Title

Enteric pathogens modulate the host to carve out a niche for expansion in the gut

Author

Miller, Brittany

Publication Date

2021

Peer reviewed|Thesis/dissertation

Enteric pathogens modulate the host to carve out a niche for expansion in the gut

By

BRITTANY MARIE MILLER
DISSERTATION

Submitted in partial satisfaction of the requirements for the degree of

DOCTOR OF PHILOSOPHY

in

Microbiology

in the

OFFICE OF GRADUATE STUDIES

of the

UNIVERSITY OF CALIFORNIA

DAVIS

Approved:

Andreas J. Bäumler, Ph.D., Chair

Mélanie G. Gareau, Ph.D.

Bennett H. Penn, M.D., Ph.D.

Committee in Charge

2021

Acknowledgements

I first and foremost like to thank my parents, who wanted nothing more of my life than for me to be happy (and for me to have health insurance). I am forever grateful for you supporting my decisions throughout my life, even when you could not understand them. Thank you to my brother Christopher for providing support as well as being my online gaming buddy.

I would like to thank Andreas Bäumler, who allowed me the freedom to develop my own projects, while always being there to lead me in the right direction. Thank you for your support and motivation. I could not have achieved this degree without your guidance.

I'd like to thank my partner, Megan Liou, whose support and love have been vital to me.

I am also grateful to many of my peers, who helped make the graduate school experience survivable. Thank you to my cohort friends Dr. Annabelle Yu, Hannah Starcevich, and Jordan Sayre.

I'd also be remiss to not thank the people in lab who have helped me along the way. Dr. Franziska Faber, for being a mentor during my rotation, teaching me many lab techniques, and helping me with projects. Dr. Christopher Lopez, for being my direct mentor, and teaching me most everything I know how to do in lab. Dr. Yael Litvak, for always making time to chat with me about science or gossip, and being the other driving force of "Team *Citrobacter*". Dr. Lillian Zhang, Dr. April Tsai, and Megan Liou, thank you for being not only instrumental to making lab and life bearable, for helping me think about my projects, helping me out with experiments, and for all the tea times. Thank you to Briana Young for the continuous support and friendship. Thank you to Andrew Rogers for being a colleague and a friend who's always down to complain with me. Thank you to Henry Nguyen who happily helps everyone, but especially for helping me, and becoming such a close friend. I'd also like to thank my committee members, Dr. Melanie Gareau and Dr. Bennet Penn for their time and input into my projects and dissertation.

Table of Contents

Abstract

Bacterial pathogens of the family *Enterobacteriaceae* must be able to successfully overcome innate host strategies for fending off invading bacteria, including competing with the resident gut microbiota, in order to obtain nutrients, replicate, and ultimately cause disease. However, mechanisms used by bacterial pathogens to outcompete the gut microbiota and establish infection are not well understood. Here, we used the murine pathogen *Citrobacter rodentium* to show the pathogen can both take advantage of host factors that are available in the gut prior to colonization for growth, as well as alter the host metabolism in a way that benefits the pathogen later on during infection. We also use the model *Salmonella enterica* serovar (*S.*) Typhimurium to show the pathogen can affect levels of a neurotransmitter, GABA, to induce an immune response that favors *S.* Typhimurium growth over competing microbes.

In chapter 2, we show that *C. rodentium*, via action of the type 3 secretion system (T3SS), can shift host colonic epithelial cell metabolism away from beta-oxidation of short chain fatty acids, a process which consumes a large amount of oxygen, to a more fermentative metabolism, leaving oxygen available for the pathogen. This phenotype was linked to colonic crypt hyperplasia, as blocking hyperplasia was able to restore the competition between a wild type and high affinity cytochrome oxidase CydAB mutant. Therefore, *C. rodentium* employs its T3SS to cause colonic crypt hyperplasia, which allows for oxygen to become available for the pathogen, thus giving the pathogen a growth advantage over competing gut microbiota members.

We next hypothesized that *C. rodentium* is respiring hydrogen peroxide prior to causing hyperplasia, to gain a foothold for growth in the gut while intimately attached to the colonic epithelium. Chapter 3 dives deeper into the observation from Chapter 2 that prior to the development of colonic crypt hyperplasia, T3SS-mediated attachment is not necessary to respire oxygen. We found that prior to hyperplasia, the cytochrome *c* peroxidase Ccp mediates respiration of hydrogen peroxide, which is produced by the epithelial NADPH oxidase NOX1. NOX1 is constitutively expressed, and acts as a habitat

filter to help shape spatial organization of the gut microbiota, however, *C. rodentium* can take advantage of this microbicidal compound for growth. *C. rodentium* thus can benefit from a presumable host defense mechanism, and in this way the pathogen is able to compete against the already established gut microbiota.

Finally, we used *S.* Typhimurium to elucidate another mechanism of overcoming colonization resistance, by establishing the hypothesis that by altering the levels of a neurotransmitter, gamma-aminobutyric acid (GABA), the pathogen can compete against other *Enterobacteriaceae* successfully. While the consumption of GABA does not provide a growth benefit directly to the pathogen, a decrease in GABA levels lead to host expression of IL-22 and downstream genes, such as lipocalin-2, allowing the pathogen to outcompete a related *Enterobacteriaceae*, *Escherichia coli* JB2. Lipocalin-2 sequesters iron from the gut lumen, which leads to growth inhibition of JB2, but *S.* Typhimurium obtains iron via salmochelin, which is resistant to lipocalin-2, thus allowing the pathogen to grow rapidly during infection.

Overall, we provide evidence that enteric pathogens have evolved methods to take advantage of immune responses to the invading pathogen, which helps them overcome habitat filters and colonization resistance.

Chapter 1

The habitat filters of microbiota-nourishing immunity

Brittany M. Miller and Andreas J. Bäumler.

Affiliations:

Department of Medical Microbiology and Immunology, School of Medicine, University of California at Davis, Davis, CA 95616, USA.

Published in:

Annual Review of Immunology, Volume 39: 1-18. (Volume publication date April 2021)

https://doi.org/10.1146/annurev-immunol-101819-024945

Abstract

An imbalance in the microbiota may contribute to many human illnesses, which has prompted efforts to rebalance it by targeting the microbes themselves. However, by supplying the habitat, the host wields a prominent influence over microbial growth at body surfaces, raising the possibility that rebalancing the microbiota by targeting our immune system would represent a viable alternative. Host control mechanisms that sculpt the microbial habitat form a functional unit with the microbiota, termed microbiota-nourishing immunity, which functions in conferring colonization resistance against pathogens. The host components of microbiota-nourishing immunity could be viewed as habitat filters that select for microbial traits licensing growth and survival in host habitat patches. Here we will review current knowledge on how host-derived habitat filters shape the size, species composition and spatial heterogeneity of the microbiota and discuss whether these host control mechanisms could be harnessed for developing approaches to rebalance microbial communities during dysbiosis.

Introduction

The advent of microbiota research has created a growing appreciation that immune responses generated during microbial infection of tissue differ in their goals from those dealing with microbial communities colonizing body surfaces (1). Microbial infection of tissue is met by sterilizing immunity, an arm of our immune system that has been studied for over a century. Sterilizing immunity is focused on detecting and distinguishing microbes from self to generate innate and adaptive immune responses that are aimed at removing microbial intruders from our tissue (**Fig. 1.1**). However, the goal of our interaction with microbial communities inhabiting body surfaces is not to detect and remove them, but rather to maintain and balance the microbiota for health. Host control mechanisms that negotiate this relationship could be viewed as habitat filters that balance the microbiota by excluding species with inappropriate trait combinations (2). In turn, a balanced microbiota orchestrates ecological priority effects to confer colonization resistance, a nonspecific immune function preventing harmful microbes from entering the body (3). Habitat filters and the microbiota thus form a host-microbe chimera, coined microbiota-nourishing immunity, which constitutes our first line of defense against continuous environmental exposure to microbes (3, 4). As colonization resistance is executed by the microbiota through effector functions that are grounded in community ecology (3, 5), the corresponding antimicrobial effector functions may seem strangely unfamiliar to immunologists accustomed to the host-derived effector functions of sterilizing immunity. However, habitat filtering shapes the size, spatial organization and species composition of microbial communities using mechanisms that partially overlap with those employed by sterilizing immunity (3), thus providing an opening for immunologists to enter this new research arena. More importantly, insights into habitat filtering provides a guide for understanding the mechanisms that underlie an imbalance in the microbiota composition (dysbiosis) (6).

Dysbiosis is associated with many non-communicable human diseases, which raises hopes that strategies to rebalance the microbiota would hold the key for developing new therapies for the corresponding illnesses (7). However, to deliver on this promise, microbiota research has to identify

treatment targets to direct the development of new therapies. Current efforts to identify potential treatment targets remain microbe-centric, as they mainly focus on finding beneficial microbes lost or harmful bacteria expanded during dysbiosis (8-11). Consequently, the field has embraced a microbe-centric approach for rebalancing the microbiota by targeting the microbes themselves with microbiota transplants, probiotics, antibiotics or dietary interventions (12-14). However, the vision of microbiota-nourishing immunity supports the alternate view that changes in the microbiota composition during dysbiosis can serve as biomarkers for an underlying weakening of habitat filters in the host (6). This vantage point suggests that the microbiota could be rebalanced with drugs that target the host to restore the functionality of its habitat filters (3, 4). The concept of microbiota-nourishing immunity thus raises the exciting prospect that host-derived habitat filters represent the treatment targets craved by contemporary microbiota research, which provides a sound rationale for reviewing current knowledge about these host control mechanisms.

Habitat filters that limit the size of microbial communities

To test the validity of the argument that a weakening of host control mechanisms is a driver of dysbiosis, let us first look at examples where the habitat filters and the disease etiology are well understood. One of the functions mediated by habitat filters is to limit the size of microbial communities, which is a prominent host control mechanism in the upper gastrointestinal tract. The stomach is generally considered an inhospitable environment for microbes, although some specialists, such as *Helicobacter pylori* (phylum *Proteobacteria*), can establish residency (15). Culture-independent methods reveal the presence of a gastric microbiota (16), but it remains controversial whether this community is truly resident or continuously reseeded from the oral cavity and then extinguished (17). A truly resident microbiota is encountered upon descent into the small intestine, which harbors a microbial community dominated by facultatively anaerobic bacteria belonging to the class *Bacilli* (phylum *Firmicutes*), whereas members of the family *Enterobacteriaceae* (phylum *Proteobacteria*) might also be present (18). Yet, bacterial densities in the duodenum and proximal jejunum remain relatively low, typically not exceeding 10^4 colony-forming units (CFU) per ml (19). The habitat filters that limit bacterial growth and survival in the upper gastrointestinal tract include gastric acid (20), pancreatic secretions (21-24), small intestinal peristalsis (25) and immunoglobulin (26) (**Table 1.1 and Fig. 1.2**).

A weakening of habitat filters that limit the size of microbial communities in the upper gastrointestinal tract is associated with small intestinal bacterial overgrowth (SIBO), a heterogenous syndrome defined by bacterial densities exceeding 10^5 CFU/ml of proximal jejunal aspiration, as determined by culture-dependent methods (19). In turn, dysbiosis can cause malabsorption, because an excess of microbes that deconjugate bile acids reduces absorption of fat and fat-soluble vitamins in the small intestine (27). Furthermore, microbial communities in the small intestine rapidly consume simple carbohydrates (18) and bacterial overgrowth therefore interferes with absorption of these nutrients by the host, which might contribute to weight loss observed in patients with SIBO (19). In addition to these quantitative changes, SIBO is associated with dysbiosis featuring changes in the microbiota composition

(28). Treatment of SIBO includes targeting the underlying disease (thereby restoring the habitat filter), providing nutritional support (thereby treating the symptoms of dysbiosis) and cyclical gastro-intestinal selective antibiotics (which reduces the bacterial burden, thereby functionally replacing habitat filters) (19). It becomes obvious from the example of SIBO that a weakening of habitat filters is a driver of dysbiosis and that, in turn, dysbiosis can exacerbate disease by adversely affecting the digestive functions of the small bowel.

Limiting the size of microbial communities is also a prominent host control mechanism operational in the lower respiratory tract. The microbial burden of the lung parenchyma and the tracheobronchial tree below the larynx is so low that these sites were long considered sterile, but advances in culture-independent approaches reveal the presence of bacterial DNA in the lower respiratory tract of healthy individuals (17, 29, 30). It remains a matter of debate whether microbes detected in the lungs represents a resident microbiota or correspond to a transient population that is continually reseeded from the microbiota of the upper respiratory tract and cleared by immune mechanisms (31). Regardless of how of this argument will be settled, it is clear that one of the habitat filters that limits bacterial growth and survival in the airways is the mucus escalator (**Table 1.1**). A weakening of mucociliary clearance is associated with dysbiosis, characterized by reduced global diversity of the oropharyngeal microbiota and elevated abundances of opportunistic pathogens, such as members of the genera *Pseudomonas* (phylum *Proteobacteria*), *Staphylococcus*, and *Streptococcus* (phylum *Firmicutes*), which might be the source of dysbiosis observed in the lower airways (32).

Notably, the mucus escalator was identified as a clearance mechanism long before the age of microbiota research, because its inactivation in individuals with cystic fibrosis leads to opportunistic infection. Cystic fibrosis is caused by loss-of-function mutations in *CFTR*, the gene encoding the cystic fibrosis transmembrane conductance regulator (CFTR), which weakens mucociliary clearance (33-35). Dysbiosis in the lungs due to impaired airway clearance gives rise to chronic inflammation and colonization with *Pseudomonas aeruginosa* and *Staphylococcus aureus,* the predominant opportunistic pathogens

associated with cystic fibrosis (36). An essential component in the management of cystic fibrosis lung disease is antibiotic therapy directed against the opportunistic bacterial pathogens (37). Viewing cystic fibrosis through the lens of microbiota-nourishing immunity suggests that antibiotic therapy functionally replaces mucociliary clearance, thereby reestablishing bacterial growth restriction in the lung. Furthermore, this vantage point suggests that a logical alternative to targeting the microbes with antibiotics would be targeting the host to restore the habitat filter. Consistent with this idea, emerging treatments for patients suffering from cystic fibrosis are aimed at restoring CFTR function in the airway epithelium through small molecule modulator drug therapy, gene therapy or gene editing strategies (38, 39). Thus, viewing cystic fibrosis as an immunodeficiency in microbiota-nourishing immunity clarifies that dysbiosis is secondary to a weakening of a habitat filter and that treatment requires restoring functionality of the habitat filter or replacing it functionally with antibiotics.

Habitat filters that shape the microbiota composition

The examples of SIBO and cystic fibrosis demonstrate that weakened habitat filters can alter microbial communities quantitatively, but dysbiosis is commonly described as a qualitative change, featuring a reduced overall microbial diversity, a demise of beneficial microbes or an expansion of harmful microorganisms (40). To explore the origin of such qualitative changes in the microbiota, we will discuss habitat filters that shape the species composition of microbial communities. Host control over the microbiota composition is overt in the vaginal mucosa of reproductive age women, where the microbial community is dominated by microbes belonging to a single genus, *Lactobacillus* (class *Bacilli*)(41, 42). The habitat filter that drives the dominance of *Lactobacillus* species is glycogen production in vaginal epithelial cells (**Table 1.1**)(43). The exfoliation of glycogen-rich epithelial cells is thought to increase glycogen availability in the vaginal lumen, where this nutrient is broken down by host-derived α-amylase into maltose and maltotriose (43-45). In turn, maltose and maltotriose drive an expansion of *Lactobacillus* species, which catabolize these nutrients into lactic acid, a metabolite that lowers the vaginal pH, thereby limiting growth of other microbes through niche modification (43, 45). The dominance of *Lactobacillus* species is not typically observed before menarche or after menopause (46, 47), pointing to a role of estrogen in controlling this habitat filter. In line with this hypothesis, a decrease in blood estrogen is associated with a reduction in glycogen-positive epithelial cells (48), low vaginal glycogen and low vaginal α-amylase (49). These data suggest that hormonal control of epithelial metabolism generates habitat characteristics that can 'filter' the vaginal microbiota so that closely related *Lactobacillus* species predominate.

Moving into the large bowel, the hypothesis that weakened habitat filters underlie dysbiosis appears to collide with the dogma that diet is the main driver of the gut microbiota composition (50). However, rather than being mutually exclusive concepts, diet could be viewed as an abiotic habitat filter that cooperates with host-derived habitat filters to select species most suited to the prevailing condition. Dietary fiber escapes digestion by host enzymes in the upper gastrointestinal tract and reaches the colon, where it forms an important nutrient source for bacterial growth (51). Members of the classes *Clostridia* (phylum

firmicutes) and *Bacteroidia* (phylum *Bacteroidetes*) possess the greatest potential for catabolizing a diverse array of dietary complex polysaccharides, because their genomes encode a broad spectrum of glycolytic enzymes (52), which might be one of the reasons these taxa dominate the adult colonic microbiota. Parameters of diet-derived filters can be changed, for example by adding new complex carbohydrates to the diet, which supports engraftment of microbes that are able to catabolize these nutrients (53, 54). Conversely, a long-term reduction in dietary fiber intake can result in an irreversible extinction of some fiber-consuming microbes from the colonic microbiota (55). However, members of the family *Bacteroidiaceae* (class *Bacteroidia*) can sustain themselves on goblet cell-derived mucus polysaccharides during periods of dietary fiber starvation (55, 56). These observations identify mucus polysaccharides as a host-derived habitat filter that maintains *Bacteroidiaceae* species within in the gut microbiota (**Table 1.1**). Consistent with the idea that this taxon is under selection by a host-derived habitat filter, co-speciation with humans and African apes is observed for clades of *Bacteroidiaceae* (57).

A second class of nutrients that are poorly absorbed in the small intestine and nourish the microbiota in the colon are dietary FODMAPs, an acronym for fermentable oligosaccharides, disaccharides, monosaccharides and polyols (58). However, delivering nutrients into the colon through this mechanism is also a host strategy to regulate microbial growth and survival in the colon. Human milk oligosaccharides do not aid in the nutrition of the infant, are poorly absorbed in the small intestine and serve as a maternal habitat filter in the colon that directs development of the infant gut microbiota (59) (**Table 1.1**). Obligate anaerobic bacteria in the family *Bifidobacteriaceae* (phylum *Actinobacteria*) contain gene clusters for the catabolism of milk oligosaccharides (60-62). Breast feeding thus drives the microbiota composition in the infant colon towards a dominance of *Bifidobacteriaceae* to guide development of a protective microbial community (63, 64). Conversely, weaning launches an ecological succession from a dominance of *Bifidobacteriaceae* to a preeminence of obligate anaerobic *Clostridia* and *Bacteroidia* in the colonic microbiota (65). Again, a dependence on maternal habitat filters for growth and survival might explain why

clades of *Bifidobacteriaceae* speciate in concert with African apes and humans, resulting in topologically identical phylogenies of these bacteria and their hosts (57).

An important host control mechanism that shapes the abundance of species inhabiting the colon is high mitochondrial oxygen consumption, which maintains the epithelial surface in a state of physiological hypoxia (66) (**Fig. 1.3**). In turn, epithelial hypoxia limits the amount of oxygen emanating from the mucosal surface, thereby maintaining anaerobiosis. Anaerobiosis is a habitat filter that checks an expansion of facultative anaerobic bacteria, thereby reducing the range of successful strategies for microbial growth in the colon (67-70) (**Table 1.1**). An expansion of facultative anaerobic *Proteobacteria* in the fecal microbiota represents a microbial signature of dysbiosis linked to a broad range of human conditions (6, 71). A fecal *Proteobacteria* expansion is a feature of dysbiosis associated with chronic alcohol consumption (72), antibiotic therapy (73), radiotherapy (74), malnutrition (75), inflammaging (76) and observed in individuals with ulcerative colitis (77), Crohn's disease (77), colorectal cancer (78), necrotizing enterocolitis (79), HIV enterophathy (80), graft versus host disease (81), infectious diarrhea (82) and a subset of patients with irritable bowel syndrome (83, 84). An expansion of facultative anaerobic bacteria is linked to a weakening of anaerobiosis, as increases in the availability of epithelial-derived respiratory electron acceptors are observed in mouse models of ulcerative colitis (85, 86), antibiotic therapy (87), colorectal cancer (86), or infectious diarrhea (88, 89), where they drive an expansion of *Proteobacteria.* During conditions of intestinal inflammation, an expansion of *Proteobacteria* might be further exacerbated by monocyte-derived nitrate, which fuels growth by anaerobic nitrate respiration (90-93). Collectively, these observations link a weakening of epithelial hypoxia to dysbiosis in a broad spectrum of diseases (69, 70), suggesting that host-derived habitat filters play a much greater role in shaping the gut microbiota than conventional wisdom on dietary control over the species composition would imply (94).

Whereas elevated epithelial oxygenation is a common cause of dysbiosis in the colon (69, 70, 95), different mechanisms can be responsible for the underlying reduction in mitochondrial oxidative phosphorylation and fatty acid oxidation. One mechanism producing an increase in epithelial oxygenation

is observed during antibiotic therapy, in which depletion of microbiota-derived short-chain fatty acids reduces epithelial PPAR-γ signaling, a pathway activating mitochondrial activity in the colonic epithelium (87). A second mechanism is associated with epithelial damage, because excessive epithelial repair responses lead to an accumulation of dividing undifferentiated epithelial cells (termed transit-amplifying cells), which obtain energy by converting glucose into lactate (aerobic glycolysis) (**Fig. 1.3**)(89, 96). In addition to increasing oxygen availability, a shift in epithelial metabolism from mitochondrial oxidative phosphorylation to aerobic glycolysis increases epithelial release of lactate, which fuels an expansion of pathogenic *Proteobacteria* during enteric infection (97-99). These mechanistic insights suggest epithelial hypoxia in the colon serves as a habitat filter that is weakened by a reduction in mitochondrial bioenergetics.

Viewing epithelial metabolism as a habitat filter raises the prospect for therapeutic intervention, because it suggests that small molecule activators of mitochondrial bioenergetics could be used to rebalance the microbiota. To explore the accuracy of this prediction, we will briefly review pertinent data on ulcerative colitis, one of the illnesses associated with a dysbiotic *Proteobacteria* expansion in the fecal microbiota (77). Colonic epithelial cells from ulcerative colitis patients exhibit impaired mitochondrial bioenergetics and reduced *PPARG* expression compared to healthy controls (100, 101). The first line of treatment for mild to moderate cases of ulcerative colitis is the PPAR-γ agonist 5-aminosalicylic acid (5-ASA) (102-105). PPAR-γ activation enhances mitochondrial bioenergetics by activating transcription of *SIRT3*, which encodes a mitochondrial protein that activates enzymes involved in oxidative phosphorylation, the tricarboxylic acid cycle and fatty acid oxidation (106-109). In patients with ulcerative colitis, 5-ASA treatment reduces the abundance of *Proteobacteria* in the fecal microbiota (110). Thus 5-ASA therapy provides a proof positive that habitat filters can be targeted with small molecule modulators of epithelial metabolism to rebalance the microbiota composition.

Habitat filters that govern the biogeography of microbial communities

Habitat filters responsible for sculpting the spatial heterogeneity of the microbiota remain under-examined, but work over the past 10 years is starting to illuminate their function in the gastrointestinal tract. To protect the single layer of colonic epithelial cells that separates us from the largest microbial community present in our body, host control mechanisms keep the colonic microbiota at a physical distance from the mucosal surface. As a result, the inner mucus layer is largely devoid of bacteria, whereas the outer mucus layer is densely colonized (111) (**Fig. 1.2**). This spatial heterogeneity has been attributed in part to physical properties of mucus, with the inner mucus layer being more densely packed, thereby preventing nanoparticles from reaching the surface (112, 113) (**Table 1.1**). However, microbiota profiling reveals a cross-sectional heterogeneity in the species composition that cannot be explained by physical properties of mucus alone.

The loose outer mucus layer is enriched in bacteria utilizing host-derived mucin, such as *Bacteroidiaceae* or *Akkermansia mucinophila* (phylum *Verrucomicrobia*) (114). Closer to the epithelium, oxygen radiating from the epithelial surface is proposed to increase the proportion of *Proteobacteria* and *Actinobacteria* phyla, which encompass "oxygen-tolerant" organisms, as suggested by expression of genes encoding catalase activity (115). However, catalase confers resistance to hydrogen peroxide, which raises the alternate possibility that the epithelial surface selects for "oxygen-tolerant" organisms by releasing hydrogen peroxide. Interestingly, epithelial cells in the colon constitutively synthesize NADPH oxidase (NOX1), (116), a potential source of hydrogen peroxide (**Table 1.1 and Fig. 1.2**). Since the vast majority of obligate anaerobic bacteria present in the colon lack oxygen tolerance, NOX1-derived hydrogen peroxide might help maintain a demilitarized zone in close proximity to the epithelial surface. Consistent with this idea, a weakening of this habitat filter allows for bacterial penetration into crypts in a mouse model (117). Furthermore, in humans, *NOX1*-deficiency results in early onset ulcerative colitis (118). However, more work is needed to determine the importance of NOX1-derived hydrogen peroxide as a host control mechanism that protects the colonic mucosal surface.

Host control also protects the epithelial surface in the small intestine, albeit through different mechanisms. Since the microbiota in the small intestine is dominated by facultative anaerobic bacteria that are oxygen tolerant (18), the usefulness of hydrogen peroxide in protecting the epithelium is diminished. The epithelium of the ileum constitutively synthesizes NOX1 and iNOS, thus driving the production of antimicrobial peroxynitrite to protect the mucosal surface (116). However, epithelial NOX1 and iNOS synthesis are absent in the duodenum and jejunum (116). Furthermore, a separation into inner and outer mucus layer is not observed in the small intestine (119). Stimulation of toll-like receptor (TLR)5 by bacterial flagellin triggers immunoglobulin (Ig)A production to limit flagella-mediated motility within the microbiota, thereby reducing bacterial penetration of the mucus layer (120) (**Fig. 1.2**). Paneth cells, which are specific to the crypts of Lieberkühn in the small intestine, release human defensin 5, which eradicates segmented filamentous bacteria (phylum *Firmicutes*), a group of microorganisms that grow in intimate attachment to the epithelial surface (121). Similarly, the antimicrobial protein REGIIIγ limits bacterial growth in close proximity to the epithelial surface in mice (122). Paneth cell dysfunction in patients with ileal Crohn's disease is associated with reduced defensin secretion (123-125) and overgrowth of adherent-invasive *Escherichia coli* (family *Enterobacteriaceae*), which inhabit a niche in close proximity to the mucosal surface (126). Thus, Paneth cells could be viewed as a habitat filter that contributes to a spatial heterogeneity of the microbiota in the small intestine by protecting the crypts and epithelial surface from bacterial overgrowth (127) (**Table 1.1**).

Control of habitat filtering

Given the importance of habitat filters in microbiota assembly, signaling pathways involved in their activation are of potential interest for restoring or maintaining homeostasis. Whereas sterilizing immunity is induced by signals that distinguish microbes from self (**Fig. 1.1**), habitat filters of microbiota-nourishing immunity often respond to metabolites that serve as biomarkers for the presence of microbial communities or changes in their composition. For example, the succinate receptor SUCNR1 is synthesized by small intestinal epithelial tuft cells. SUCNR1 responds to succinate, a microbial metabolite whose concentration increases during helminth infection, thereby inducing type 2 responses that filter the habitat to exclude the parasite (128) (**Fig. 1.4**). Another metabolite that can become elevated during dysbiosis is lactate (97, 98), which is detected by G-protein-coupled receptor 31(GPR31) present on dendritic cells. GPR31 directs protrusion of dendrites into the lumen that function in microbial sampling to generate antibody responses (129), a habitat filter in the small intestine (**Table 1.1**). Thus, monitoring the luminal concentrations of succinate or lactate could be viewed as mechanisms to sense dysbiosis and rebalance the microbiota through habitat filtering.

Microbiota-derived tryptophan metabolites are ligands of the aryl hydrocarbon receptor (AHR), which is expressed on dendritic cells, T helper type 17 (T_H17) cells and innate lymphoid cells (130, 131). Stimulation of AHR leads to production of interleukin (IL)-22, a cytokine that induces the epithelial release of the antimicrobial protein REGIIIγ (132-134) (**Fig. 1.4**), which filters the habitat in close proximity to the mucosal surface (122). Microbiota-derived short-chain fatty acids are sensed by G-protein-coupled receptor 43 (GPR43) on regulatory T cells (135-138), GPR109A on antigen presenting cells (139), PPAR-γ in colonic epithelial cells (140) and through downregulation of histone deacetylases (HDACs) in macrophages (141). Signals detected through these short-chain fatty acid sensors maintain the regulatory T cell pool (135-139), thereby preserving epithelial hypoxia, a habitat filter in the colon (87).

These examples illustrate that host signaling pathways involved in balancing the microbiota can be identified by elucidating the mechanisms through which metabolites control habitat filters of microbiota-nourishing immunity.

Conclusions

The surprising revelation that diseases ranging from colorectal cancer to autism are associated with dysbiosis has generated the expectation that microbiome research will generate new therapies for a broad spectrum of human illnesses (7). However, defining the microbiome as the microbiota and its genes (142) has focused major initiatives, such as he human microbiome project, on cataloguing microbial genes and species names (143, 144), which has not generated the anticipated bonanza of new treatment targets (145). Breaking from the confines of a microbe-centric viewpoint requires defining the microbiome ecologically as the microbiota and its host habitat (146), a perspective that integrates host control over the microbial environment into the picture (147, 148). This vantage point suggests that habitat filters of microbiota-nourishing immunity balance the microbiota composition by selecting for phenotypic characteristics of microbes that license their growth and survival in the host. A weakening of habitat filters is a major driver of dysbiosis, which can feature changes in the size, species composition or spatial organization of the microbiota. Consequently, dysbiosis could be considered a microbial signature of dysfunctional habitat filtering, which in turn identifies the microbiota as a biomarker that can be used for monitoring the functionality of these host control mechanisms.

There is considerable overlap between effector functions of sterilizing immunity and the mechanisms habitat filters employ to shape the microbiota, which include immunoglobulin, antimicrobial peptides and reactive oxygen species. However, some habitat filters literally nourish the microbiota through milk oligosaccharides, mucus carbohydrates or α-amylase-derived maltose and maltotriose. Shaping the microbiota using a combination of nutrition and antimicrobial control is a carrot-and-stick approach that is unique to microbiota-nourishing immunity, because sterilizing immunity never deliberately feeds microbes. As functions that nourish the microbiota are often linked to epithelial metabolism, changes in intracellular metabolic pathways can weaken the functionality of habitat filters (**Fig. 1.3**). This feature finds a parallel in sterilizing immunity, where changes in intracellular metabolic pathways can alter the function of immune

cells (149). Thus, strategies to manipulate immunometabolism might turn out to be useful tools to strengthen microbiota-nourishing immunity as well.

Great challenges remain in detecting additional habitat filters, particularly those acting on fungi, protozoa or viruses. However, microbiome research also creates countless opportunities for identifying new therapeutic targets to strengthen microbiota-nourishing immunity. Expanding the microbe-centric approach of microbiome research to incorporate the concept of microbiota-nourishing immunity will speed up meeting these challenges and opportunities and help the field to live up to its expectations by identifying host-derived habitat filters as potential treatment targets.

References

1. Kisseleva EP. 2014. Innate immunity underlies symbiotic relationships. *Biochemistry (Mosc)* 79: 1273-85

2. Costello EK, Stagaman K, Dethlefsen L, Bohannan BJ, Relman DA. 2012. The application of ecological theory toward an understanding of the human microbiome. *Science* 336: 1255-62

3. Litvak Y, Baumler AJ. 2019. Microbiota-Nourishing Immunity: A Guide to Understanding Our Microbial Self. *Immunity* 51: 214-24

4. Byndloss MX, Litvak Y, Baumler AJ. 2019. Microbiota-nourishing Immunity and Its Relevance for Ulcerative Colitis. *Inflamm Bowel Dis*

5. Litvak Y, Baumler AJ. 2019. The founder hypothesis: A basis for microbiota resistance, diversity in taxa carriage, and colonization resistance against pathogens. *PLoS Pathog* 15: e1007563

6. Tiffany CR, Baumler AJ. 2019. Dysbiosis: from fiction to function. *Am J Physiol Gastrointest Liver Physiol* 317: G602-G8

7. Cani PD. 2017. Gut microbiota - at the intersection of everything? *Nat Rev Gastroenterol Hepatol*

8. Shreiner A, Huffnagle GB, Noverr MC. 2008. The "Microflora Hypothesis" of allergic disease. *Adv Exp Med Biol* 635: 113-34

9. Packey CD, Sartor RB. 2009. Commensal bacteria, traditional and opportunistic pathogens, dysbiosis and bacterial killing in inflammatory bowel diseases. *Curr Opin Infect Dis* 22: 292-301

10. Round JL, Mazmanian SK. 2009. The gut microbiota shapes intestinal immune responses during health and disease. *Nat Rev Immunol* 9: 313-23

11. Bjorksten B. 2009. The hygiene hypothesis: do we still believe in it? *Nestle Nutr Workshop Ser Pediatr Program* 64: 11-8; discussion 8-22, 251-7

12. Gagliardi A, Totino V, Cacciotti F, Iebba V, Neroni B, Bonfiglio G, Trancassini M, Passariello C, Pantanella F, Schippa S. 2018. Rebuilding the Gut Microbiota Ecosystem. *Int J Environ Res Public Health* 15

13. Kumar V, Fischer M. 2019. Expert opinion on fecal microbiota transplantation for the treatment of Clostridioides difficile infection and beyond. *Expert Opin Biol Ther*: 1-9

14. Chen CC, Chen YN, Liou JM, Wu MS, Taiwan Gastrointestinal D, Helicobacter C. 2019. From germ theory to germ therapy. *Kaohsiung J Med Sci* 35: 73-82

15. Marshall BJ, Warren JR. 1984. Unidentified curved bacilli in the stomach of patients with gastritis and peptic ulceration. *Lancet* 1: 1311-5

16. Bik EM, Eckburg PB, Gill SR, Nelson KE, Purdom EA, Francois F, Perez-Perez G, Blaser MJ, Relman DA. 2006. Molecular analysis of the bacterial microbiota in the human stomach. *Proc Natl Acad Sci U S A* 103: 732-7

17. Bassis CM, Erb-Downward JR, Dickson RP, Freeman CM, Schmidt TM, Young VB, Beck JM, Curtis JL, Huffnagle GB. 2015. Analysis of the upper respiratory tract microbiotas as the source of the lung and gastric microbiotas in healthy individuals. *MBio* 6: e00037

18. Zoetendal EG, Raes J, van den Bogert B, Arumugam M, Booijink CC, Troost FJ, Bork P, Wels M, de Vos WM, Kleerebezem M. 2012. The human small intestinal microbiota is driven by rapid uptake and conversion of simple carbohydrates. *ISME J* 6: 1415-26

19. Bures J, Cyrany J, Kohoutova D, Forstl M, Rejchrt S, Kvetina J, Vorisek V, Kopacova M. 2010. Small intestinal bacterial overgrowth syndrome. *World J Gastroenterol* 16: 2978-90

20. Sarker SA, Ahmed T, Brussow H. 2017. Hunger and microbiology: is a low gastric acid-induced bacterial overgrowth in the small intestine a contributor to malnutrition in developing countries? *Microb Biotechnol* 10: 1025-30

21. Trespi E, Ferrieri A. 1999. Intestinal bacterial overgrowth during chronic pancreatitis. *Curr Med Res Opin* 15: 47-52

22. Stenwall A, Ingvast S, Skog O, Korsgren O. 2019. Characterization of host defense molecules in the human pancreas. *Islets* 11: 89-101

23. Ahuja M, Schwartz DM, Tandon M, Son A, Zeng M, Swaim W, Eckhaus M, Hoffman V, Cui Y, Xiao B, Worley PF, Muallem S. 2017. Orai1-Mediated Antimicrobial Secretion from Pancreatic Acini Shapes the Gut Microbiome and Regulates Gut Innate Immunity. *Cell Metab* 25: 635-46

24. Minelli EB, Benini A, Bassi C, Abbas H, Falconi M, Locatelli F, de Marco R, Pederzoli P. 1996. Antimicrobial activity of human pancreatic juice and its interaction with antibiotics. *Antimicrob Agents Chemother* 40: 2099-105

25. Kongara KR, Soffer EE. 2000. Intestinal motility in small bowel diverticulosis: a case report and review of the literature. *J Clin Gastroenterol* 30: 84-6

26. Pignata C, Budillon G, Monaco G, Nani E, Cuomo R, Parrilli G, Ciccimarra F. 1990. Jejunal bacterial overgrowth and intestinal permeability in children with immunodeficiency syndromes. *Gut* 31: 879-82

27. Fan X, Sellin JH. 2009. Review article: Small intestinal bacterial overgrowth, bile acid malabsorption and gluten intolerance as possible causes of chronic watery diarrhoea. *Aliment Pharmacol Ther* 29: 1069-77

28. Bouhnik Y, Alain S, Attar A, Flourie B, Raskine L, Sanson-Le Pors MJ, Rambaud JC. 1999. Bacterial populations contaminating the upper gut in patients with small intestinal bacterial overgrowth syndrome. *Am J Gastroenterol* 94: 1327-31

29. Dickson RP, Erb-Downward JR, Freeman CM, McCloskey L, Beck JM, Huffnagle GB, Curtis JL. 2015. Spatial Variation in the Healthy Human Lung Microbiome and the Adapted Island Model of Lung Biogeography. *Ann Am Thorac Soc* 12: 821-30

30. Charlson ES, Bittinger K, Haas AR, Fitzgerald AS, Frank I, Yadav A, Bushman FD, Collman RG. 2011. Topographical continuity of bacterial populations in the healthy human respiratory tract. *Am J Respir Crit Care Med* 184: 957-63

31. Budden KF, Gellatly SL, Wood DL, Cooper MA, Morrison M, Hugenholtz P, Hansbro PM. 2017. Emerging pathogenic links between microbiota and the gut-lung axis. *Nat Rev Microbiol* 15: 55-63

32. Boutin S, Depner M, Stahl M, Graeber SY, Dittrich SA, Legatzki A, von Mutius E, Mall M, Dalpke AH. 2017. Comparison of Oropharyngeal Microbiota from Children with Asthma and Cystic Fibrosis. *Mediators Inflamm* 2017: 5047403

33. Kerem B, Rommens JM, Buchanan JA, Markiewicz D, Cox TK, Chakravarti A, Buchwald M, Tsui LC. 1989. Identification of the cystic fibrosis gene: genetic analysis. *Science* 245: 1073-80

34. Riordan JR, Rommens JM, Kerem B, Alon N, Rozmahel R, Grzelczak Z, Zielenski J, Lok S, Plavsic N, Chou JL, et al. 1989. Identification of the cystic fibrosis gene: cloning and characterization of complementary DNA. *Science* 245: 1066-73

35. Rommens JM, Iannuzzi MC, Kerem B, Drumm ML, Melmer G, Dean M, Rozmahel R, Cole JL, Kennedy D, Hidaka N, et al. 1989. Identification of the cystic fibrosis gene: chromosome walking and jumping. *Science* 245: 1059-65

36. Shukla SD, Budden KF, Neal R, Hansbro PM. 2017. Microbiome effects on immunity, health and disease in the lung. *Clin Transl Immunology* 6: e133

37. Gibson RL, Burns JL, Ramsey BW. 2003. Pathophysiology and management of pulmonary infections in cystic fibrosis. *Am J Respir Crit Care Med* 168: 918-51

38. Miah KM, Hyde SC, Gill DR. 2019. Emerging gene therapies for cystic fibrosis. *Expert Rev Respir Med* 13: 709-25

39. Yan Z, McCray PB, Jr., Engelhardt JF. 2019. Advances in gene therapy for cystic fibrosis lung disease. *Hum Mol Genet* 28: R88-R94

40. Petersen C, Round JL. 2014. Defining dysbiosis and its influence on host immunity and disease. *Cell Microbiol* 16: 1024-33

41. Ravel J, Gajer P, Abdo Z, Schneider GM, Koenig SS, McCulle SL, Karlebach S, Gorle R, Russell J, Tacket CO, Brotman RM, Davis CC, Ault K, Peralta L, Forney LJ. 2011. Vaginal microbiome of reproductive-age women. *Proc Natl Acad Sci U S A* 108 Suppl 1: 4680-7

42. Chen C, Song X, Wei W, Zhong H, Dai J, Lan Z, Li F, Yu X, Feng Q, Wang Z, Xie H, Chen X, Zeng C, Wen B, Zeng L, Du H, Tang H, Xu C, Xia Y, Xia H, Yang H, Wang J, Wang J, Madsen L, Brix S, Kristiansen K, Xu X, Li J, Wu R, Jia H. 2017. The microbiota continuum along the female reproductive tract and its relation to uterine-related diseases. *Nat Commun* 8: 875

43. Spear GT, French AL, Gilbert D, Zariffard MR, Mirmonsef P, Sullivan TH, Spear WW, Landay A, Micci S, Lee BH, Hamaker BR. 2014. Human alpha-amylase present in lower-genital-tract mucosal fluid processes glycogen to support vaginal colonization by Lactobacillus. *J Infect Dis* 210: 1019-28

44. Mirmonsef P, Hotton AL, Gilbert D, Burgad D, Landay A, Weber KM, Cohen M, Ravel J, Spear GT. 2014. Free glycogen in vaginal fluids is associated with Lactobacillus colonization and low vaginal pH. *PLoS One* 9: e102467

45. Nasioudis D, Beghini J, Bongiovanni AM, Giraldo PC, Linhares IM, Witkin SS. 2015. alpha-Amylase in Vaginal Fluid: Association With Conditions Favorable to Dominance of Lactobacillus. *Reprod Sci* 22: 1393-8

46. Brotman RM, Shardell MD, Gajer P, Fadrosh D, Chang K, Silver MI, Viscidi RP, Burke AE, Ravel J, Gravitt PE. 2014. Association between the vaginal microbiota, menopause status, and signs of vulvovaginal atrophy. *Menopause* 21: 450-8

47. Thoma ME, Gray RH, Kiwanuka N, Aluma S, Wang MC, Sewankambo N, Wawer MJ. 2011. Longitudinal changes in vaginal microbiota composition assessed by gram stain among never sexually active pre- and postmenarcheal adolescents in Rakai, Uganda. *J Pediatr Adolesc Gynecol* 24: 42-7

48. Miller L, Patton DL, Meier A, Thwin SS, Hooton TM, Eschenbach DA. 2000. Depomedroxyprogesterone-induced hypoestrogenism and changes in vaginal flora and epithelium. *Obstet Gynecol* 96: 431-9

49. Wessels JM, Lajoie J, Cooper M, Omollo K, Felker AM, Vitali D, Dupont HA, Nguyen PV, Mueller K, Vahedi F, Kimani J, Oyugi J, Cheruiyot J, Mungai JN, Deshiere A, Tremblay MJ, Mazzulli T, Stearns JC, Ashkar AA, Fowke KR, Surette MG, Kaushic C. 2019. Medroxyprogesterone acetate alters the vaginal microbiota and microenvironment in women and increases susceptibility to HIV-1 in humanized mice. *Dis Model Mech* 12

50. David LA, Maurice CF, Carmody RN, Gootenberg DB, Button JE, Wolfe BE, Ling AV, Devlin AS, Varma Y, Fischbach MA, Biddinger SB, Dutton RJ, Turnbaugh PJ. 2014. Diet rapidly and reproducibly alters the human gut microbiome. *Nature* 505: 559-63

51. Singh RK, Chang HW, Yan D, Lee KM, Ucmak D, Wong K, Abrouk M, Farahnik B, Nakamura M, Zhu TH, Bhutani T, Liao W. 2017. Influence of diet on the gut microbiome and implications for human health. *J Transl Med* 15: 73

52. El Kaoutari A, Armougom F, Gordon JI, Raoult D, Henrissat B. 2013. The abundance and variety of carbohydrate-active enzymes in the human gut microbiota. *Nat Rev Microbiol* 11: 497-504

53. Shepherd ES, DeLoache WC, Pruss KM, Whitaker WR, Sonnenburg JL. 2018. An exclusive metabolic niche enables strain engraftment in the gut microbiota. *Nature* 557: 434-8

54. Kearney SM, Gibbons SM, Erdman SE, Alm EJ. 2018. Orthogonal Dietary Niche Enables Reversible Engraftment of a Gut Bacterial Commensal. *Cell Rep* 24: 1842-51

55. Sonnenburg ED, Smits SA, Tikhonov M, Higginbottom SK, Wingreen NS, Sonnenburg JL. 2016. Diet-induced extinctions in the gut microbiota compound over generations. *Nature* 529: 212-5

56. Sonnenburg JL, Xu J, Leip DD, Chen CH, Westover BP, Weatherford J, Buhler JD, Gordon JI. 2005. Glycan foraging in vivo by an intestine-adapted bacterial symbiont. *Science* 307: 1955-9

57. Moeller AH, Caro-Quintero A, Mjungu D, Georgiev AV, Lonsdorf EV, Muller MN, Pusey AE, Peeters M, Hahn BH, Ochman H. 2016. Cospeciation of gut microbiota with hominids. *Science* 353: 380-2

58. Reddel S, Putignani L, Del Chierico F. 2019. The Impact of Low-FODMAPs, Gluten-Free, and Ketogenic Diets on Gut Microbiota Modulation in Pathological Conditions. *Nutrients* 11

59. Sela DA, Chapman J, Adeuya A, Kim JH, Chen F, Whitehead TR, Lapidus A, Rokhsar DS, Lebrilla CB, German JB, Price NP, Richardson PM, Mills DA. 2008. The genome sequence of Bifidobacterium longum subsp. infantis reveals adaptations for milk utilization within the infant microbiome. *Proc Natl Acad Sci U S A* 105: 18964-9

60. Ward RE, Ninonuevo M, Mills DA, Lebrilla CB, German JB. 2006. In vitro fermentation of breast milk oligosaccharides by Bifidobacterium infantis and Lactobacillus gasseri. *Appl Environ Microbiol* 72: 4497-9

61. LoCascio RG, Desai P, Sela DA, Weimer B, Mills DA. 2010. Broad conservation of milk utilization genes in Bifidobacterium longum subsp. infantis as revealed by comparative genomic hybridization. *Appl Environ Microbiol* 76: 7373-81

62. Sela DA, Garrido D, Lerno L, Wu S, Tan K, Eom HJ, Joachimiak A, Lebrilla CB, Mills DA. 2012. Bifidobacterium longum subsp. infantis ATCC 15697 alpha-fucosidases are active on fucosylated human milk oligosaccharides. *Appl Environ Microbiol* 78: 795-803

63. Sela DA, Mills DA. 2010. Nursing our microbiota: molecular linkages between bifidobacteria and milk oligosaccharides. *Trends Microbiol* 18: 298-307

64. Garrido D, Dallas DC, Mills DA. 2013. Consumption of human milk glycoconjugates by infant-associated bifidobacteria: mechanisms and implications. *Microbiology* 159: 649-64

65. Mackie RI, Sghir A, Gaskins HR. 1999. Developmental microbial ecology of the neonatal gastrointestinal tract. *Am J Clin Nutr* 69: 1035S-45S

66. Kelly CJ, Zheng L, Campbell EL, Saeedi B, Scholz CC, Bayless AJ, Wilson KE, Glover LE, Kominsky DJ, Magnuson A, Weir TL, Ehrentraut SF, Pickel C, Kuhn KA, Lanis JM, Nguyen V, Taylor CT, Colgan SP. 2015. Crosstalk between Microbiota-Derived Short-Chain Fatty Acids and Intestinal Epithelial HIF Augments Tissue Barrier Function. *Cell Host Microbe* 17: 662-71

67. Rigottier-Gois L. 2013. Dysbiosis in inflammatory bowel diseases: the oxygen hypothesis. *ISME J* 7: 1256-61

68. Rivera-Chavez F, Lopez CA, Baumler AJ. 2017. Oxygen as a driver of gut dysbiosis. *Free Radic Biol Med* 105: 93-101

69. Litvak Y, Byndloss MX, Tsolis RM, Baumler AJ. 2017. Dysbiotic Proteobacteria expansion: a microbial signature of epithelial dysfunction. *Curr Opin Microbiol* 39: 1-6

70. Litvak Y, Byndloss MX, Baumler AJ. 2018. Colonocyte metabolism shapes the gut microbiota. *Science* 362

71. Shin NR, Whon TW, Bae JW. 2015. Proteobacteria: microbial signature of dysbiosis in gut microbiota. *Trends Biotechnol* 33: 496-503

72. Dubinkina VB, Tyakht AV, Odintsova VY, Yarygin KS, Kovarsky BA, Pavlenko AV, Ischenko DS, Popenko AS, Alexeev DG, Taraskina AY, Nasyrova RF, Krupitsky EM, Shalikiani NV, Bakulin IG, Shcherbakov PL, Skorodumova LO, Larin AK, Kostryukova ES, Abdulkhakov RA, Abdulkhakov SR, Malanin SY, Ismagilova RK, Grigoryeva TV, Ilina EN, Govorun VM. 2017. Links of gut microbiota composition with alcohol dependence syndrome and alcoholic liver disease. *Microbiome* 5: 141

73. Vollaard EJ, Clasener HA, Janssen AJ. 1992. Co-trimoxazole impairs colonization resistance in healthy volunteers. *J Antimicrob Chemother* 30: 685-91

74. Wang Z, Wang Q, Wang X, Zhu L, Chen J, Zhang B, Chen Y, Yuan Z. 2019. Gut microbial dysbiosis is associated with development and progression of radiation enteritis during pelvic radiotherapy. *J Cell Mol Med* 23: 3747-56

75. Pham TA, Clare S, Goulding D, Arasteh JM, Stares MD, Browne HP, Keane JA, Page AJ, Kumasaka N, Kane L, Mottram L, Harcourt K, Hale C, Arends MJ, Gaffney DJ, Sanger Mouse Genetics P, Dougan G, Lawley TD. 2014. Epithelial IL-22RA1-mediated fucosylation promotes intestinal colonization resistance to an opportunistic pathogen. *Cell Host Microbe* 16: 504-16

76. Mueller S, Saunier K, Hanisch C, Norin E, Alm L, Midtvedt T, Cresci A, Silvi S, Orpianesi C, Verdenelli MC, Clavel T, Koebnick C, Zunft HJ, Dore J, Blaut M. 2006. Differences in fecal microbiota in different European study populations in relation to age, gender, and country: a cross-sectional study. *Appl Environ Microbiol* 72: 1027-33

77. Frank DN, St Amand AL, Feldman RA, Boedeker EC, Harpaz N, Pace NR. 2007. Molecular-phylogenetic characterization of microbial community imbalances in human inflammatory bowel diseases. *Proceedings of the National Academy of Sciences of the United States of America* 104: 13780-5

78. Arthur JC, Perez-Chanona E, Muhlbauer M, Tomkovich S, Uronis JM, Fan TJ, Campbell BJ, Abujamel T, Dogan B, Rogers AB, Rhodes JM, Stintzi A, Simpson KW, Hansen JJ, Keku TO, Fodor AA, Jobin C. 2012. Intestinal inflammation targets cancer-inducing activity of the microbiota. *Science* 338: 120-3

79. Normann E, Fahlen A, Engstrand L, Lilja HE. 2013. Intestinal microbial profiles in extremely preterm infants with and without necrotizing enterocolitis. *Acta paediatrica* 102: 129-36

80. Vujkovic-Cvijin I, Dunham RM, Iwai S, Maher MC, Albright RG, Broadhurst MJ, Hernandez RD, Lederman MM, Huang Y, Somsouk M, Deeks SG, Hunt PW, Lynch SV, McCune JM. 2013. Dysbiosis of the gut microbiota is associated with HIV disease progression and tryptophan catabolism. *Sci Transl Med* 5: 193ra91

81. Fredricks DN. 2019. The gut microbiota and graft-versus-host disease. *J Clin Invest* 129: 1808-17

82. Braun T, Di Segni A, BenShoshan M, Asaf R, Squires JE, Farage Barhom S, Glick Saar E, Cesarkas K, Smollan G, Weiss B, Amit S, Keller N, Haberman Y. 2017. Fecal microbial characterization of hospitalized patients with suspected infectious diarrhea shows significant dysbiosis. *Sci Rep* 7: 1088

83. Krogius-Kurikka L, Lyra A, Malinen E, Aarnikunnas J, Tuimala J, Paulin L, Makivuokko H, Kajander K, Palva A. 2009. Microbial community analysis reveals high level phylogenetic alterations in the overall gastrointestinal microbiota of diarrhoea-predominant irritable bowel syndrome sufferers. *BMC gastroenterology* 9: 95

84. Carroll IM, Ringel-Kulka T, Siddle JP, Ringel Y. 2012. Alterations in composition and diversity of the intestinal microbiota in patients with diarrhea-predominant irritable bowel syndrome. *Neurogastroenterology and motility : the official journal of the European Gastrointestinal Motility Society* 24: 521-30, e248

85. Hughes ER, Winter MG, Duerkop BA, Spiga L, Furtado de Carvalho T, Zhu W, Gillis CC, Buttner L, Smoot MP, Behrendt CL, Cherry S, Santos RL, Hooper LV, Winter SE. 2017. Microbial Respiration and Formate Oxidation as Metabolic Signatures of Inflammation-Associated Dysbiosis. *Cell Host Microbe* 21: 208-19

86. Cevallos SA, Lee JY, Tiffany CR, Byndloss AJ, Johnston L, Byndloss MX, Baumler AJ. 2019. Increased Epithelial Oxygenation Links Colitis to an Expansion of Tumorigenic Bacteria. *MBio* 10

87. Byndloss MX, Olsan EE, Rivera-Chávez F, Tiffany CR, Cevallos SA, Lokken KL, Torres TP, Byndloss AJ, Faber F, Gao Y, Litvak Y, Lopez CA, Xu G, Napoli E, Giulivi C, Tsolis RM, Revzin A, Lebrilla CB, Bäumler AJ. 2017. Microbiota-activated PPAR-g signaling inhibits dysbiotic Enterobacteriaceae expansion. *Science* 357: 570-5

88. Rivera-Chavez F, Zhang LF, Faber F, Lopez CA, Byndloss MX, Olsan EE, Xu G, Velazquez EM, Lebrilla CB, Winter SE, Baumler AJ. 2016. Depletion of Butyrate-Producing Clostridia from the Gut Microbiota Drives an Aerobic Luminal Expansion of Salmonella. *Cell Host Microbe* 19: 443-54

89. Lopez CA, Miller BM, Rivera-Chávez F, Velazquez EM, Byndloss MX, Chávez-Arroyo A, Lokken KL, Tsolis RM, Winter SE, Bäumler AJ. 2016. Virulence factors enhance Citrobacter rodentium expansion through aerobic respiration. *Science* 353: 1249-53

90. Winter SE, Winter MG, Xavier MN, Thiennimitr P, Poon V, Keestra AM, Laughlin RC, Gomez G, Wu J, Lawhon SD, Popova IE, Parikh SJ, Adams LG, Tsolis RM, Stewart VJ, Baumler AJ. 2013. Host-derived nitrate boosts growth of E. coli in the inflamed gut. *Science* 339: 708-11

91. Lopez CA, Winter SE, Rivera-Chavez F, Xavier MN, Poon V, Nuccio SP, Tsolis RM, Baumler AJ. 2012. Phage-mediated acquisition of a type III secreted effector protein boosts growth of salmonella by nitrate respiration. *MBio* 3

92. Lopez CA, Rivera-Chavez F, Byndloss MX, Baumler AJ. 2015. The Periplasmic Nitrate Reductase NapABC Supports Luminal Growth of Salmonella enterica Serovar Typhimurium during Colitis. *Infect Immun* 83: 3470-8

93. McLaughlin PA, Bettke JA, Tam JW, Leeds J, Bliska JB, Butler BP, van der Velden AWM. 2019. Inflammatory monocytes provide a niche for Salmonella expansion in the lumen of the inflamed intestine. *PLoS Pathog* 15: e1007847

94. Thursby E, Juge N. 2017. Introduction to the human gut microbiota. *Biochem J* 474: 1823-36

95. Byndloss MX, Baumler AJ. 2018. The germ-organ theory of non-communicable diseases. *Nat Rev Microbiol* 16: 103-10

96. Carson D, Barry R, Hopkins EGD, Roumeliotis TI, Garcia-Weber D, Mullineaux-Sanders C, Elinav E, Arrieumerlou C, Choudhary JS, Frankel G. 2019. Citrobacter rodentium induces rapid and unique metabolic and inflammatory responses in mice suffering from severe disease. *Cell Microbiol*: e13126

97. Gillis CC, Winter MG, Chanin RB, Zhu W, Spiga L, Winter SE. 2019. Host-Derived Metabolites Modulate Transcription of Salmonella Genes Involved in l-Lactate Utilization during Gut Colonization. *Infect Immun* 87

98. Gillis CC, Hughes ER, Spiga L, Winter MG, Zhu W, Furtado de Carvalho T, Chanin RB, Behrendt CL, Hooper LV, Santos RL, Winter SE. 2018. Dysbiosis-Associated Change in Host Metabolism Generates Lactate to Support Salmonella Growth. *Cell Host Microbe* 23: 54-64 e6

99. Rivera-Chavez F, Mekalanos JJ. 2019. Cholera toxin promotes pathogen acquisition of host-derived nutrients. *Nature* 572: 244-8

100. Roediger WE. 1980. The colonic epithelium in ulcerative colitis: an energy-deficiency disease? *Lancet* 2: 712-5

101. Dubuquoy L, Jansson EA, Deeb S, Rakotobe S, Karoui M, Colombel JF, Auwerx J, Pettersson S, Desreumaux P. 2003. Impaired expression of peroxisome proliferator-activated receptor gamma in ulcerative colitis. *Gastroenterology* 124: 1265-76

102. Azad Khan AK, Piris J, Truelove SC. 1977. An experiment to determine the active therapeutic moiety of sulphasalazine. *Lancet* 2: 892-5

103. Iacucci M, de Silva S, Ghosh S. 2010. Mesalazine in inflammatory bowel disease: a trendy topic once again? *Can J Gastroenterol* 24: 127-33

104. Criscuoli V, Modesto I, Orlando A, Cottone M. 2013. Mesalazine for the treatment of inflammatory bowel disease. *Expert Opin Pharmacother* 14: 1669-78

105. Rousseaux C, El-Jamal N, Fumery M, Dubuquoy C, Romano O, Chatelain D, Langlois A, Bertin B, Buob D, Colombel JF, Cortot A, Desreumaux P, Dubuquoy L. 2013. The 5-aminosalicylic acid antineoplastic effect in the intestine is mediated by PPARgamma. *Carcinogenesis* 34: 2580-6

106. Giralt A, Hondares E, Villena JA, Ribas F, Diaz-Delfin J, Giralt M, Iglesias R, Villarroya F. 2011. Peroxisome proliferator-activated receptor-gamma coactivator-1alpha controls transcription of the Sirt3 gene, an essential component of the thermogenic brown adipocyte phenotype. *J Biol Chem* 286: 16958-66

107. Finley LW, Haas W, Desquiret-Dumas V, Wallace DC, Procaccio V, Gygi SP, Haigis MC. 2011. Succinate dehydrogenase is a direct target of sirtuin 3 deacetylase activity. *PLoS One* 6: e23295

108. Hirschey MD, Shimazu T, Goetzman E, Jing E, Schwer B, Lombard DB, Grueter CA, Harris C, Biddinger S, Ilkayeva OR, Stevens RD, Li Y, Saha AK, Ruderman NB, Bain JR, Newgard CB, Farese RV, Jr., Alt FW, Kahn CR, Verdin E. 2010. SIRT3 regulates mitochondrial fatty-acid oxidation by reversible enzyme deacetylation. *Nature* 464: 121-5

109. Ahn BH, Kim HS, Song S, Lee IH, Liu J, Vassilopoulos A, Deng CX, Finkel T. 2008. A role for the mitochondrial deacetylase Sirt3 in regulating energy homeostasis. *Proc Natl Acad Sci U S A* 105: 14447-52

110. Xu J, Chen N, Wu Z, Song Y, Zhang Y, Wu N, Zhang F, Ren X, Liu Y. 2018. 5-Aminosalicylic Acid Alters the Gut Bacterial Microbiota in Patients With Ulcerative Colitis. *Front Microbiol* 9: 1274

111. Johansson ME, Phillipson M, Petersson J, Velcich A, Holm L, Hansson GC. 2008. The inner of the two Muc2 mucin-dependent mucus layers in colon is devoid of bacteria. *Proc Natl Acad Sci U S A* 105: 15064-9

112. Johansson ME, Gustafsson JK, Holmen-Larsson J, Jabbar KS, Xia L, Xu H, Ghishan FK, Carvalho FA, Gewirtz AT, Sjovall H, Hansson GC. 2014. Bacteria penetrate the normally impenetrable inner colon mucus layer in both murine colitis models and patients with ulcerative colitis. *Gut* 63: 281-91

113. van der Post S, Jabbar KS, Birchenough G, Arike L, Akhtar N, Sjovall H, Johansson MEV, Hansson GC. 2019. Structural weakening of the colonic mucus barrier is an early event in ulcerative colitis pathogenesis. *Gut*

114. Li H, Limenitakis JP, Fuhrer T, Geuking MB, Lawson MA, Wyss M, Brugiroux S, Keller I, Macpherson JA, Rupp S, Stolp B, Stein JV, Stecher B, Sauer U, McCoy KD, Macpherson AJ. 2015. The outer mucus layer hosts a distinct intestinal microbial niche. *Nat Commun* 6: 8292

115. Albenberg L, Esipova TV, Judge CP, Bittinger K, Chen J, Laughlin A, Grunberg S, Baldassano RN, Lewis JD, Li H, Thom SR, Bushman FD, Vinogradov SA, Wu GD. 2014. Correlation between intraluminal oxygen gradient and radial partitioning of intestinal microbiota. *Gastroenterology* 147: 1055-63 e8

116. Matziouridou C, Rocha SDC, Haabeth OA, Rudi K, Carlsen H, Kielland A. 2018. iNOS- and NOX1-dependent ROS production maintains bacterial homeostasis in the ileum of mice. *Mucosal Immunol* 11: 774-84

117. Aviello G, Singh AK, O'Neill S, Conroy E, Gallagher W, D'Agostino G, Walker AW, Bourke B, Scholz D, Knaus UG. 2019. Colitis susceptibility in mice with reactive oxygen species deficiency is mediated by mucus barrier and immune defense defects. *Mucosal Immunol* 12: 1316-26

118. Schwerd T, Bryant RV, Pandey S, Capitani M, Meran L, Cazier JB, Jung J, Mondal K, Parkes M, Mathew CG, Fiedler K, McCarthy DJ, Consortium WGS, Oxford IBDcsi, investigators CiIg, Consortium UIG, Sullivan PB, Rodrigues A, Travis SPL, Moore C, Sambrook J, Ouwehand WH, Roberts DJ, Danesh J, Study I, Russell RK, Wilson DC, Kelsen JR, Cornall R, Denson LA, Kugathasan S, Knaus UG, Serra EG, Anderson CA, Duerr RH, McGovern DP, Cho J, Powrie F, Li VS, Muise AM, Uhlig HH. 2018. NOX1 loss-of-function genetic variants in patients with inflammatory bowel disease. *Mucosal Immunol* 11: 562-74

119. Johansson ME, Sjovall H, Hansson GC. 2013. The gastrointestinal mucus system in health and disease. *Nat Rev Gastroenterol Hepatol* 10: 352-61

120. Cullender TC, Chassaing B, Janzon A, Kumar K, Muller CE, Werner JJ, Angenent LT, Bell ME, Hay AG, Peterson DA, Walter J, Vijay-Kumar M, Gewirtz AT, Ley RE. 2013. Innate and

adaptive immunity interact to quench microbiome flagellar motility in the gut. *Cell Host Microbe* 14: 571-81

121. Salzman NH, Hung K, Haribhai D, Chu H, Karlsson-Sjoberg J, Amir E, Teggatz P, Barman M, Hayward M, Eastwood D, Stoel M, Zhou Y, Sodergren E, Weinstock GM, Bevins CL, Williams CB, Bos NA. 2010. Enteric defensins are essential regulators of intestinal microbial ecology. *Nat Immunol* 11: 76-83

122. Vaishnava S, Yamamoto M, Severson KM, Ruhn KA, Yu X, Koren O, Ley R, Wakeland EK, Hooper LV. 2011. The antibacterial lectin RegIIIgamma promotes the spatial segregation of microbiota and host in the intestine. *Science* 334: 255-8

123. Bevins CL, Stange EF, Wehkamp J. 2009. Decreased Paneth cell defensin expression in ileal Crohn's disease is independent of inflammation, but linked to the NOD2 1007fs genotype. *Gut* 58: 882-3; discussion 3-4

124. Wehkamp J, Salzman NH, Porter E, Nuding S, Weichenthal M, Petras RE, Shen B, Schaeffeler E, Schwab M, Linzmeier R, Feathers RW, Chu H, Lima H, Jr., Fellermann K, Ganz T, Stange EF, Bevins CL. 2005. Reduced Paneth cell alpha-defensins in ileal Crohn's disease. *Proc Natl Acad Sci U S A* 102: 18129-34

125. Wehkamp J, Harder J, Weichenthal M, Schwab M, Schaffeler E, Schlee M, Herrlinger KR, Stallmach A, Noack F, Fritz P, Schroder JM, Bevins CL, Fellermann K, Stange EF. 2004. NOD2 (CARD15) mutations in Crohn's disease are associated with diminished mucosal alpha-defensin expression. *Gut* 53: 1658-64

126. Darfeuille-Michaud A, Boudeau J, Bulois P, Neut C, Glasser AL, Barnich N, Bringer MA, Swidsinski A, Beaugerie L, Colombel JF. 2004. High prevalence of adherent-invasive Escherichia coli associated with ileal mucosa in Crohn's disease. *Gastroenterology* 127: 412-21

127. Salzman NH, Bevins CL. 2013. Dysbiosis--a consequence of Paneth cell dysfunction. *Semin Immunol* 25: 334-41

128. Nadjsombati MS, McGinty JW, Lyons-Cohen MR, Jaffe JB, DiPeso L, Schneider C, Miller CN, Pollack JL, Nagana Gowda GA, Fontana MF, Erle DJ, Anderson MS, Locksley RM, Raftery D, von Moltke J. 2018. Detection of Succinate by Intestinal Tuft Cells Triggers a Type 2 Innate Immune Circuit. *Immunity* 49: 33-41 e7

129. Morita N, Umemoto E, Fujita S, Hayashi A, Kikuta J, Kimura I, Haneda T, Imai T, Inoue A, Mimuro H, Maeda Y, Kayama H, Okumura R, Aoki J, Okada N, Kida T, Ishii M, Nabeshima R, Takeda K. 2019. GPR31-dependent dendrite protrusion of intestinal CX3CR1(+) cells by bacterial metabolites. *Nature* 566: 110-4

130. Miller CA, 3rd. 1997. Expression of the human aryl hydrocarbon receptor complex in yeast. Activation of transcription by indole compounds. *The Journal of biological chemistry* 272: 32824-9

131. Heath-Pagliuso S, Rogers WJ, Tullis K, Seidel SD, Cenijn PH, Brouwer A, Denison MS. 1998. Activation of the Ah receptor by tryptophan and tryptophan metabolites. *Biochemistry* 37: 11508-15

132. Zelante T, Iannitti RG, Cunha C, De Luca A, Giovannini G, Pieraccini G, Zecchi R, D'Angelo C, Massi-Benedetti C, Fallarino F, Carvalho A, Puccetti P, Romani L. 2013. Tryptophan catabolites from microbiota engage aryl hydrocarbon receptor and balance mucosal reactivity via interleukin-22. *Immunity* 39: 372-85

133. Monteleone I, Rizzo A, Sarra M, Sica G, Sileri P, Biancone L, MacDonald TT, Pallone F, Monteleone G. 2011. Aryl hydrocarbon receptor-induced signals up-regulate IL-22 production and inhibit inflammation in the gastrointestinal tract. *Gastroenterology* 141: 237-48, 48 e1

134. Fukumoto S, Toshimitsu T, Matsuoka S, Maruyama A, Oh-Oka K, Takamura T, Nakamura Y, Ishimaru K, Fujii-Kuriyama Y, Ikegami S, Itou H, Nakao A. 2014. Identification of a probiotic bacteria-derived activator of the aryl hydrocarbon receptor that inhibits colitis. *Immunology and cell biology*

135. Arpaia N, Campbell C, Fan X, Dikiy S, van der Veeken J, deRoos P, Liu H, Cross JR, Pfeffer K, Coffer PJ, Rudensky AY. 2013. Metabolites produced by commensal bacteria promote peripheral regulatory T-cell generation. *Nature* 504: 451-5

136. Atarashi K, Tanoue T, Shima T, Imaoka A, Kuwahara T, Momose Y, Cheng G, Yamasaki S, Saito T, Ohba Y, Taniguchi T, Takeda K, Hori S, Ivanov, II, Umesaki Y, Itoh K, Honda K. 2011. Induction of colonic regulatory T cells by indigenous Clostridium species. *Science* 331: 337-41

137. Furusawa Y, Obata Y, Fukuda S, Endo TA, Nakato G, Takahashi D, Nakanishi Y, Uetake C, Kato K, Kato T, Takahashi M, Fukuda NN, Murakami S, Miyauchi E, Hino S, Atarashi K, Onawa S, Fujimura Y, Lockett T, Clarke JM, Topping DL, Tomita M, Hori S, Ohara O, Morita T, Koseki H, Kikuchi J, Honda K, Hase K, Ohno H. 2013. Commensal microbe-derived butyrate induces the differentiation of colonic regulatory T cells. *Nature* 504: 446-50

138. Smith PM, Howitt MR, Panikov N, Michaud M, Gallini CA, Bohlooly YM, Glickman JN, Garrett WS. 2013. The microbial metabolites, short-chain fatty acids, regulate colonic Treg cell homeostasis. *Science* 341: 569-73

139. Singh N, Gurav A, Sivaprakasam S, Brady E, Padia R, Shi H, Thangaraju M, Prasad PD, Manicassamy S, Munn DH, Lee JR, Offermanns S, Ganapathy V. 2014. Activation of Gpr109a, receptor for niacin and the commensal metabolite butyrate, suppresses colonic inflammation and carcinogenesis. *Immunity* 40: 128-39

140. Alex S, Lange K, Amolo T, Grinstead JS, Haakonsson AK, Szalowska E, Koppen A, Mudde K, Haenen D, Al-Lahham S, Roelofsen H, Houtman R, van der Burg B, Mandrup S, Bonvin AM,

Kalkhoven E, Muller M, Hooiveld GJ, Kersten S. 2013. Short-chain fatty acids stimulate angiopoietin-like 4 synthesis in human colon adenocarcinoma cells by activating peroxisome proliferator-activated receptor gamma. *Mol Cell Biol* 33: 1303-16

141. Chang PV, Hao L, Offermanns S, Medzhitov R. 2014. The microbial metabolite butyrate regulates intestinal macrophage function via histone deacetylase inhibition. *Proc Natl Acad Sci U S A* 111: 2247-52

142. Hooper LV, Gordon JI. 2001. Commensal host-bacterial relationships in the gut. *Science* 292: 1115-8

143. Human Microbiome Project C. 2012. Structure, function and diversity of the healthy human microbiome. *Nature* 486: 207-14

144. Integrative HMPRNC. 2019. The Integrative Human Microbiome Project. *Nature* 569: 641-8

145. Proctor L. 2019. Priorities for the next 10 years of human microbiome research. *Nature* 569: 623-5

146. Tipton L, Darcy JL, Hynson NA. 2019. A Developing Symbiosis: Enabling Cross-Talk Between Ecologists and Microbiome Scientists. *Front Microbiol* 10: 292

147. Foster KR, Schluter J, Coyte KZ, Rakoff-Nahoum S. 2017. The evolution of the host microbiome as an ecosystem on a leash. *Nature* 548: 43-51

148. Byndloss MX, Pernitzsch SR, Baumler AJ. 2018. Healthy hosts rule within: ecological forces shaping the gut microbiota. *Mucosal Immunol*

149. Mills EL, Kelly B, O'Neill LAJ. 2017. Mitochondria are the powerhouses of immunity. *Nat Immunol* 18: 488-98

150. Quie PG. 1986. Lung defense against infection. *J Pediatr* 108: 813-6

151. Borges S, Silva J, Teixeira P. 2014. The role of lactobacilli and probiotics in maintaining vaginal health. *Arch Gynecol Obstet* 289: 479-89

152. Johansson ME, Gustafsson JK, Sjoberg KE, Petersson J, Holm L, Sjovall H, Hansson GC. 2010. Bacteria penetrate the inner mucus layer before inflammation in the dextran sulfate colitis model. *PLoS One* 5: e12238

153. Colomer V, Lal K, Hoops TC, Rindler MJ. 1994. Exocrine granule specific packaging signals are present in the polypeptide moiety of the pancreatic granule membrane protein GP2 and in amylase: implications for protein targeting to secretory granules. *EMBO J* 13: 3711-9

154. Yu S, Lowe AW. 2009. The pancreatic zymogen granule membrane protein, GP2, binds Escherichia coli Type 1 fimbriae. *BMC Gastroenterol* 9: 58

Table 1.1: Habitat filters of microbiota-nourishing immunity

Organ	Habitat filter	Functional category	Weakening is associated with	References
Lower respiratory tract	Mucus escalator	Reducing community size	Cystic fibrosis; opportunistic infections with *Staphylococcus aureus*, or *Pseudomonas aeruginosa*	(150)
Female reproductive tract	Glycogen catabolism by α-amylase	Shaping the microbiota composition	Reduced abundance of *Lactobacillus*, vaginosis	(43, 151)
Upper gastrointestinal tract	Hydrochloric acid secretion by parietal cells	Reducing community size	Small intestinal bacterial overgrowth (SIBO)	(20)
	Pancreatic secretions			(21-24)
	Peristalsis			(25)
	Immunoglobulin			(26)

	Defensin secretion by Paneth cells	Maintaining the spatial organization of microbial communities	Ileal Crohn's disease	(123, 125)
	Epithelial release of REGIIIγ		Increased bacterial colonization of the intestinal epithelial surface	(122)
	TLR5-dependent IgA production		Increased bacterial motility and mucus penetration	(120)
Large intestine	Epithelial hypoxia	Shaping the microbiota composition	Dysbiosis characterized by *Proteobacteria* expansion	(69, 70)
	Milk oligo-saccharides		Absence of species consuming milk oligo-saccharides	(63, 64)
	Mucus polysaccharide		Defect in retaining *Bacteroidiaceae* during fiber-starvation	(55-57)
	Inner mucus layer	Maintaining the spatial	Bacterial penetration into	(111, 112, 152)

		organization of microbial communities	the crypts; ulcerative colitis	
	Epithelial release of NOX1-derived hydrogen peroxide		Bacterial penetration into the crypts; early-onset ulcerative colitis	(117, 118)
	Oxygen gradient		Accumulation of oxygen tolerant species at the mucosal surface	(115)

Figures

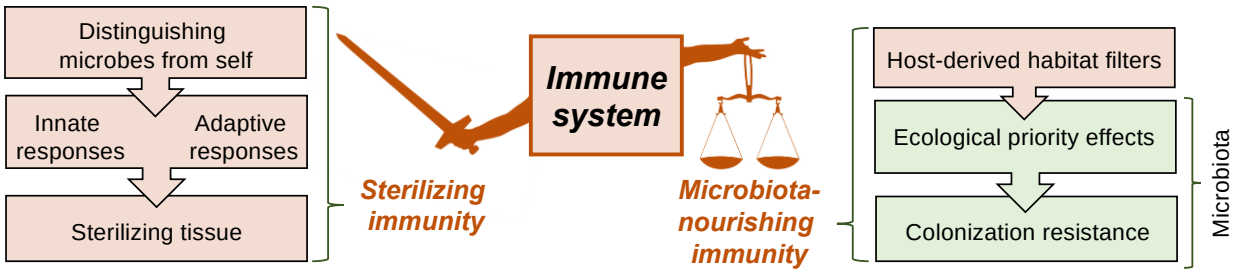

Figure 1.1: Immune responses that maintain the sanctity of our tissue differ from those balancing microbial communities on body surfaces. Sterilizing immunity is an arm of the immune system that functions in distinguishing microbes from self and eliciting responses to remove microbial intruders from tissue. In contrast, balancing microbial communities on body surfaces is not aimed at detecting and removing the microbiota. Instead, habitat filters of our immune system balance microbial communities by picking microbial attributes that enable growth and survival in the host. Habitat filters and the microbiota form a host microbe chimera, termed microbiota-nourishing immunity, which uses ecological priority effects to confer colonization resistance against pathogens, a non-specific immune function.

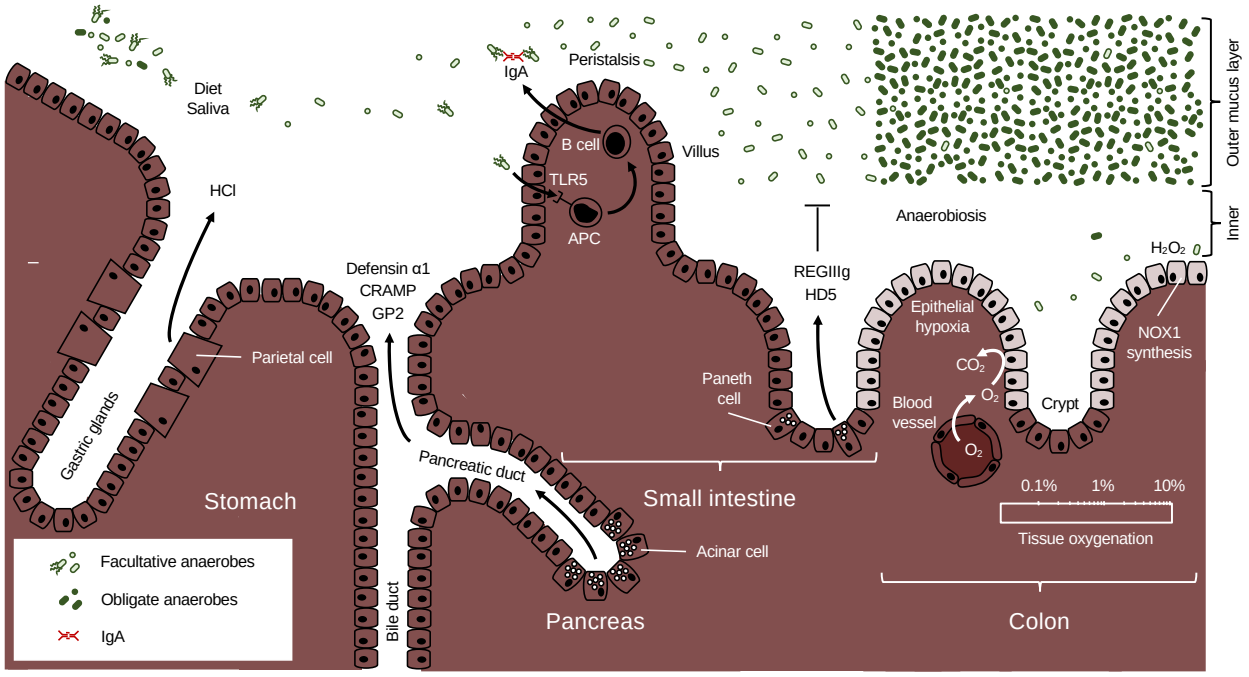

Figure 1.2: Habitat filters controlling microbial communities in the gastrointestinal tract. Microbes entering the stomach are decimated by gastric acid (HCl), which reduces the community size. Pancreatic juice contains additional antimicrobials that control the microbial community size, including glycoprotein 2 (GP2) and defensin α1 in humans and cathelicidin-related antimicrobial peptide (CRAMP) in the mouse. GP2, defensin α1 and CRAMP are excreted by pancreatic acinar cells and transport along ductal epithelium into the small intestine. GP2 that binds surface appendages of *E. coli* (153, 154). Reduced pancreatic levels of CRAMP trigger small intestinal bacterial outgrowth and dysbiosis in mice (23). Motile bacteria that venture close to the mucosal surface elicit a TLR5-dependent production of anti-flagellin IgA by B cells, which reduces flagella expression by the microbiota to protect the epithelial surface (120). Epithelial release of REGIIIγ and human defensin α 5 (HD5) provide additional help to protects the epithelial surface of the small intestine (122, 123, 125). Peristalsis ensures contents move swiftly into the large intestine without providing excessive time for bacterial cell division. Once in the large intestine, host control over the size of microbial communities is muted, leading to a steep rise in bacterial density. Epithelial hypoxia helps maintain anaerobiosis, thereby shaping the microbiota composition in the colon to be dominated by obligate anaerobic bacteria (87). Constitutive NOX1 synthesis in colonic epithelial cells generates a hydrogen

peroxide gradient that might contribute to a spatial heterogeneity of the microbiota. PC, antigen presenting cell.

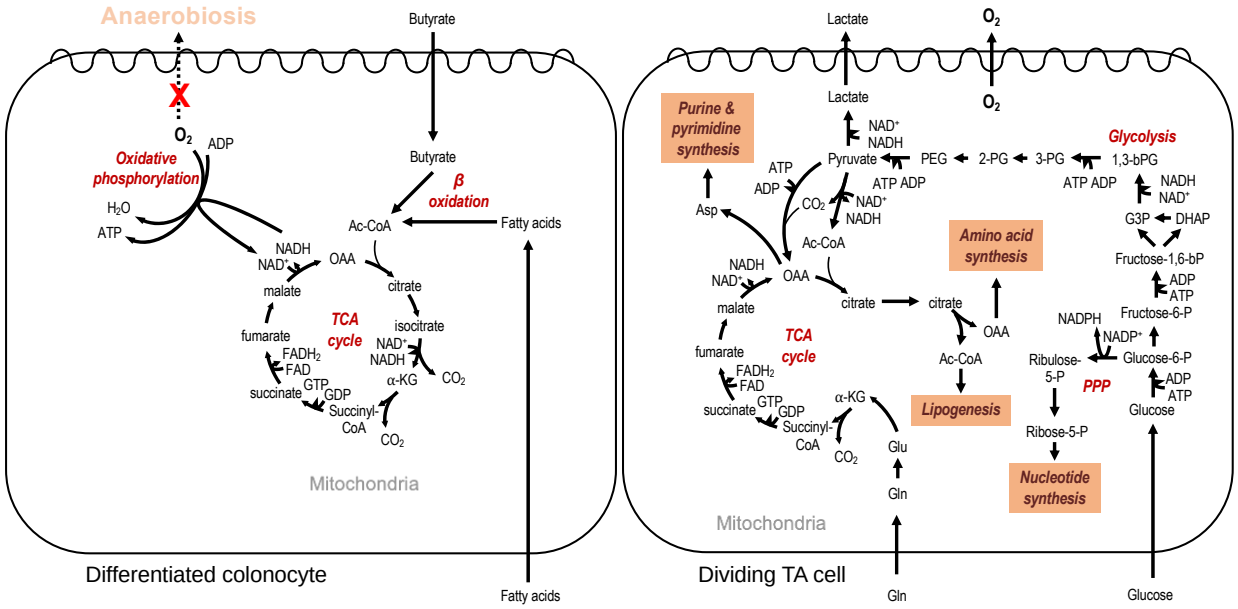

Figure 1.3: Epithelial metabolism shapes the habitat of the colonic microbiota. The schematic on the left depicts the energy metabolism of differentiated colonic epithelial cells (colonocytes), which catabolize fatty acids and microbiota-derived butyrate using β oxidation, the tricarboxylic acid (TCA) cycle and oxidative phosphorylation in the mitochondria. Elevated mitochondrial bioenergetics result in high mitochondrial oxygen consumption, thus limiting the amount of oxygen (O_2) diffusing into the intestinal lumen, which helps maintain anaerobiosis in the lumen. The schematic on the right depicts the metabolism of dividing transit-amplifying (TA) cells, which obtain energy during conversion of glucose into lactate (aerobic glycolysis) through substrate level phosphorylation. Lactate generated during aerobic glycolysis is released into the intestinal lumen. A fraction of glucose is metabolized through the pentose phosphate pathway (PPP) to synthesize nucleotides for cell division. To support cell division, TCA cycle intermediates are exported from the mitochondria into the cytosol to synthesize amino acids, lipids, purines and pyrimidines. Glutamine (Gln) and pyruvate are used in anaplerotic reactions to replenish TCA cycle intermediates that have been extracted for biosynthesis. Reduced mitochondrial bioenergetics result in increased epithelial oxygenation, thereby disrupting anaerobiosis in the intestinal lumen. OAA, oxaloacetate; α-KG, α-ketoglutarate; Ac-CoA, acetyl-coenzyme A; H_2O, water; CO_2, carbon dioxide; NO,

nitric oxide; NO_3^-, nitrate; ADP, adenosine diphosphate; ATP, adenosine triphosphate; NAD^+/NADH, nicotinamide adenine dinucleotide redox pair; Asp, aspartate; Glu, glutamate; Gln, glutamine; G3P, glyceraldehyde 3-phosphate ; DHAP, dihydroxyacetone phosphate; 1.3-bPG, 1,3-bisphosphateglycerate; 3-PG, 3-phosphoglycerate ; 2-PG, 2-phosphoglycerate ; PEG, phosphoenolpyruvate.

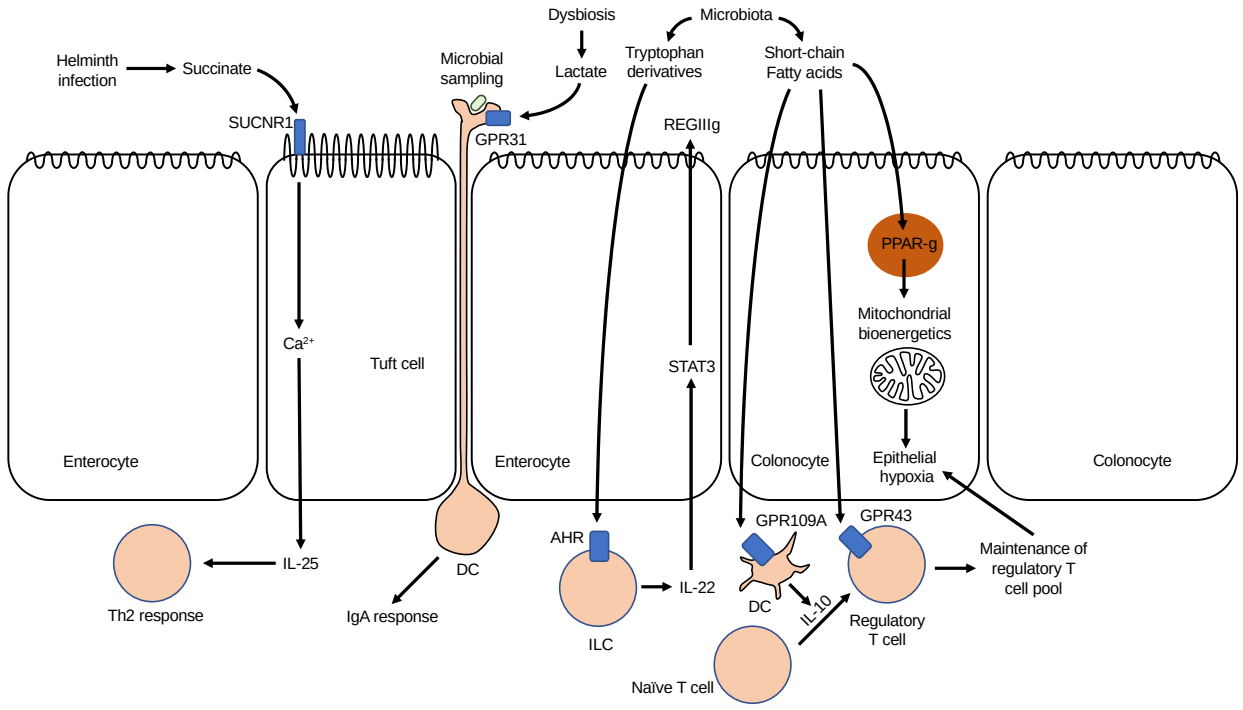

Figure 1.4: Control of habitat filters by metabolites. The schematic illustrates how receptors for succinate (SUCNR1), lactate (GPR31), tryptophan-derivatives (AHR) and short-chain fatty acids (GPR109A, GPR43 and PPAR-γ) orchestrate habitat filtering through the induction of Th2 responses, IgA responses, epithelial release of REGIIIγ and maintenance of epithelial hypoxia, respectively.

Chapter 2

Virulence factors enhance *Citrobacter rodentium* expansion through aerobic respiration

Christopher A. Lopez[1], Brittany M. Miller[1], Fabian Rivera-Chávez[1], Eric Velazquez[1], Mariana X. Byndloss[1], Alfredo Chávez-Arroyo[1], Kristen L. Lokken[1], Renée M. Tsolis[1], Sebastian E. Winter[2], Andreas J. Bäumler[1,*]

Short Title: Virulence factors drive aerobic pathogen expansion

Affiliations:

[1] Department of Medical Microbiology and Immunology, School of Medicine, University of California, Davis, One Shields Avenue, Davis, CA, USA.

[2] Department of Microbiology, University of Texas Southwestern Medical Center, 5323 Harry Hines Blvd, Dallas, TX, USA.

Published in:

Lopez CA, Miller BM, Rivera-Chávez F, Velazquez E, Byndloss MX, Chávez-Arroyo A, et al. (2016) Virulence factors enhance *Citrobacter rodentium* expansion through aerobic respiration. Science 353(6305): 1249-53. DOI: 10.1126/science.aag3042

Statement of Author Contribution:

The main contributor of figures to this paper was the first author, CAL. BMM aided in finding the discovery that hyperplasia and oxygen are linked. BMM began work after figure 2.1 was already created, and was responsible for the following:

BMM generated the *Citrobacter rodentium* mutants *cfcH*, *cfcH cydAB*, *espH cesF map*, and *espH cesF map cydAB*.

BMM and CAL together performed experiments for figures 2.2, 2.3, S2.8, and S2.11. BMM aided in mouse experiments by collecting fecal pellets, performing necropsies, and plating samples for CFU enumeration. BMM performed staining for fluorescent microscopy, as well as obtaining images used in quantification.

Abstract

Citrobacter rodentium uses a type III secretion system (T3SS) to induce colonic crypt hyperplasia in mice, thereby gaining an edge during its competition with the gut microbiota through an unknown mechanism. Here we show that by triggering colonic crypt hyperplasia, the *C. rodentium* T3SS induced an excessive expansion of undifferentiated Ki67-positive epithelial cells, which increased oxygenation of the mucosal surface and drove an aerobic *C. rodentium* expansion in the colon. Treatment of mice with the γ-secretase inhibitor dibenzazepine to diminish Notch-driven colonic crypt hyperplasia curtailed the fitness advantage conferred by aerobic respiration during *C. rodentium* infection. We conclude that *C. rodentium* uses its T3SS to induce histopathological lesions that generate an intestinal microenvironment in which growth of the pathogen is fueled by aerobic respiration.

Attaching and effacing (AE) pathogens are defined by virulence characteristics encoded by a pathogenicity island known as the locus of enterocyte effacement (LEE) (*1, 2*), which contains genes encoding for a T3SS (*3*) and an adhesin termed intimin (*4*). The T3SS injects the intimin receptor Tir into the host cell cytosol (*5*), resulting in intimate attachment of bacteria to the effaced epithelial surface (*6*). The LEE encoded T3SS of the AE pathogen *C. rodentium* injects additional effector proteins that are required for causing transmissible colonic crypt hyperplasia in mice (*7, 8*) (**Fig. S2.1**). Following the development of colonic crypt hyperplasia, *C. rodentium* blooms in the lumen of the murine large bowel (*9*). The LEE encoded T3SS is required for this rapid luminal expansion possibly by allowing *C. rodentium* to compete with the microbiota for carbon sources, because the T3SS provides no benefit in germ-free mice (*10*). These data suggest that the T3SS places *C. rodentium* in a microenvironment that somehow provides a growth advantage during its competition with the resident microbiota, but it remains obscure which resources might become available in this niche to fuel pathogen expansion.

Electron acceptors, such as nitrate, are produced as a by-product of the inflammatory host response and boost luminal growth of pathogenic *Salmonella enterica* or commensal *Escherichia coli* by anaerobic respiration in mouse models of colitis (*11-13*). Since *C. rodentium* infection triggers colonic crypt hyperplasia, we wanted to determine whether the inflammatory host response would enable the pathogen to grow by anaerobic respiration. The respiratory reductases for nitrate, dimethyl sulfoxide (DMSO) and trimethylamine N-oxide (TMAO) as well as the formate dehydrogenases FdnGHI and FdoGHI contain a molybdopterin cofactor. Thus, to explore a possible role of anaerobic respiration during *C. rodentium* growth in the mouse gut, we constructed a *C. rodentium* mutant lacking a gene required for molybdopterin cofactor biosynthesis (*moaA* mutant) (**Fig. S2.2A**) (*14*). Mice (C57BL/6) were inoculated with an equal mixture of wild-type *C. rodentium* and an isogenic *moaA* mutant to compare the fitness of both strains. Mice developed intestinal inflammation as indicated by increased transcript levels of pro-inflammatory markers in the colonic mucosa (**Fig. S2.3A and S2.3B**). The *C. rodentium* wild type was recovered in significantly ($P < 0.05$) higher numbers than the *moaA* mutant (**Fig. 2.1A**). Similar results were observed

with genetically susceptible C3H/HeJ mice that experience more severe intestinal inflammation during *C. rodentium* infection (**Fig. S2.3C and S2.3D**). In contrast, when germ-free mice were inoculated with an equal mixture of the *C. rodentium* wild type and a *moaA* mutant, both strains were recovered in similar numbers (**Fig. 2.1B and S2.3E**), suggesting that either anaerobic respiration or the utilization of formate provided an edge during competition of the pathogen with the resident microbiota.

C. rodentium infection resulted in a markedly increased colonic expression of *Nos2* (**Fig. S2.3B and S2.3D**), the gene encoding inducible nitric oxide synthase (iNOS), an enzyme necessary for generating nitric oxide, which is converted to nitrate in the intestinal lumen (*11*). To determine whether nitrate respiration enhances growth, we constructed a mutant deficient for the three nitrate reductases encoded by *C. rodentium* (*narG napA narZ* mutant) (**Fig. S2.2B and S2.2F**). Remarkably, in mice inoculated with an equal mixture of the *C. rodentium* wild type and a *narG napA narZ* mutant, both strains were recovered in equal numbers from colon contents and feces (**Fig. 2.1A, S2.3C and S2.3E**), suggesting that nitrate respiration did not provide a fitness advantage.

We next examined the possibility that the phenotype of the *moaA* mutant was due to an inability to utilize formate as an electron donor rather than nitrate as an electron acceptor. Since formate dehydrogenases FdnGHI and FdoGHI can couple electron transfer from formate through the quinone pool to nitrate (*15*) or oxygen (*16*), respectively, we envisioned that analysis of this pathway would provide indirect information about the electron acceptor used by *C. rodentium* in the gut. To test whether the nitrate-dependent and/or the oxygen-dependent formate dehydrogenase contributed to growth of *C. rodentium* during colitis, mice were inoculated with an equal mixture of the *C. rodentium* wild type and either an *fdnG* mutant or *fdoG* mutant (**Fig. S2.2C and S2.2D**). Consistent with our observation that nitrate respiration did not contribute to fitness (**Fig. 2.1A**), inactivation of the nitrate-dependent *fdnG* did not reduce growth of *C. rodentium* (**Fig. 2.1B**). However, inactivation of the oxygen-dependent *fdoG* reduced fitness of *C. rodentium* in conventional (C57BL/6) mice ($P < 0.05$), while little benefit was observed in germ-free (Swiss Webster) mice (**Fig. 2.1B and S2.3E**). The finding that *fdoG* was required for pathogen expansion was

intriguing, because it suggested that *C. rodentium* might utilize oxygen as a terminal electron acceptor during luminal growth.

We thus wanted to test the hypothesis that aerobic respiration fuels *C. rodentium* growth during infection. To test this idea, we deleted the *C. rodentium cydAB* genes (**Fig. S2.2E**), which encode a high-affinity cytochrome *bd* oxidase required for aerobic respiration in microaerobic environments. *In vitro*, the *C. rodentium* wild type was recovered in higher numbers than the *cydAB* mutant when both strains were co-cultured under conditions mimicking hypoxia (1% O_2) or normal tissue oxygenation (4% or 8% O_2), but not under anaerobic conditions (0% O_2) or at atmospheric oxygen levels (21% O_2) (**Fig. 2.1C**). Next, we compared the fitness of the *C. rodentium* wild type and a *cydAB* mutant by infecting C57BL/6 mice with a 1:1 mixture of both strains. Remarkably, the *C. rodentium* wild type was recovered in 20,000-fold higher numbers ($P < 0.01$) than the *cydAB* mutant from colon contents seven days after infection (**Fig. 2.1D**), suggesting that aerobic respiration contributed to growth of the pathogen. Expression of *ler*, encoding the master regulator of T3SS synthesis, was reduced in the *cydAB* mutant, but this difference did not reach statistical significance (**Fig. S2.4A**). When infection with a 1:1 mixture of the *C. rodentium* wild type and a *cydAB* mutant was repeated in germ-free (Swiss Webster) mice, the fitness advantage provided by *cydAB* was greatly reduced (**Fig. 2.1D**). Collectively, these data suggested that aerobic respiration drove an uncontrolled luminal expansion of *C. rodentium* in an environment occupied by the gut microbiota.

To test whether tissue/mucus-associated bacteria have a respiratory metabolism compared to luminal bacteria, we investigated transcription of the *sucA* gene, which encodes a subunit of 2-ketoglutarate dehydrogenase, an enzyme required for the aerobic tricarboxylic acid (TCA) cycle. Under anaerobic conditions, SucA is no longer required as the normally cyclic TCA pathway switches to a non-cyclic series of reactions. Higher expression of *sucA* under aerobic than anaerobic conditions can serve as an indicator for a respiratory central metabolism (*17*). *C. rodentium sucA* was transcribed at significantly ($P < 0.05$) higher levels when bacteria were cultured *in vitro* under microaerobic conditions compared to anaerobic conditions (**Fig. 2.1E and S2.4B**). To investigate *sucA* expression *in vivo*, RNA was isolated from mucus

scrapings or colon contents of mice infected with *C. rodentium. C. rodentium* residing in close proximity to tissue (i.e. mucus scrapings) transcribed *sucA* at significantly ($P < 0.05$) higher levels than bacteria located in colon contents (**Fig. 2.1F and S2.4C**). These results provided further support for the idea that bacteria in close proximity to the mucosal surface had an oxidative metabolism *in vivo*.

Intestinal inflammation caused by *Salmonella enterica* drives a depletion of *Clostridia*, which in turn increases epithelial oxygenation (*18*). We thus wanted to determine whether *C. rodentium*-induced colonic crypt hyperplasia would increase oxygen availability in the gut by driving a depletion of *Clostridia.* The numbers of *C. rodentium* recovered from colon contents of mice infected with the *C. rodentium* wild type were 1,000-fold higher ($P < 0.05$) than those recovered from colon contents of mice infected with a *cydAB* mutant (**Fig. 2.1G**), which correlated with reduced colonic inflammation ($P < 0.05$) (**Fig. 2.1H and S2.5**). Consistent with a previous report (*9*), infection of mice with the *C. rodentium* wild type resulted in a shift in the microbial community structure (**Fig. 2.1I and S2.6**). The absolute abundances of members of the *Enterobacteriaceae* (**Fig. S2.7A**) and *Erythrobacteraceae* (**Fig. S2.7B**) were significantly ($P < 0.05$) increased in mice infected with the *C. rodentium* wild type, a shift in the community structure previously associated with increased oxygen availability in the gut (*19*). However, infection with the *C. rodentium* wild type resulted in an increased ($P < 0.05$) abundance of *Clostridia* (**Fig. 2.1I**), which was most pronounced for members of the *Lachnospiraceae* belonging to the genus *Dorea* (**Fig. S2.7C**) and the genus *Coprococcus* (**Fig. S2.7D**). These changes in the microbial population profile were reduced or absent in mice infected with a *cydAB* mutant (**Fig. 2.1I, S2.6 and S2.7**). In conclusion, our data were not consistent with the hypothesis that colonic crypt hyperplasia increased oxygen availability by depleting *Clostridia.*

C. rodentium attaches to murine colonic epithelial cells (colonocytes) using a Type IV pilus encoded by the *cfc* operon (*20*). To test whether this adhesin contributed to establishing a niche in which the pathogen could grow by CydAB-mediated respiration, we constructed a *cfcH* mutant (**Fig. S2.1F**). Genetic ablation of Type IV pilus biosynthesis did not change the CydAB-dependent growth advantage

seven days after infection of mice (**Fig. 2.2A and Fig. S2.8A**), possibly because a *cfcH* mutant still occupied a niche near the epithelium (**Fig. S2.8B**).

C. rodentium intimately attaches to colonocytes in a T3SS-dependent fashion using intimin. To test whether the T3SS and intimin contributed to CydAB-dependent growth, we constructed mutations in *escN*, encoding a component of the T3SS, and *eae*, the gene encoding intimin (**Fig. S2.1G and S2.1H**). Interestingly, the fitness advantage conferred by CydAB-dependent respiration seven days after infection was significantly reduced in *C. rodentium* strains lacking *eae* or *escN* (**Fig. 2.2A and S2.8A**), suggesting that in the absence of intimate attachment or a functional T3SS, oxygen respiration no longer conferred a marked fitness advantage. However, at three days after infection, when intestinal inflammation was just beginning to develop (**Fig. S2.8C and S2.8D**), inactivation of *escN* did not significantly reduce the fitness advantage conferred by the *cydAB* genes (**Fig. S2.8E**). Since the *escN* mutation did not reduce the fitness advantage conferred by the *cydAB* genes in the absence of overt crypt hyperplasia (i.e. at three days after infection), we considered the possibility that enhanced access to oxygen might not depend on intimate attachment, but require T3SS-mediated host responses.

Colonocytes mature as they migrate from the bottom of the crypt to the luminal surface. The mature surface colonocyte population functions in water absorption, which is driven by electrolyte transport (*21*). To energize absorption of electrolytes, mature colonocytes respire butyrate in their mitochondria (*22*), a process consuming oxygen and rendering the mucosal surface hypoxic (< 7.6 mmHg pO_2 or < 1% O_2) (*23, 24*) (**Fig. S2.1**). To investigate whether T3SS-induced colonic crypt hyperplasia, which developed by seven days after infection (**Fig. S2.9A and S2.9B**), would alter epithelial oxygenation *in vivo*, we visualized the "physiologic hypoxia" of surface colonocytes using the exogenous hypoxic marker pimonidazole (*25*) (**Fig. 2.2B**). Remarkably, a lack of hypoxia staining at the mucosal surface suggested that infection with the *C. rodentium* wild type significantly ($P < 0.05$) reduced epithelial hypoxia by seven days after infection (**Fig. 2.2B, 2.2C and S2.10**), indicative of a marked increase in epithelial oxygenation. This increased epithelial

oxygenation was T3SS-dependent, because it was not observed in mice infected with the *escN* mutant (**Fig. 2.2B and 2.2C**), which did not develop inflammation in the colon (**Fig. S2.8**).

T3SS-induced colonic crypt hyperplasia is characterized by an excessive intestinal epithelial repair response (reviewed in (*26*)). To further investigate the mechanism by which the T3SS increases epithelial oxygenation, we deleted the *map*, *cesF* and *espH* genes to reduce damage to colonocytes (**Fig. S2.2H**). Map and EspH are T3SS effector proteins that damage mitochondria (which might impair respiration of butyrate) or activate caspase-3 to induce cytotoxicity, respectively (*27, 28*), while the *cesF* gene encodes a chaperone for the mitochondria-associated T3SS effector EspF (*29*). Deletion of the *map*, *cesF* and *espH* genes significantly ($P < 0.05$) reduced the fitness advantage conferred by CydAB-dependent respiration seven days after infection of mice (**Fig. 2.2A**), but it was not clear whether this was simply due to an overall lower level of colonization (**Fig. S2.8A**). When mice were infected with either the *C. rodentium* wild type or an *espH cesF map* mutant, both strains were detected in association with the mucosal surface, although the *espH cesF map* mutant appeared impaired for colonization (**Fig. S2.11A**) and the *C. rodentium* wild type was recovered in higher numbers than a *espH cesF map* mutant from colon contents seven days after infection (**Fig. 2.3A)**. Only infection with the *C. rodentium* wild type significantly reduced epithelial hypoxia, while the colonic surface remained hypoxic in mice infected with a *espH cesF map* mutant (**Fig. S2.11B and S2.11C**).

While mature colonocytes at the luminal surface respire butyrate, undifferentiated colonocytes in the crypts exhibit the Warburg metabolism of dividing cells, which is characterized by fermenting glucose to lactate (*30*). *C. rodentium* infection induces epithelial regeneration and repair mechanisms, which drives a marked expansion of undifferentiated colonocytes, resulting in crypt elongation and the presence of undifferentiated colonocytes at the luminal surface (*31, 32*)(**Fig. S2.1**). Since the Warburg metabolism does not consume oxygen, we wanted to determine whether reduced hypoxia of surface colonocytes observed during *C. rodentium* infection (**Fig. 2.2B, 2.2C, S2.11B and S2.11C**) was due to an accumulation of undifferentiated colonocytes at the luminal surface. Interestingly, infection with a *espH cesF map* mutant

triggered significantly ($P < 0.05$) less mitotic divisions in the colonic epithelium than infection with wild-type *C. rodentium* (**Fig. S2.8C**), suggesting that deletion of the *espH*, *cesF* and *map* genes might reduce crypt hyperplasia. To test this idea, we stained colonic sections from mock-infected mice or mice infected with the *C. rodentium* wild type or an *espH cesF map* mutant with Ki67, a cellular marker for proliferation. Infection with the *C. rodentium* wild type induced a marked expansion of Ki67-positive colonocytes, resulting in crypt elongation, a thickening of the colonic mucosa and an accumulation of Ki67-positive colonocytes along the length of the crypt and at the luminal surface (**Fig. 2.3B and 2.3C**). Interestingly, this host response was blunted in mice infected with a *C. rodentium espH cesF map* mutant (**Fig. 2.3B and 2.3C**), which correlated with increased epithelial hypoxia (**Fig. S2.11B and S2.11C**).

We next wanted to determine whether colonic crypt hyperplasia was a driver of CydAB-dependent pathogen expansion. To this end, mice were mock infected or infected with a 1:1 mixture of the *C. rodentium* wild type and *cydAB* mutant and then treated with dibenzazepine (DBZ) or with vehicle control. DBZ is a Notch and Wnt (wingless-related integration site) signaling pathway inhibitor that prevents colonic crypt hyperplasia during *C. rodentium* infection (*31*). Ki67 staining suggested that mice infected with the *C. rodentium* strain mixture developed colonic crypt hyperplasia, which was significantly ($P < 0.05$) blunted by DBZ treatment (**Fig. 2.3D and 2.3E**), although DBZ treatment did not reduce the severity of other histopathological changes (**Fig. S2.12A and S2.12B**). Remarkably, inhibition of colonic crypt hyperplasia by DBZ treatment abrogated the fitness advantage conferred by the *cydAB* genes (**Fig. 2.3F**), suggesting that crypt hyperplasia was a main driver of aerobic pathogen expansion.

Our finding that the LEE-encoded T3SS provides *C. rodentium* access to oxygen *in vivo* helps explain why the mechanism by which this trademark virulence factor confers a benefit to AE pathogens has not been apparent from *in vitro* studies, because such experiments are commonly performed in a 95% air (79% N_2/21% O_2) atmosphere, supplemented by 5% of carbon dioxide, thus providing 19.95% O_2 (150 mmHg). This oxygenation is considerably higher than normal tissue oxygenation (23–70 mmHg or 3%-10% oxygen) (*35*) or oxygenation of colonocytes *in vivo* (< 7.6 mmHg or < 1% O_2) (*23, 24*). While oxygen

emanating from the mucosal surface is a very limited resource in the lumen of the large intestine (*36*), epithelial oxygenation was markedly elevated during T3SS-induced colonic crypt hyperplasia. As a result, T3SS-induced colonic crypt hyperplasia drove growth of *C. rodentium* through CydAB-mediated aerobic respiration, presumably because a respiratory metabolism enables the pathogen to utilize carbon sources more effectively than competing microbes that rely on fermentation for growth. In conclusion, our results revealed how histopathological changes triggered by a trademark virulence factor of AE pathogens create a unique nutrient-niche to fuel an uncontrolled luminal expansion of *C. rodentium*.

References and notes

1. T. E. Staley, E. W. Jones, L. D. Corley, Attachment and penetration of Escherichia coli into intestinal epithelium of the ileum in newborn pigs. *The American journal of pathology* **56**, 371-392 (1969).

2. H. W. Moon, S. C. Whipp, R. A. Argenzio, M. M. Levine, R. A. Giannella, Attaching and effacing activities of rabbit and human enteropathogenic Escherichia coli in pig and rabbit intestines. *Infection and immunity* **41**, 1340-1351 (1983).

3. K. G. Jarvis *et al.*, Enteropathogenic Escherichia coli contains a putative type III secretion system necessary for the export of proteins involved in attaching and effacing lesion formation. *Proceedings of the National Academy of Sciences of the United States of America* **92**, 7996-8000 (1995).

4. A. E. Jerse, J. Yu, B. D. Tall, J. B. Kaper, A genetic locus of enteropathogenic Escherichia coli necessary for the production of attaching and effacing lesions on tissue culture cells. *Proceedings of the National Academy of Sciences of the United States of America* **87**, 7839-7843 (1990).

5. B. Kenny *et al.*, Enteropathogenic E. coli (EPEC) transfers its receptor for intimate adherence into mammalian cells. *Cell* **91**, 511-520 (1997).

6. W. Deng, B. A. Vallance, Y. Li, J. L. Puente, B. B. Finlay, Citrobacter rodentium translocated intimin receptor (Tir) is an essential virulence factor needed for actin condensation, intestinal colonization and colonic hyperplasia in mice. *Mol Microbiol* **48**, 95-115 (2003).

7. J. P. Nataro, J. B. Kaper, Diarrheagenic Escherichia coli. *Clin Microbiol Rev* **11**, 142-201 (1998).

8. S. A. Luperchio, D. B. Schauer, Molecular pathogenesis of Citrobacter rodentium and transmissible murine colonic hyperplasia. *Microbes Infect* **3**, 333-340 (2001).

9. C. Lupp *et al.*, Host-mediated inflammation disrupts the intestinal microbiota and promotes the overgrowth of Enterobacteriaceae. *Cell Host Microbe* **2**, 204 (2007).

10. N. Kamada *et al.*, Regulated virulence controls the ability of a pathogen to compete with the gut microbiota. *Science* **336**, 1325-1329 (2012).

11. C. A. Lopez *et al.*, Phage-mediated acquisition of a type III secreted effector protein boosts growth of salmonella by nitrate respiration. *MBio* **3**, (2012).

12. S. E. Winter *et al.*, Host-derived nitrate boosts growth of E. coli in the inflamed gut. *Science* **339**, 708-711 (2013).

13. S. E. Winter *et al.*, Gut inflammation provides a respiratory electron acceptor for Salmonella. *Nature* **467**, 426-429 (2010).

14. S. L. Rivers, E. McNairn, F. Blasco, G. Giordano, D. H. Boxer, Molecular genetic analysis of the moa operon of Escherichia coli K-12 required for molybdenum cofactor biosynthesis. *Molecular microbiology* **8**, 1071-1081 (1993).

15. B. L. Berg, V. Stewart, Structural genes for nitrate-inducible formate dehydrogenase in Escherichia coli K-12. *Genetics* **125**, 691-702 (1990).

16. G. Sawers, J. Heider, E. Zehelein, A. Bock, Expression and operon structure of the sel genes of Escherichia coli and identification of a third selenium-containing formate dehydrogenase isoenzyme. *Journal of bacteriology* **173**, 4983-4993 (1991).

17. C. R. Amarasingham, B. D. Davis, Regulation of alpha-ketoglutarate dehydrogenase formation in Escherichia coli. *J Biol Chem* **240**, 3664-3668 (1965).

18. F. Rivera-Chavez *et al.*, Depletion of Butyrate-Producing Clostridia from the Gut Microbiota Drives an Aerobic Luminal Expansion of Salmonella. *Cell Host Microbe* **19**, 443-454 (2016).

19. L. Albenberg *et al.*, Correlation between intraluminal oxygen gradient and radial partitioning of intestinal microbiota. *Gastroenterology* **147**, 1055-1063 e1058 (2014).

20. R. Mundy *et al.*, Identification of a novel type IV pilus gene cluster required for gastrointestinal colonization of Citrobacter rodentium. *Molecular microbiology* **48**, 795-809 (2003).

21. R. B. Lomax, C. M. McNicholas, M. Lombes, G. I. Sandle, Aldosterone-induced apical Na+ and K+ conductances are located predominantly in surface cells in rat distal colon. *Am J Physiol* **266**, G71-82 (1994).

22. O. C. Velazquez, H. M. Lederer, J. L. Rombeau, Butyrate and the colonocyte. Production, absorption, metabolism, and therapeutic implications. *Adv Exp Med Biol* **427**, 123-134 (1997).

23. G. T. Furuta *et al.*, Hypoxia-inducible factor 1-dependent induction of intestinal trefoil factor protects barrier function during hypoxia. *J Exp Med* **193**, 1027-1034 (2001).

24. C. J. Kelly *et al.*, Crosstalk between Microbiota-Derived Short-Chain Fatty Acids and Intestinal Epithelial HIF Augments Tissue Barrier Function. *Cell Host Microbe* **17**, 662-671 (2015).

25. N. Terada, N. Ohno, S. Saitoh, S. Ohno, Immunohistochemical detection of hypoxia in mouse liver tissues treated with pimonidazole using "in vivo cryotechnique". *Histochem Cell Biol* **128**, 253-261 (2007).

26. J. W. Collins *et al.*, Citrobacter rodentium: infection, inflammation and the microbiota. *Nat Rev Microbiol* **12**, 612-623 (2014).

27. A. R. Wong, A. Clements, B. Raymond, V. F. Crepin, G. Frankel, The interplay between the Escherichia coli Rho guanine nucleotide exchange factor effectors and the mammalian RhoGEF inhibitor EspH. *MBio* **3**, (2012).

28. C. Ma *et al.*, Citrobacter rodentium infection causes both mitochondrial dysfunction and intestinal epithelial barrier disruption in vivo: role of mitochondrial associated protein (Map). *Cell Microbiol* **8**, 1669-1686 (2006).

29. J. P. Nougayrede, M. S. Donnenberg, Enteropathogenic Escherichia coli EspF is targeted to mitochondria and is required to initiate the mitochondrial death pathway. *Cell Microbiol* **6**, 1097-1111 (2004).

30. Y. Y. Fan *et al.*, A bioassay to measure energy metabolism in mouse colonic crypts, organoids, and sorted stem cells. *American journal of physiology. Gastrointestinal and liver physiology* **309**, G1-9 (2015).

31. I. Ahmed *et al.*, Critical roles of Notch and Wnt/beta-catenin pathways in the regulation of hyperplasia and/or colitis in response to bacterial infection. *Infect Immun* **80**, 3107-3121 (2012).

32. P. Chandrakesan *et al.*, Novel changes in NF-{kappa}B activity during progression and regression phases of hyperplasia: role of MEK, ERK, and p38. *J Biol Chem* **285**, 33485-33498 (2010).

33. E. Caron *et al.*, Subversion of actin dynamics by EPEC and EHEC. *Curr Opin Microbiol* **9**, 40-45 (2006).

34. G. Frankel *et al.*, Enteropathogenic and enterohaemorrhagic Escherichia coli: more subversive elements. *Molecular microbiology* **30**, 911-921 (1998).

35. A. Carreau, B. El Hafny-Rahbi, A. Matejuk, C. Grillon, C. Kieda, Why is the partial oxygen pressure of human tissues a crucial parameter? Small molecules and hypoxia. *J Cell Mol Med* **15**, 1239-1253 (2011).

36. M. G. Espey, Role of oxygen gradients in shaping redox relationships between the human intestine and its microbiota. *Free radical biology & medicine* **55**, 130-140 (2013).

37. V. Stewart, J. Parales, Jr., Identification and expression of genes narL and narX of the nar (nitrate reductase) locus in Escherichia coli K-12. *Journal of bacteriology* **170**, 1589-1597 (1988).

38. J. G. Caporaso *et al.*, QIIME allows analysis of high-throughput community sequencing data. *Nat Methods* **7**, 335-336 (2010).

39. D. H. Huson, S. Mitra, H. J. Ruscheweyh, N. Weber, S. C. Schuster, Integrative analysis of environmental sequences using MEGAN4. *Genome Res* **21**, 1552-1560 (2011).

40. C. E. Robertson *et al.*, Explicet: graphical user interface software for metadata-driven management, analysis and visualization of microbiome data. *Bioinformatics* **29**, 3100-3101 (2013).

41. D. Arndt *et al.*, METAGENassist: a comprehensive web server for comparative metagenomics. *Nucleic Acids Res* **40**, W88-95 (2012).

42. N. Kamada *et al.*, Humoral Immunity in the Gut Selectively Targets Phenotypically Virulent Attaching-and-Effacing Bacteria for Intraluminal Elimination. *Cell Host Microbe* **17**, 617-627 (2015).

43. I. Godinez *et al.*, Interleukin-23 orchestrates mucosal responses to Salmonella enterica serotype Typhimurium in the intestine. *Infect Immun* **77**, 387-398 (2009).

44. C. A. Schneider, W. S. Rasband, K. W. Eliceiri, NIH Image to ImageJ: 25 years of image analysis. *Nat Methods* **9**, 671-675 (2012).

45. S. W. Barthold, G. L. Coleman, P. N. Bhatt, G. W. Osbaldiston, A. M. Jonas, The etiology of transmissible murine colonic hyperplasia. *Lab Anim Sci* **26**, 889-894 (1976).

46. D. Pal, T. Venkova-Canova, P. Srivastava, D. K. Chattoraj, Multipartite regulation of rctB, the replication initiator gene of Vibrio cholerae chromosome II. *Journal of bacteriology* **187**, 7167-7175 (2005).

47. R. Simon, U. Priefer, A. Puhler, A Broad Host Range Mobilization System for Invivo Genetic-Engineering - Transposon Mutagenesis in Gram-Negative Bacteria. *Bio-Technology* **1**, 784-791 (1983).

48. R. F. Wang, S. R. Kushner, Construction of versatile low-copy-number vectors for cloning, sequencing and gene expression in Escherichia coli. *Gene* **100**, 195-199 (1991).

49. V. L. Miller, J. J. Mekalanos, A novel suicide vector and its use in construction of insertion mutations: osmoregulation of outer membrane proteins and virulence determinants in Vibrio cholerae requires toxR. *Journal of bacteriology* **170**, 2575-2583 (1988).

50. R. A. Kingsley *et al.*, Ferrioxamine-mediated Iron(III) utilization by Salmonella enterica. *Appl Environ Microbiol* **65**, 1610-1618 (1999).

51. S. A. Kinder, J. L. Badger, G. O. Bryant, J. C. Pepe, V. L. Miller, Cloning of the YenI restriction endonuclease and methyltransferase from Yersinia enterocolitica serotype O8 and construction of a transformable R-M+ mutant. *Gene* **136**, 271-275 (1993).

52. M. Raffatellu *et al.*, Lipocalin-2 resistance confers an advantage to Salmonella enterica serotype Typhimurium for growth and survival in the inflamed intestine. *Cell Host Microbe* **5**, 476-486 (2009).

We would like to acknowledge the Host-Microbe Systems Biology Core (HMSB Core) at the UC Davis School of Medicine for expert technical assistance with microbiota sequence analysis. The data reported in the manuscript are tabulated in the main paper and in the supplementary materials. Work in A.J.B.'s laboratory was supported by Public Health Service Grants AI044170, AI096528, AI107393, and AI112949. Work in R.M.T.'s lab was supported by Public Health Service Grant AI098078. Work in

S.E.W.'s lab was supported by Public Health Service Grant AI103248. C.A.L was supported by Public Health Service Grant AI112241. E.M.V. was supported by Public Health Service Grant OD010931.

Figures

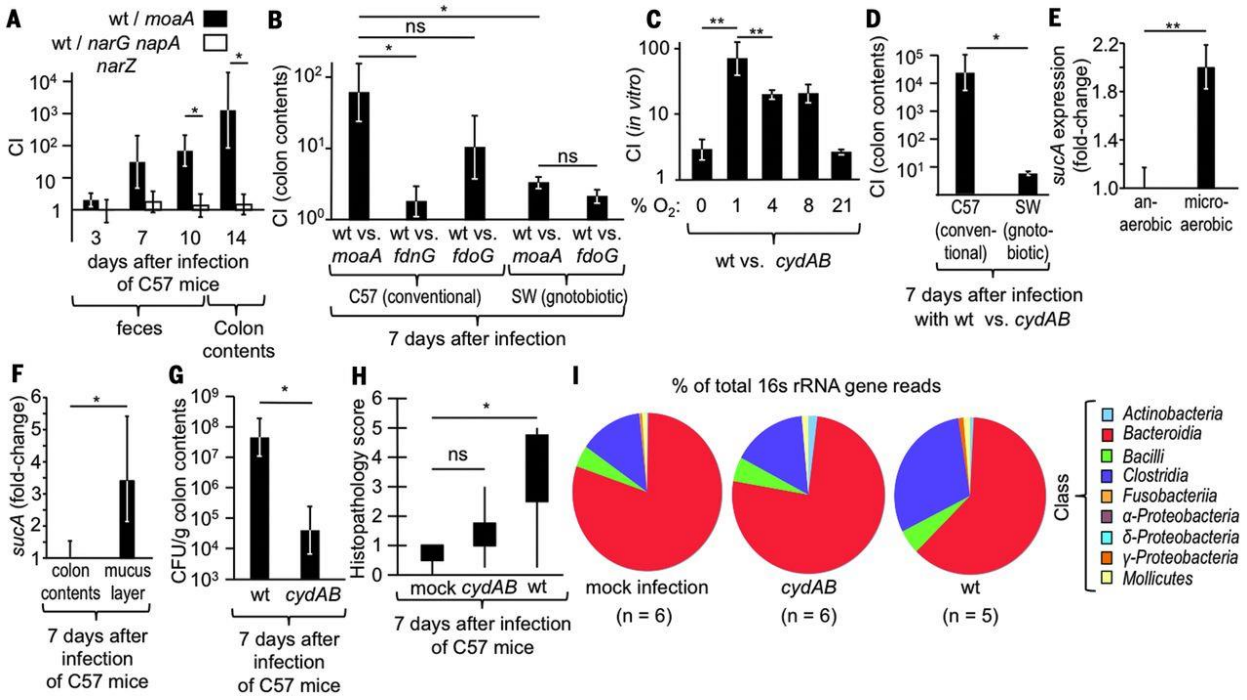

Figure 2.1: Oxygen respiration supports *C. rodentium* expansion in the mouse colon.

(A) C57BL/6 (C57) mice were infected with *C. rodentium* wild type (wt, DBS100) and either a *moaA* mutant (CAL142) or a *napA narG narZ* mutant (CAL93). **(B)** Conventional C57 or germ-free Swiss Webster (SW) mice were infected with wt *C. rodentium* and either a *moaA* mutant, a *fdnG* mutant (CAL210 [pWSK129]), or a *fdoG* mutant (CAL261). *N* is indicated in Fig. S3E. **(C)** Competitive *in vitro* growth (*N* =8) of *C. rodentium* wild type (wt) and a *cydAB* mutant (CAL247) for 16 hours in minimal medium in the presence of the indicated oxygen levels (% O_2). **(D)** Conventional or germ-free mice were infected with an equal mixture of the *C. rodentium* wild type (wt) and a *cydAB* mutant. (**A and D**) *N* = 4. **(E)** *C. rodentium* was grown in minimal medium supplemented with mannose as a carbon source under either microaerobic or anaerobic conditions. **(F)** Bacterial RNA was isolated from either mucus scrapings or colon contents of *C. rodentium*-infected mice. (**E-F**) The transcript levels of *sucA* were quantified by real-time PCR, normalized to 16S rRNA levels and shown as fold-changes. *N* is shown in Fig. S4B and S4C. **(G-I)** Mice (*N* indicated in **I**) were either mock-treated, infected with the *C. rodentium* wild type (wt) or with a *cydAB*

mutant (CAL247). **(G)** Enumeration of *C. rodentium* by plating on selective media. (**A-G**) Bars represent geometric mean ± standard error. **(H)** Boxes in Whisker plots represent the second and third quartiles of combined histopathology scores, while lines indicate the first and fourth quartiles. **(I)** Microbial representation at the class-level based on 16S rRNA gene sequencing of colon contents 7 days after infection. Color-coding for classes is shown on the right. *, $P < 0.05$; **, $P < 0.01$; ns, not statistically significantly different.

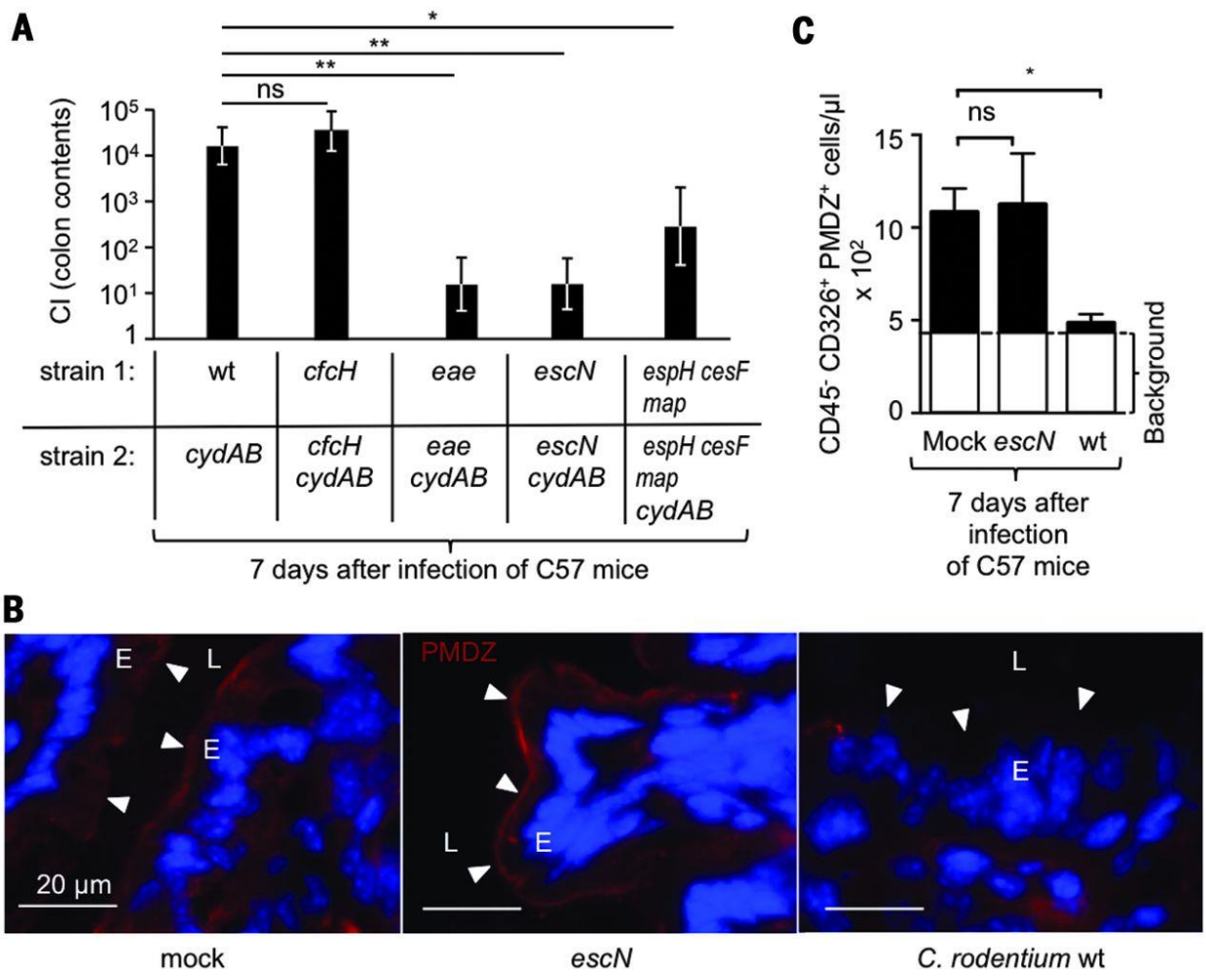

Figure 2.2: A functional T3SS increases epithelial oxygenation and drives a CydAB-dependent *C. rodentium* expansion.

(A) Mice (*N* is indicated in Fig. S8A) were infected with the indicated *C. rodentium* strain mixtures. Bars represent geometric means of the competitive index (CI) ± standard error. **(B)** Representative images of colonic sections stained to detect pimonidazole hypoxia stain (red fluorescence) and counterstained with DAPI nuclear stain (blue fluorescence). Arrow heads point to the mucosal surface. E, epithelial cell; L, lumen. **(C)** Pimonidazole staining ($PMDZ^+$) was quantified by flow cytometry in colonic epithelial ($CD45^-$ $CD326^+$) cells. White bars indicate the level of background staining observed in mice that were not injected with PMDZ. Bars represent geometric mean ± standard error. **, $P < 0.01$; *, $P < 0.05$; ns, not statistically significantly different; wt, DBS100; *cydAB*, CAL247; *cfcH*, BMM12; *cfcH cydAB*,

BMM11; *eae*, CAL290; *eae cydAB*, CAL291; *escN*, CAL286; *escN cydAB*, CAL287; *espH cesF map*, BMM30; *espH cesF map cydAB*, BMM40.

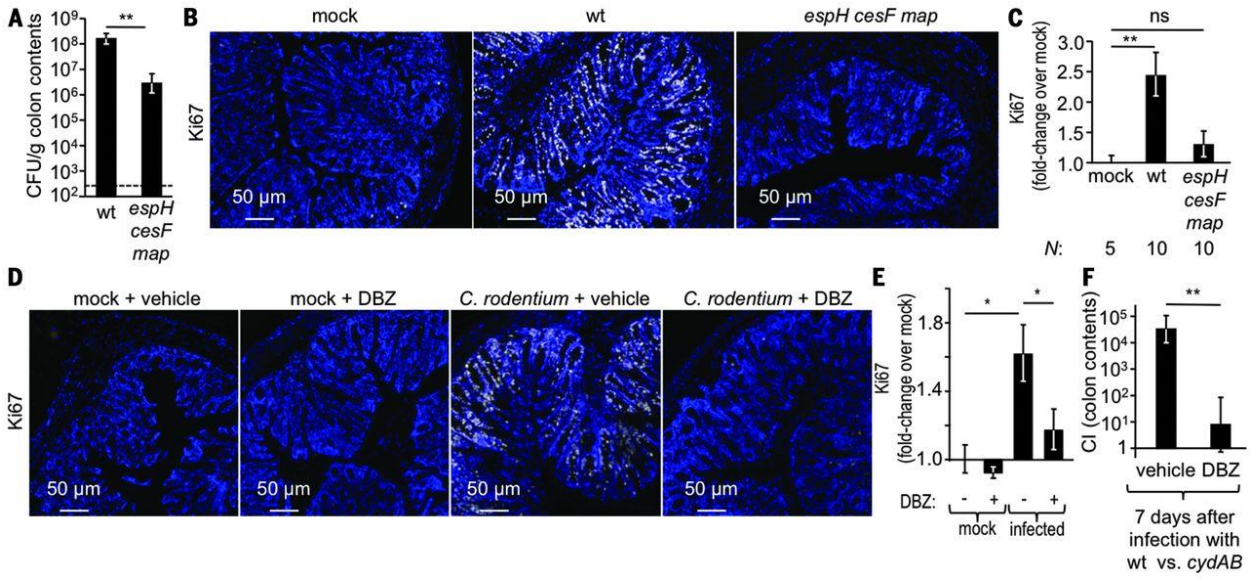

Figure 2.3: Colonic crypt hyperplasia drives a CydAB-dependent *C. rodentium* expansion.

(**A-C**) C57BL/6 mice were mock infected or infected with the *C. rodentium* wild type (wt, DBS100) or an *espH cesF map* mutant (BMM30). (**D-F**) C57BL/6 mice were mock infected or infected with a 1:1 mixture of the *C. rodentium* wild type (wt) and a *cydAB* mutant (CAL247). Mice were either treated with dibenzazepine (DBZ) or with vehicle control. (**A-F**) Organs were collected seven days after infection. (**A**) CFU recovered from colon contents. (**B and D**) Representative images of colonic sections were stained to detect Ki67 (yellow fluorescence) and counterstained with DAPI nuclear stain (blue fluorescence). (**C and E**) Ki67 staining was quantified by image analysis. (**F**) Enumeration of wt and *cydAB* mutant recovered from colon contents was used to calculate the competitive index (CI). (**A, C, E and F**) Bars represent geometric mean ± standard error. **, $P < 0.01$; *, $P < 0.05$; ns, not statistically significantly different.

Supplementary materials

Materials and Methods

Bacterial strains and culture conditions. For the *Escherichia coli* and *Citrobacter rodentium* strains used in this study, see Table S1. Strains were routinely grown in Luria-Burtani broth (BD Biosciences #244620) or on LB plates unless otherwise indicated. Antibiotics were used at the following concentrations: carbenicillin (Carb), 0.1 mg/ml; chloramphenicol (Cm), 0.015mg/ml; kanamycin (Kan), 0.1 mg/ml; tetracycline (Tet), 0.02 mg/ml.

***In vitro* competitive growth assay.** Bacteria were grown in 10 ml M9 minimal media (2mM $MgS0_4$, 0.2mM $CaCl_2$, M9 salts [Na_2HPO_4, 6.8 g/l; KH_2PO_4, 3 g/l; NaCl, 0.5 g/l; NH_4Cl, 1 g/l]) with 0.4% glycerol, 1% casamino acids (BD Biosciences). Bacteria for the assay were grown overnight at 37°C in an anaerobe chamber (Shellab) with an environment of 5 % CO_2, 5 % H_2, and the remainder N_2. Pre-reduced media was inoculated with a 1:1 ratio of two *C. rodentium* strains at a concentration of $1x10^5$ total CFU in the anaerobe chamber. The inoculated media was then either left in the anaerobe chamber (0% oxygen) or moved to a hypoxia chamber in an airtight container. The hypoxia chamber was set at either 1 %, 4 %, 8 %, or 21 % oxygen, with the remaining atmosphere being composed of 5 % CO_2 and 95 % N_2. Cultures were left to incubate for 24 hours and then plated on selective MacConkey agar to differentiate between the two strains. Data represents eight replicates per group.

Nitrate reductase assay. Bacterial cultures were grown overnight in LB broth, then diluted 1:1000 into fresh LB broth containing 40 mM $NaNO_3$. Cultures were grown statically at 37°C for 3 hours. The assay was then performed as described previously (*37*). Briefly, 50 µl of a washed cell suspension was permeabilized in 0.1% sodium dodecyl sulfate and chloroform. Next methyl viologen (0.5 mg/ml) and a solution of bicarbonate (8 mg/ml), sodium hydrosulfite (8 mg/ml), and nitrate (0.5 M) were added to cells and left to incubate at room temperature for 5 minutes. Assay was terminated with vigorous vortexing, then sulfanilic HCl (1% sulfanilic acid and 20% HCl) and Marshall's reagent (0.13 % N-1-

naphthylethylenediamine 2HCl) were added to the solution. Absorbance was next read at 540 nm and 420 nm. To calculate nitrate reductase activity, we used the following equation: $\{[A_{540} – (0.72 * A_{420})]/(t * v * A_{600})\} * 100$ where t is the time (minutes) of the reaction, v is the volume (ml) of the cell suspension in the assay, and A_{600} is the optical density of the original cell suspension.

Construction of *C. rodentium* mutants. To construct a *napA* mutant, upstream and downstream regions of approximately 1kb in length flanking *C. rodentium napA* were amplified via PCR, run on an agarose gel, and purified using the QiaexII kit (Qiagen). These flanking regions were digested with XbaI (NEB), ligated, and PCR amplified to form one fragment of approximately 2kb that was then inserted into pCR2.1. The plasmid was propagated in Top10 *E. coli*. This plasmid was next digested with SphI (NEB) and the fragment was inserted into pRDH10 to form pCAL7 and cloned into *E. coli* DH5α λ*pir*. To insert a tetracylin resistance cassette, pCAL7 was digested with XbaI while pSPN23 was digested with NheI (NEB). The tetracycline resistance cassette from pSPN23 was ligated with pCAL7 to form pCAL17. Plasmid pCAL17 was then transformed into *E. coli* strain S17-1 λ*pir* and conjugation performed with *C. rodentium* that was transformed with pWSK129 to have a selectable marker for the recipient. After selection to pick *C. rodentium* colonies containing a single crossover mutation, sucrose selection was performed to select for colonies that lost the vector backbone along with the *napA* gene, but retained the tetracycline resistance cassette. After confirming the mutation via PCR, this strain was named CAL60. To generate a nonpolar *napA* mutant, CAL60 was conjugated with *E. coli* S17-1 λ*pir* containing pCAL7. After selection for single crossover *C. rodentium* colonies, sucrose selection was performed to select for colonies that lost the tetracycline cassette (CAL77).

To construct the *narZ* mutation, upstream and downstream regions of approximately 1kb in length flanking *C. rodentium narZ* were amplified via PCR, run on an agarose gel, and purified using the QiaexII kit. These flanking regions were digested with XbaI, ligated, and PCR amplified to form one fragment of approximately 2kb that was then inserted into pCR2.1 and propagated in *E. coli* Top10. This plasmid was next digested with SphI and the fragment was inserted into pRDH10 to form pCAL8, which was propagated

in DH5α λ*pir* *E. coli*. To insert a tetracycline resistance cassette, pCAL8 was digested with XbaI while pSPN23 was digested with NheI. The tetracycline resistance cassette was ligated with pCAL8 to form pCAL15. Plasmid pCAL15 was transformed into *E. coli* S17-1 λ*pir* and conjugation performed with CAL77. After selection to pick *C. rodentium* colonies containing a single crossover mutation, sucrose selection was performed to select for colonies that lost the vector backbone and *narZ* gene, but retained the tetracycline resistance cassette. After confirming the mutation via PCR, the *napA narZ* mutant was named CAL92.

To construct the *narG* mutation, a region within *C. rodentium narG* was amplified via PCR, inserted into pCR2.1, and propagated in Top10 *E. coli*. This plasmid and the plasmid pGP704 were then digested with XbaI and SphI. The *narG* fragment was ligated into pGP704 to produce the plasmid pCAL6 and propagated in *E. coli* DH5α λ*pir*. Plasmid pCAL6 was then transformed into *E. coli* S17-1 λ*pir* conjugation performed with CAL92. *C. rodentium* colonies with a single crossover were selected and PCR confirmed the mutation in *narG*. The *napA narZ narG* mutant was named CAL93.

To construct a *moaA* mutant, a region within *C. rodentium moaA* was amplified via PCR, inserted into pCR2.1, and propagated in *E. coli* Top10. This plasmid and the plasmid pEP185.2 were then digested with XhoI (NEB) and SacI (NEB). The *moaA* fragment was ligated into pEP185.2 to generate the plasmid pCAL34, which was subsequently propagated in *E. coli* DH5α λ*pir.* To aid in selection during conjugation, wild type *C. rodentium* was transformed with the temperature-sensitive plasmid pSW172. Plasmid pCAL34 was then introduced into *E. coli* S17-1 λ*pir* and conjugation performed with *C. rodentium* (SW172) at 30°C. Since *C. rodentium* exhibits low-level resistance to carbenicillin naturally, a higher concentration of this antibiotic (0.2 mg/ml) was used to select for *C. rodentium* colonies that retained the $Carb^R$ plasmid pSW172 and also contained a single crossover event at the *moaA* locus. The plasmid pSW172 was cured after growth at 40°C and PCR was used to confirm the *moaA* mutation. The *moaA* mutant was named CAL142.

To construct a non-polar *cydAB* mutant, upstream and downstream regions of approximately 1kb in length flanking the *C. rodentium cydAB* operon were amplified via PCR, run on an agarose gel, and

purified using the QiaexII kit. These flanking regions were digested with XbaI, ligated, and PCR amplified to form one fragment of approximately 2kb that was then inserted into pCR2.1 and propagated in *E. coli* Top10. While cloning in *C. rodentium*, we observed that sucrose selection does not efficiently prevent the growth of *Citrobacter* colonies that retained a suicide vector encoding *sacRB*. To improve screening for double crossover events, we amplified the *phoN* gene of *Salmonella enterica* serovar Typhimurium via PCR and inserted it into pCR2.1 followed by propagation in *E. coli* Top10. This plasmid was subsequently digested with EcoRI (NEB) and *phoN* was inserted into the EcoRI-digested pRDH10 plasmid to generate pCAL52. *C. rodentium* colonies with this plasmid will turn blue when grown on plates containing X-phos (5-bromo-4-chloro-3-indolyl phosphate). The plasmid pCR2.1 containing the *cydAB* flanking regions was next digested with SalI (NEB) and the fragment was inserted into pCAL52 to generate pCAL59. To insert a kanamycin resistance cassette, pCAL59 and pUC4 KSAC were first digested with XbaI. The kanamycin resistance cassette from pUC4 KSAC was then ligated with pCAL59 to form pCAL60 and propagated in *E. coli* DH5α λ*pir*. Plasmid pCAL60 was then transformed into *E. coli* strain S17-1 λ*pir* and conjugation performed with *C. rodentium* (SW172). *C. rodentium* colonies containing a single crossover mutation were then grown overnight in LB broth at 30°C and plated on LB agar plates containing X-phos (40mg/l). White colonies were screened for resistance to kanamycin, but sensitivity to chloramphenicol, confirming loss of the pCAL52 vector backbone but retaining the kanamycin resistance cassette. After confirming the *cydAB* deletion via PCR, the plasmid pSW172 was cured after growth at 40°C and the strain named CAL247. To generate a non-polar *cydAB* mutant, CAL247 was conjugated with *E. coli* S17-1 λ*pir* containing pCAL59. After selection for single crossover *C. rodentium* colonies, we performed blue-white screening on LB agar plates containing X-phos as described above to select for colonies that lost the kanamycin cassette and generated CAL267.

To construct a non-polar *fdnG* mutant, upstream and downstream regions of approximately 1kb in length flanking the *C. rodentium fdnG* gene were amplified via PCR, run on an agarose gel, and purified using the QiaexII kit. These flanking regions were digested with XbaI, ligated, and PCR amplified to form

one fragment of approximately 2kb in size that was then inserted into pCR2.1 and propagated in *E. coli* Top10. This plasmid was next digested with SphI and inserted into pCAL52 to generate pCAL55 and propagated in *E. coli* DH5α λ*pir.* Plasmid pCAL55 was transformed into *E. coli* S17-1 λ*pir*, conjugation performed with *C. rodentium* (SW172) and single crossover events were selected for using the appropriate antibiotics. Blue-white screening with X-phos was performed as described above. A double crossover event was confirmed via PCR. The plasmid pSW172 was cured after growth at 40°C and the non-polar *fdnG* mutant was named CAL210. To aid in selection during mouse experiments, CAL210 was transformed with pWSK129.

To construct the *fdoG* mutant, upstream and downstream regions of approximately 1kb in length flanking the *C. rodentium fdoG* gene were amplified via PCR, run on an agarose gel, and purified using the QiaexII kit. These flanking regions were digested with XbaI, ligated, and PCR amplified to form one fragment of approximately 2kb that was then inserted into pCR2.1 and propagated in *E. coli* Top10. This plasmid, containing the *fdoG* flanking regions, was next digested with SphI and the fragment was inserted into pCAL52 to generate pCAL72. To insert a kanamycin resistance cassette, pCAL72 and pUC4 KSAC were first digested with XbaI. The kanamycin resistance cassette from pUC4 KSAC was then ligated with pCAL72 to form pCAL74 and propagated in *E. coli* DH5α λ*pir*. Plasmid pCAL74 was then transformed into *E. coli* strain S17-1 λ*pir* and conjugation performed with *C. rodentium* (SW172). Single crossover events were selected for by growing on the appropriate antibiotics. Blue-white screening with Xphos was performed as described above to identify a colony that lost the vector backbone and the *fdoG* gene, but retained the kanamycin resistance cassette. Plasmid pSW172 was cured after growth at 40°C. After PCR confirmation of the *fdoG* mutation, this strain was named CAL261.

To construct a *escN* mutant, the Gibson Assembly method (New England Biolabs) was used to generate plasmid pCAL81 with a pEP185.2 vector backbone and an insert of an internal amplified region of *escN*. Plasmid pCAL81 was first propagated in *E. coli* DH5α λ*pir*, then transformed into *E. coli* S17-1 λ*pir* and conjugation performed with *C. rodentium* (SW172) at 30°C. After selection for single crossover

events, the plasmid pSW172 was cured after growth at 40°C and PCR was used to confirm the *escN* mutation. This *escN* mutant was named CAL286.

To construct a *cydAB escN* double mutant, the *E. coli* S17-1 λ*pir* strain containing pCAL81 was conjugated with CAL247. After selection for single crossover events, PCR was used to confirm the *escN* mutation. The *cydAB escN* mutant was named CAL287.

For generation of a *cfcH* mutant, a region within the *C. rodentium cfcH* was amplified via PCR. Fragments were run on an agarose gel and purified using the Zymoclean Gel DNA Recovery kit (Zymo Research). Creation of pBMM1 was accomplished by insertion of the purified fragment into pEP185.2 via the Gibson Assembly (New England Biolabs), and propagation in *E. coli* DH5α λ*pir*. pBMM1 was then transformed into *E. coli* S17-1 λ*pir,* followed by conjugation with *C. rodentium* (SW172). *C. rodentium* colonies with a single crossover were selected, and PCR was used to confirm the mutation in *cfcH*. The *cfcH* mutant was named BMM12.

For construction of a *cydAB cfcH* double mutant, the *E. coli* S17-1 λ*pir* strain containing pBMM1 was conjugated with a *cydAB* mutant. *C. rodentium* colonies carrying a single crossover were selected, and PCR was used to confirm the *cfcH* mutation. This *cydAB cfcH* double mutant was then named BMM11.

To construct an *eae* mutant, primers were designed using NEBuilder Assembly Tool (New England Biolabs) to amplify an *eae* intragenic region with overlapping regions with the plasmid pEP185.2. The intragenic region was amplified using Q5 high-fidelity master mix (New England Biolabs) and ligated via Gibson Assembly with pEP185.2 after the vector was digested with SacI. The assembled plasmid, named pCAL82, was transformed into *E. coli* DH5α λ*pir* then into *E. coli* S17-1 λ*pir*. *C. rodentium* (SW172) or the Δ*cydAB*::Kan^R mutant (CAL247) were next conjugated with *E. coli* S17-1 λ*pir* containing pCAL82. A *C. rodentium* colony resistant to Cm was verified by PCR to contain a single crossover at the *eae* locus. The strain was then cured of the temperature sensitive plasmid after growth at 40°C and designated

CAL290. A *C. rodentium* Δ*cydAB* mutant resistant to Kan and Cm was verified by PCR to contain a single crossover at the *eae* locus in addition to the deletion of *cydAB* and this strain was named CAL291.

To construct a non-polar *espH cesF map* mutant, regions of approximately 400bp in length flanking the *espH*, *cesF*, and *map* genes were amplified via PCR using Q5 high fidelity master mix, run on an agarose gel, and purified using Zymoclean Gel DNA Recovery kit (Zymo Research). Fragments were ligated into pRDH10 via Gibson Assembly after the vector was digested with SphI. The resulting plasmid pBMM3 was transformed into *E. coli E. coli* S17-1 λ*pir* and conjugated with *C. rodentium* wild type or a *cydAB* mutant (CAL247), which had been transformed with the temperature-sensitive plasmid pSW172. Exconjugants were selected for loss of the plasmid using sucrose selection and screened via PCR to confirm deletion of the target genes. The strains were then cured of the temperature sensitive plasmid after growth overnight at 42°C and were named BMM30 and BMM40, respectively.

Animal experiments. The Institutional Animal Care and Use Committee at the University of California, Davis, approved all animal experiments. For experiments involving mice colonized with conventional specific pathogen free microbiota, either C57BL/6J or C3H/HeJ strains (Jackson Laboratories) aged 6-8 weeks were inoculated with $1x10^9$ colony forming units (CFU)/mouse of a single *C. rodentium* strain in LB broth intragastrically. In competitive infections, a 1:1 ratio of two *C. rodentium* strains were given intragastrically at a combined final concentration of $1x10^9$ CFU/mouse. Fecal pellets were collected on days 3, 7, or 10 and mice were sacrificed between 3 and 14 days after infection. Colon contents were stored in phosphate-buffered saline (PBS) on ice. Colon tissue for histopathology was fixed in 10% buffered formalin phosphate while colon sections for murine RNA analysis were flash frozen and stored at -80°C. *C. rodentium* from feces and colon contents were enumerated by plating serial ten-fold dilutions of samples on LB agar or MacConkey agar (BD Biosciences) containing the appropriate antibiotics based on the resistance markers listed for each strain in Table S1. Plates were incubated overnight at 37°C under atmospheric oxygen conditions.

Germ-free Swiss Webster mice were bred and housed at the Teaching and Research Animal Care Services facilities at UC Davis. These mice were infected and euthanized as described above.

To inhibit hyperplasia, mice were first mock infected or infected with a 1:1 mixture of the indicated C. rodentium strains as described above. Dibenzazepine (DBZ) was initially dissolved in DMSO and then suspended in a solution of hydroxypropyl methylcellulose (0.5 %)(Sigma) and Tween80 (0.1 %). Mice were given 0.1ml of the DBZ solution or DMSO vehicle control starting at day 2 after infection (approximately 10 μmol/kg) and continuing daily up to day 6 post-infection, or a total of 5 doses. On day 7 after infection, mice were given pimonidazole (PMDZ) one hour before euthanasia was performed.

Microbiota analysis. Seven days after treatment of mice, DNA from the colon content was extracted using the PowerSoil DNA Isolation kit (Mo-Bio, Carlsbad, CA) according to the manufacturer's protocol. Bacterial DNA was amplified via a PCR enrichment of the 16S rDNA (V4 region) using primers 515F and 806R modified by addition of barcodes for multiplexing. Libraries were sequenced with an Illumina MiSeq system. Sample sequences were demultiplexed and trimmed, followed by filtering for quality. QIIME open-source software (http://qiime.org) (*38*) was used for initial identification of operational taxonomic units (OTU), clustering, and phylogenetic analysis. Samples containing less than 1000 quality reads were removed from dataset. Subsequent data transformation was performed using MEGAN 4 software (http://ab.inf.uni-tuebingen.de/software/megan4/) (*39*) and then further analyzed using Explicet version 2.10.5 (http://www.explicet.org/) (*40*). Data analyzed using METAGENassist (http://www.metagenassist.ca/) was first normalized by logarithmically transforming the reads to yield a more normal distribution (*41*).

Histopathology. Fixed colon sections were stained with hematoxylin and eosin. A veterinary pathologist scored histopathological changes of blinded samples using the scoring scheme described in Figure S4A. For mitotic divisions, the data represent the number of mitotic figures per high power field (40X), with the average of five fields per slide displayed.

RNA isolation. For murine RNA isolation, colon tissue sections were homogenized in a Mini-Beadbeater (BioSpec Products, Bartlesville, OK) and RNA was isolated by the TRI-Reagent method (Molecular Research Center, Inc.) following the manufacturer's protocol. Contaminating DNA was removed using the DNA-free kit (Applied Biosystems) and RNA was stored at -80°C.

Upon *C. rodentium* infection of mice, bacterial RNA was isolated from two compartments: the intestinal colon contents and mucus layer. During necropsy, a section of the middle colon containing a fecal pellet was removed and cut longitudinally. The fecal pellet was carefully removed to avoid pellet disintegration and stored in RNAlater (Ambion) overnight at 4°C. Forceps were next used to gently scrape off the mucus layer from the underlying tissue. The mucus layer was also stored in RNAlater overnight at 4°C. Sample isolation was performed at atmospheric oxygen tensions. Excess solution was subsequently removed from the pellet and Trizol (Invitrogen) was added. Next chloroform was added and the solution was transferred to 2 ml phase-lock tubes (5 Prime) and centrifuged at 14000g. The upper phase was removed and RNA was precipitated with 100% ethanol at -20°C overnight. RNA was collected after centrifugation and washed with 70% ethanol. Contaminating DNA was removed as described above.

For bacterial RNA isolation from cultures, 1 ml of bacterial culture was processed using the Aurum Total RNA mini kit (BioRad) following the manufacturer's protocol. Contaminating DNA was removed as described above.

Quantitative real-time PCR. Isolated RNA was reverse transcribed using random hexamers and Moloney murine leukemia virus reverse transcriptase (Applied Biosystems). Quantitative real-time PCR was performed using SYBR green (Applied Biosystems) PCR mix and the appropriate primer sets (see Table S2) at a final concentration of 0.25 mM. Absolute values were calculated using a series of standards and a standard curve. To generate standards, the above mentioned primer sets were used in standard PCR reaction to amplify the target genes, which were subsequently inserted into pCR2.1 using the TOPO cloning kit (Life Technologies). The resulting plasmids were sequenced for accuracy and the concentration

quantified to create a set of standards ranging from 10^8 to 10^1 copies/µl diluted in a 0.02 mg/ml yeast RNA (Sigma) solution.

To quantify transcription of the regulator of the LEE pathogenicity island, *ler*, RNA was isolated from the colon contents (see above) and qRT-PCR was applied with a published primer pair (*42*). To quantify transcription of *sucA* expression *in vivo*, RNA was isolated from both the mucus layer and colon contents (see above) and qRT-PCR was applied using the primers in Table S2.

Flow cytometry: Flow cytometry analysis was performed for detection of PMDZ staining on whole colon epithelial cells isolated from mock, *C. rodentium*-infected and *C. rodentium escN* mutant-infected mice. Single cell suspensions of colonocytes were obtained as described previously (*43*). Cells were suspended in 2 ml of dPBS and stained with Aqua Live/Dead cell discriminator (Invitrogen) according to the manufacturer's protocol. After Live/Dead staining, cells were washed with dPBS and re-suspended in 100 µl of PBS containing 3.6% of M.O.M.™ mouse Ig blocking reagent (Vector Laboratories) and incubated in the dark at 4°C for 20 min. Cells were washed with 2 ml of dPBS containing 1% bovine serum albumin and 2 mM EDTA (fluorescence-activated cell sorter [FACS] buffer) and then re-suspended in 50 µl of FACS. Cells were stained with a FC receptor blocking antibody, anti-CD16/32 (Biolegend), for 5 minutes at 4°C and then stained for 30 min at 4°C with a cocktail of anti-CD45 PerCp-Cy5.5 (Biolegend) and anti-EpCam FITC (Biolegend). Cells were washed in FACS buffer, fixed and permeabilized with BD Cytofix/Cytoperm™ (BD Biosciences) for 20 minutes at 4°C and then washed with BD Perm/Wash buffer™ (BD Biosciences). Cells were re-suspended in 100 µl of BD Perm/Wash buffer™ containing 3.6% of M.O.M.™ mouse Ig blocking reagent and incubated in the dark at 4°C for 20 min. Cells were washed with BD Perm/Wash buffer™ and then stained with an anti-PMDZ PE antibody (Hypoxyprobe), diluted in BD Perm/Wash buffer™ for 30 min at 4°C. Cells were washed in BD Perm/Wash buffer™ and re-suspended in FACS. For quantification of cell populations, 50 µl of SPHERO AccuCount Fluorescent Particles 10.1 µm (Spherotech) were added to each sample prior to analysis. Calculation of absolute counts

was performed according to manufacturer's protocol. Flow cytometry analysis was performed using a BD (Becton Dickinson) LSRII, and 4.0 x 10^5 events were collected per mouse. Data were analyzed using FlowJo software (Treestar, inc. Ashland, OR) and gates were based on fluorescence-minus-one (FMO) controls.

Fluorescent Imaging. For mouse colon imaging, 10-15 mm sections of mid-colon were frozen in Optimal Cutting Temperature (OCT) compound (Fisher HealthCare) and cut in transverse sections to a thickness of 7μm. Sections were fixed with 4% PFA and permeabilized with 0.2% Triton-X 100. *C. rodentium* cells were stained with a rabbit anti-*Citrobacter* primary antibody (Abcam, ab37056) and a goat anti-rabbit Alexafluor 647conjugate (Abcam, ab150079). Proliferating cells were visualized with a primary rabbit antibody targeting the nuclear protein Ki67 (Abcam, ab15580) and a goat anti-rabbit Alexafluor 647 conjugate. Nuclei were stained with DAPI in SlowFade mounting media (Invitrogen). Actin was stained using phalloidin-tetramethylrhodamine B isothiocyanate (Sigma Aldrich).

For imaging of intestinal hypoxia, at the day of euthanasia mice were treated intraperitoneally with 20 mg per mouse of pimonidazole HCl (Hypoxyprobe). One hour after treatment, mice were euthanized and colon sections were frozen and cryosectioned as stated above. These PMDZ adducts were detected with a mouse monoclonal antibody MAb1 (Hypoxyprobe) followed by a secondary goat anti-mouse IgG antibody (Alexafluor 546, ThermoFisher). After fixation and permeabilization sections were incubated first with Universal Block (KPL) then with an IgG blocking reagent from a Mouse on Mouse (M.O.M) kit (Vector Laboratories). Sections were finally incubated with the anti-PMDZ primary antibody and the secondary anti-mouse Alexafluor 546 antibody.

PMDZ and Ki67 staining was quantified using ImageJ 1.49v software (*44*). For PMDZ quantification, staining intensity of the outer colonocytes was normalized to the staining intensity of DAPI. This ratio was then expressed as fold change over the mock control group. For Ki67 quantification, staining intensity of all the cells within a colonic crypt was normalized to the staining intensity of DAPI. This ratio was then expressed as fold change over the mock control group. For both PMDZ and Ki67 quantification, three to four non-overlapping images were used per mouse.

***In vitro* bacterial RNA expression.** To measure gene expression *in vitro*, wild type *C. rodentium* was grown in M9 media supplemented with 1% casamino acids and 0.4% mannose for 16 hours at 37°C under either microaerobic or anaerobic conditions. A microaerobic environment was created by growing bacteria without shaking under environmental oxygen tension while anaerobiosis was achieved by growing bacteria in pre-reduced media in an anaerobe chamber. Experiments were performed in triplicate. RNA was then isolated as described above.

Statistical analysis. Data for our experiments displayed as bar graphs represent the geometric mean and the standard error of the mean. For most experiments, data points were first log transformed and differences between experimental groups were determined on the transformed data using a Student's T-test (for comparing two groups) or ANOVA followed by Fisher's LSD post hoc test (for comparison of more than two groups). If appropriate, outliers were removed using Grubb's test. Data representing the percent of PMDZ positive colonocytes were first arc-sine transformed before applying the ANOVA test. A one-way ANOVA using METAGENassist online software was used to determine statistical significance on the changes in the proportion of microbial taxa from the16S sequencing reads. A *P*-value of less than 0.05 was considered significant.

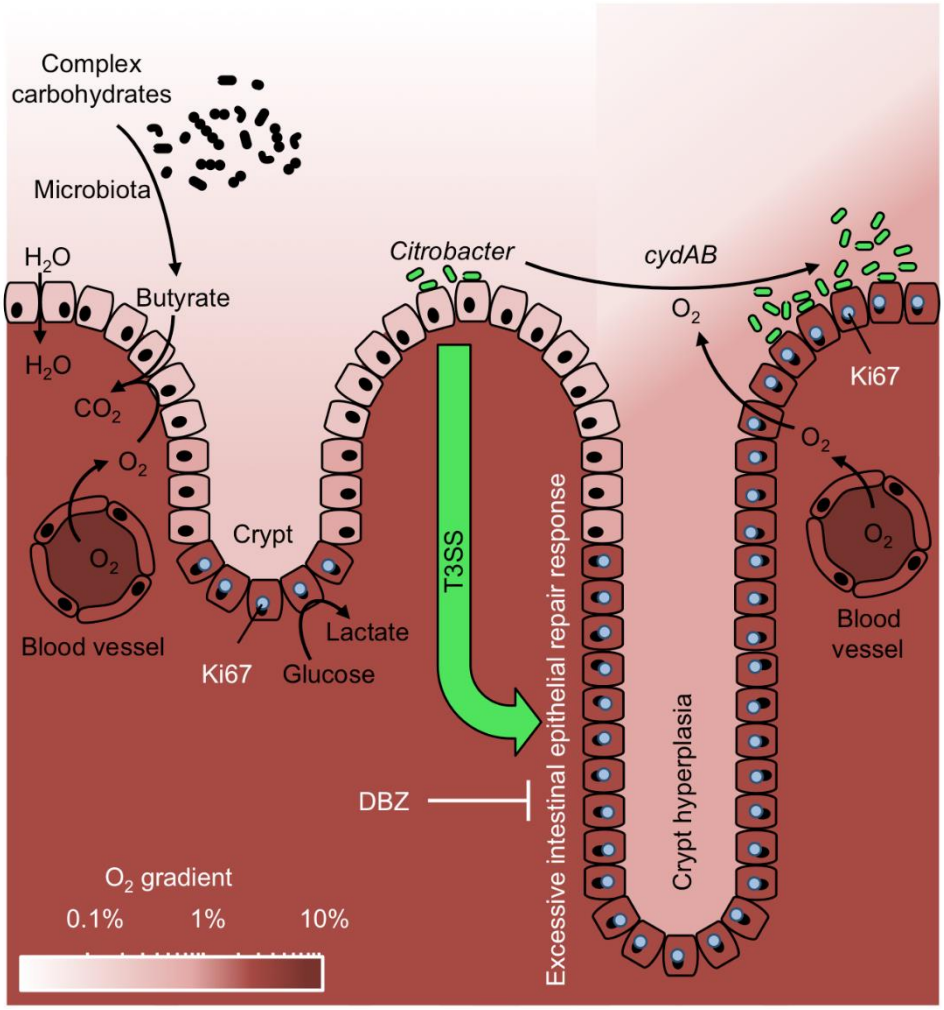

Fig. S2.1: Model for a virulence factor-mediated aerobic expansion of *C. rodentium*.

Mature colonocytes in the healthy colon (left) oxidize microbiota-derived butyrate to carbon dioxide (CO_2) to obtain energy for water (H_2O) absorption, a metabolism that renders the colonic surface hypoxic. In contrast, undifferentiated colonocytes in the crypts, which express the nuclear proliferation marker Ki67, do not consume oxygen (O_2), because they ferment glucose to lactate, an energy metabolism characteristic of growing cells. *C. rodentium* uses its T3SS to induce an excessive epithelial repair response (center). The resulting excessive proliferation of undifferentiated colonocytes leads to crypt hyperplasia, which can be blocked by treatment with the Notch and Wnt signaling pathway inhibitor dibenzazepine (DBZ). Crypt hyperplasia places Ki67-positive undifferentiated colonocytes at the mucosal surface, which

abrogates hypoxia of the colonic surface, thereby driving an aerobic luminal expansion of *C. rodentium* using the *cydAB* genes (right). The scale shown at the left bottom indicates oxygen availability.

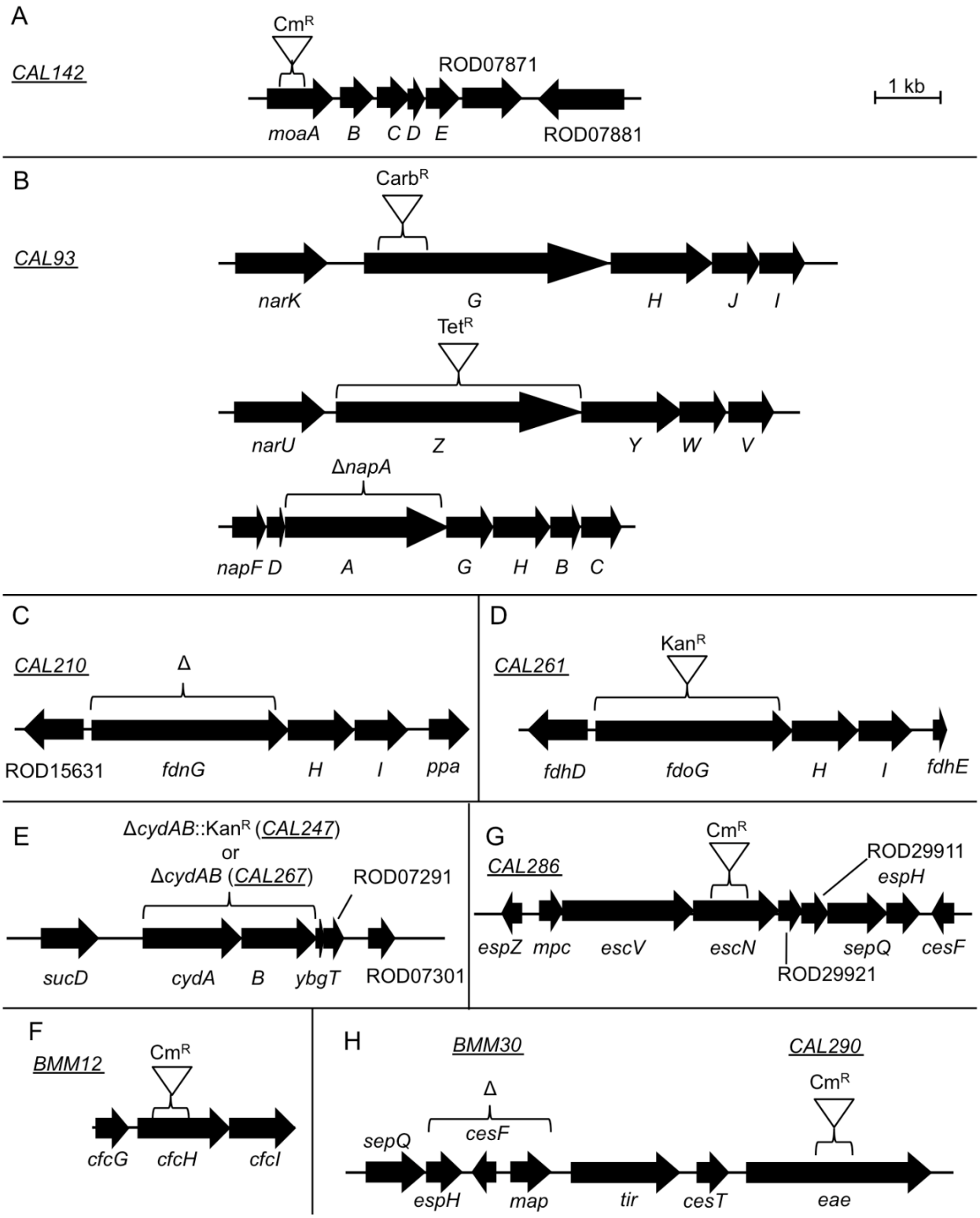
A
CAL142
Cm^R
ROD07871
moaA B C D E
ROD07881
1 kb
B
CAL93
Carb^R
narK G H J I
Tet^R
narU Z Y W V
ΔnapA
napF D A G H B C
C
CAL210
Δ
ROD15631 fdnG H I ppa
D
CAL261
Kan^R
fdhD fdoG H I fdhE
E
ΔcydAB::Kan^R (CAL247)
or
ΔcydAB (CAL267)
ROD07291
sucD cydA B ybgT
ROD07301
G
CAL286
Cm^R
ROD29911
espH
espZ mpc escV escN sepQ cesF
ROD29921
F
BMM12
Cm^R
cfcG cfcH cfcI
H
BMM30
Δ
cesF
sepQ
espH map tir cesT
CAL290
Cm^R
eae

Figure S2.2: Schematic drawing of *C. rodentium* DNA regions relevant for this study. Arrows designate genes. Brackets above arrows indicate size and location of DNA regions deleted in the indicated mutants (CAL142, CAL93, CAL210, CAL261, CAL247, CAL267, CAL286, BMM12, BMM30 or CAL290).

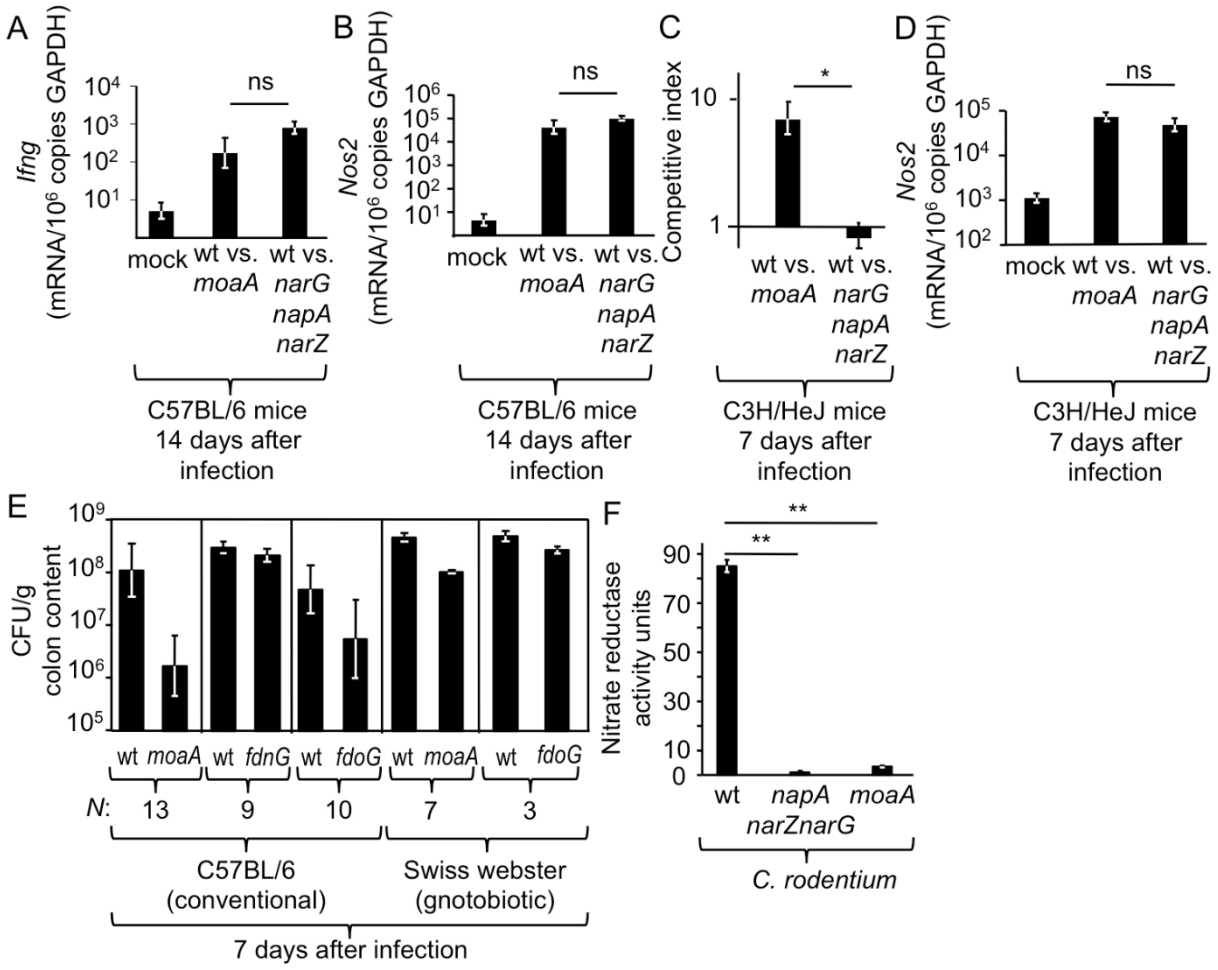

Figure S2.3: Nitrate respiration does not provide an advantage to *C. rodentium* during intestinal growth. C57BL/6 (**A-B**) or C3H/HeJ (**C-D**) mice ($N = 4$) were either mock treated or infected with an equal mixture of the indicated *C. rodentium* strains. Murine mRNA transcript levels for *Ifng* (encoding gamma interferon) (**A**) or *Nos2* (encoding inducible nitric oxide synthase) (**B** and **D**) were quantified in the colon using real time PCR at 14 (**A-B**) or 7 (**D**) days after infection. **(C)** The ratio of *C. rodentium* strains recovered from colon contents 7 days after infection was enumerated on selective media. (**E**) Conventional C57BL/6 mice or germ-free Swiss Webster mice were infected with *C. rodentium* wild type (wt) and either a *moaA* mutant, a *fdnG* mutant, or a *fdoG* mutant. CFU for each strain was determined in colon contents. (**F**) Nitrate reductase activity was determined for the indicated *C. rodentium* strains grown in LB broth

containing 40 mM $NaNO_3$. (**A-E**) Bars represent geometric mean ± standard error. *, $P < 0.05$; **, $P < 0.01$; ns, not statistically significantly different.

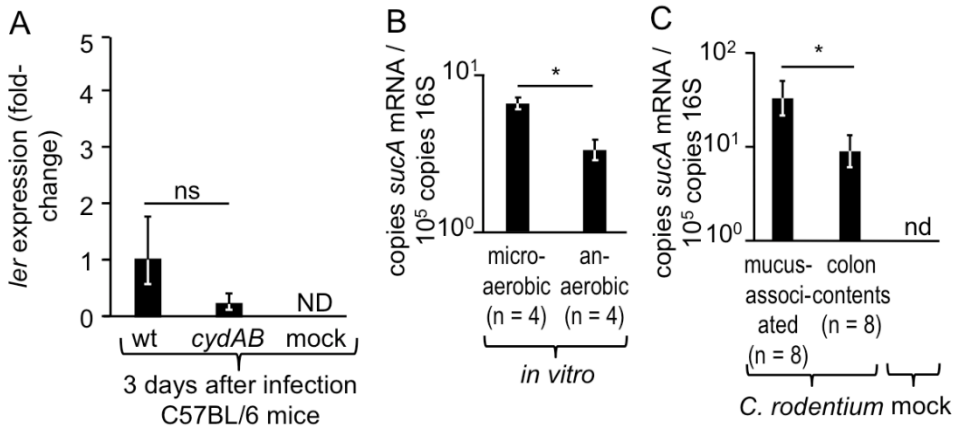

Figure S2.4: Aerobic respiration provides a fitness advantage during *C. rodentium* infection.

(**A**) Transcript levels of the *ler* gene were determined by real-time PCR in colon contents of mock-infected mice or mice infected with the indicated *C. rodentium* strains. Expression is shown as fold-increase over levels observed for *C. rodentium* wild type. **(B)** *C. rodentium* was grown in minimal medium supplemented with mannose as a carbon source under either microaerobic or anaerobic conditions. **(C)** Bacterial RNA was isolated from either mucus scrapings or colon contents of *C. rodentium*-infected mice. (**B-C**) Absolute transcript levels of *sucA* were quantified by real-time PCR and normalized to 16S rRNA levels. See Fig. 1E and 1F for fold-increases in *sucA* transcripts. (**A-C**) Bars represent geometric mean ± standard error. *, $P < 0.05$; ns, not statistically significantly different; ND, none detected.

A Histopathology scoring for colon

Score	Infiltration with inflammatory cells*	Submucosal edema	Epithelial damage	Combined score	Description
0	no infiltration	not present	not present	0 to 1	normal
1	mild multifocal to diffuse infiltration	mild (1-20%)	mild focal to multifocal enterocyte hyperplasia; mild loss of goblet cells	2 to 4	mild inflammation
2	moderate multifocal to diffuse infiltration	moderate (20-40%)	moderate multifocal enterocyte hyperplasia; moderate loss of goblet cells	5 to 7	moderate inflammation
3	severe diffuse infiltration	severe (>40%)	severe multifocal to diffuse enterocyte hyperplasia; severe loss of goblet cells	> 7	severe inflammation

* accumulation of mononuclear cells and neutrophils in the lamina propria

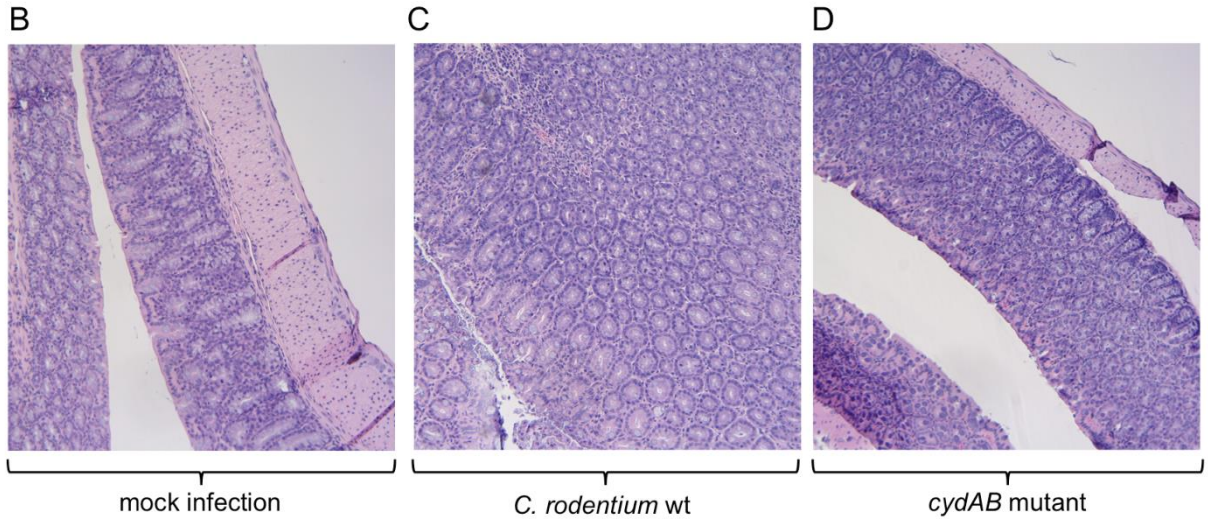

Figure S2.5: Histopathology scoring for colon. (**A**) Criteria for scoring blinded hematoxylin and eosin (H&E) stained sections from the colon is shown on the left. Interpretation of combined overall histopathology scores is shown on the right. (**B-D**) Representative images (10x) objective of colonic sections from mock-treated mice (**B**), mice infected with *C. rodentium* wild type (wt) (**C**) or mice infected with a *cydAB* mutant (**D**) seven days after infection.

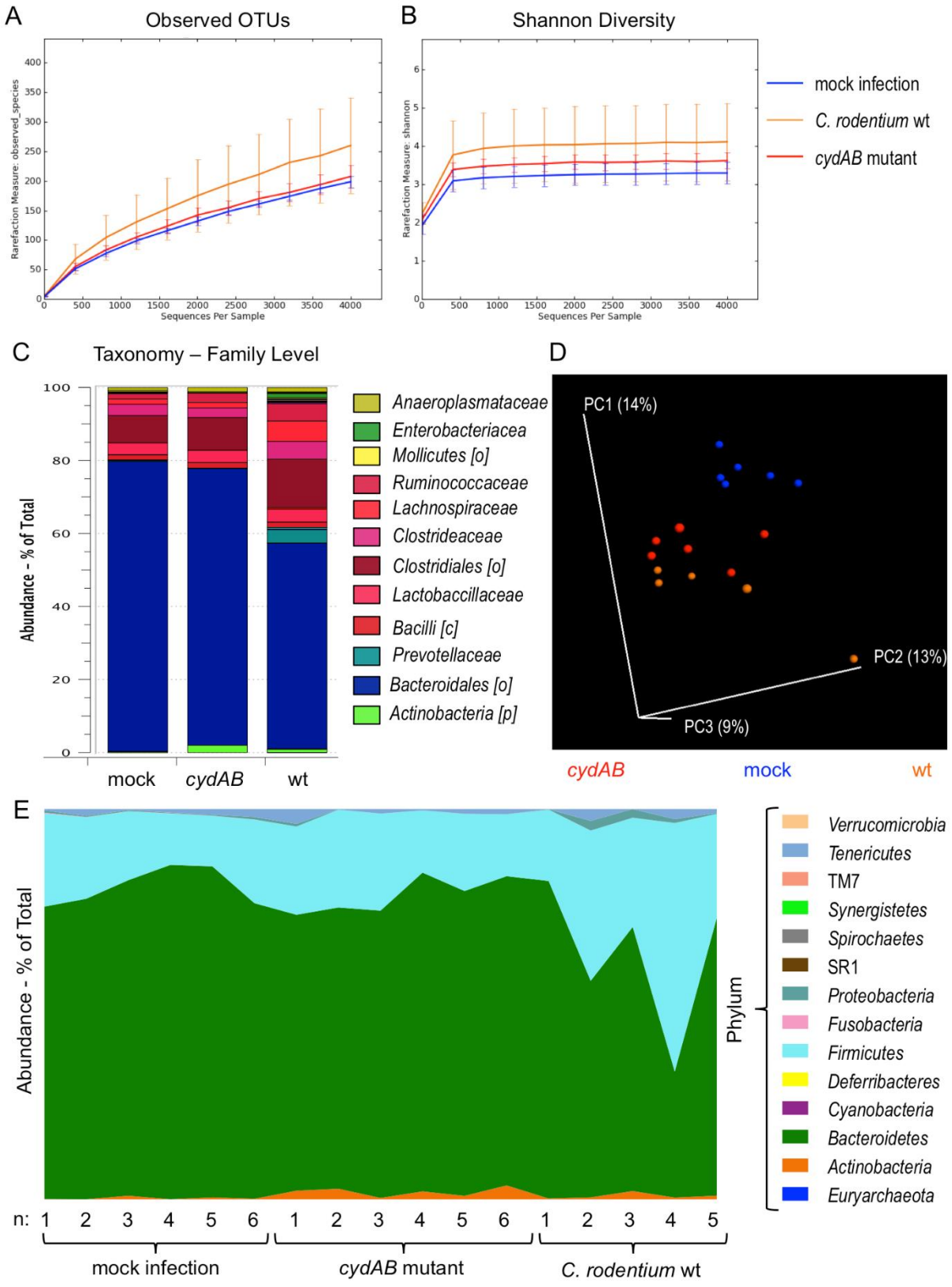
A
Observed OTUs
Rarefaction Measure: observed_species
Sequences Per Sample
B
Shannon Diversity
Rarefaction Measure: shannon
Sequences Per Sample
mock infection
C. rodentium wt
cydAB mutant
C
Taxonomy – Family Level
Abundance - % of Total
mock
cydAB
wt
Anaeroplasmataceae
Enterobacteriacea
Mollicutes [o]
Ruminococcaceae
Lachnospiraceae
Clostrideaceae
Clostridiales [o]
Lactobaccillaceae
Bacilli [c]
Prevotellaceae
Bacteroidales [o]
Actinobacteria [p]
D
PC1 (14%)
PC2 (13%)
PC3 (9%)
cydAB
mock
wt
E
Abundance - % of Total
n: 1 2 3 4 5 6 1 2 3 4 5 6 1 2 3 4 5
mock infection
cydAB mutant
C. rodentium wt
Phylum
Verrucomicrobia
Tenericutes
TM7
Synergistetes
Spirochaetes
SR1
Proteobacteria
Fusobacteria
Firmicutes
Deferribacteres
Cyanobacteria
Bacteroidetes
Actinobacteria
Euryarchaeota

Figure S2.6: Microbiota analysis. Mice (n indicated in **C**) were either mock-treated, infected with the *C. rodentium* wild type (wt) or a with a *cydAB* mutant and microbial diversity in colon contents analyzed 7 days later by 16S rRNA gene sequencing. **(A)** Rarefaction curve reflecting number of observed operational taxonomic units (OTUs, labeled as 'species' on Y axis) per number of sequences. **(B)** Species diversity based on Shannon Diversity measure. Plots generated using QIIME software with data representing combined data from all samples in each group. (**C**) Percent of total abundance for family-level taxa. Plot generated using Explicet software with data representing averages for all mice in each group that contained greater than 1000 quality reads. Color-coding for families is shown on the right. (**D**) Area plot showing percent of total abundance for phyla-level taxa. The plot was generated using QIIME software. Color-coding for phyla is shown on the right. (**E**) Principle component analysis of 16S profiling data. Each dot represents data from one animal.

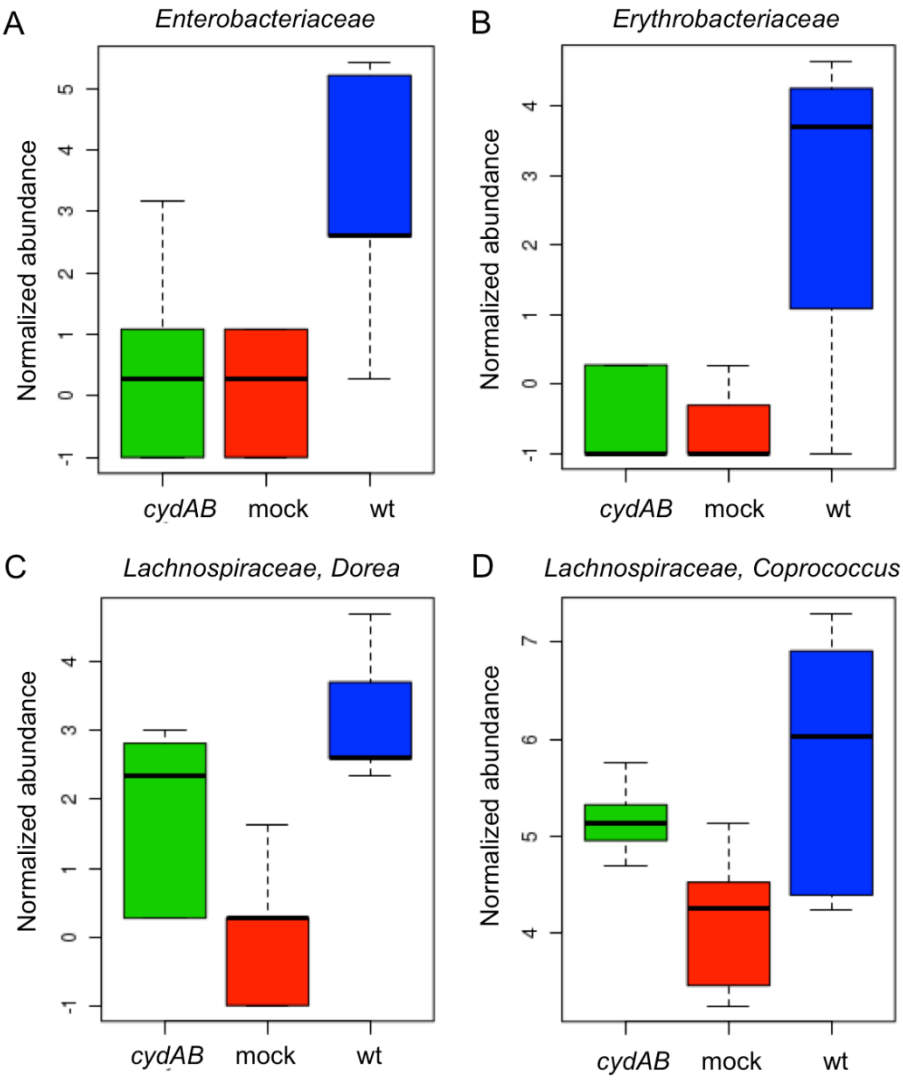

Figure S2.7: Normalized abundances of selected groupings. Normalized abundances of members of the family *Enterobacteriaceae* (**A**), of the family *Erythrobacteriaceae* (**B**) of the genus *Dorea* (family *Lachnospiraceae*) (**C**) and the genus *Coprococcus* (family *Lachnospiraceae*) (**D**) in colon contents at seven days after infection. Boxes in whisker plots represent the second and third quartiles, while lines indicate the first and fourth quartiles.

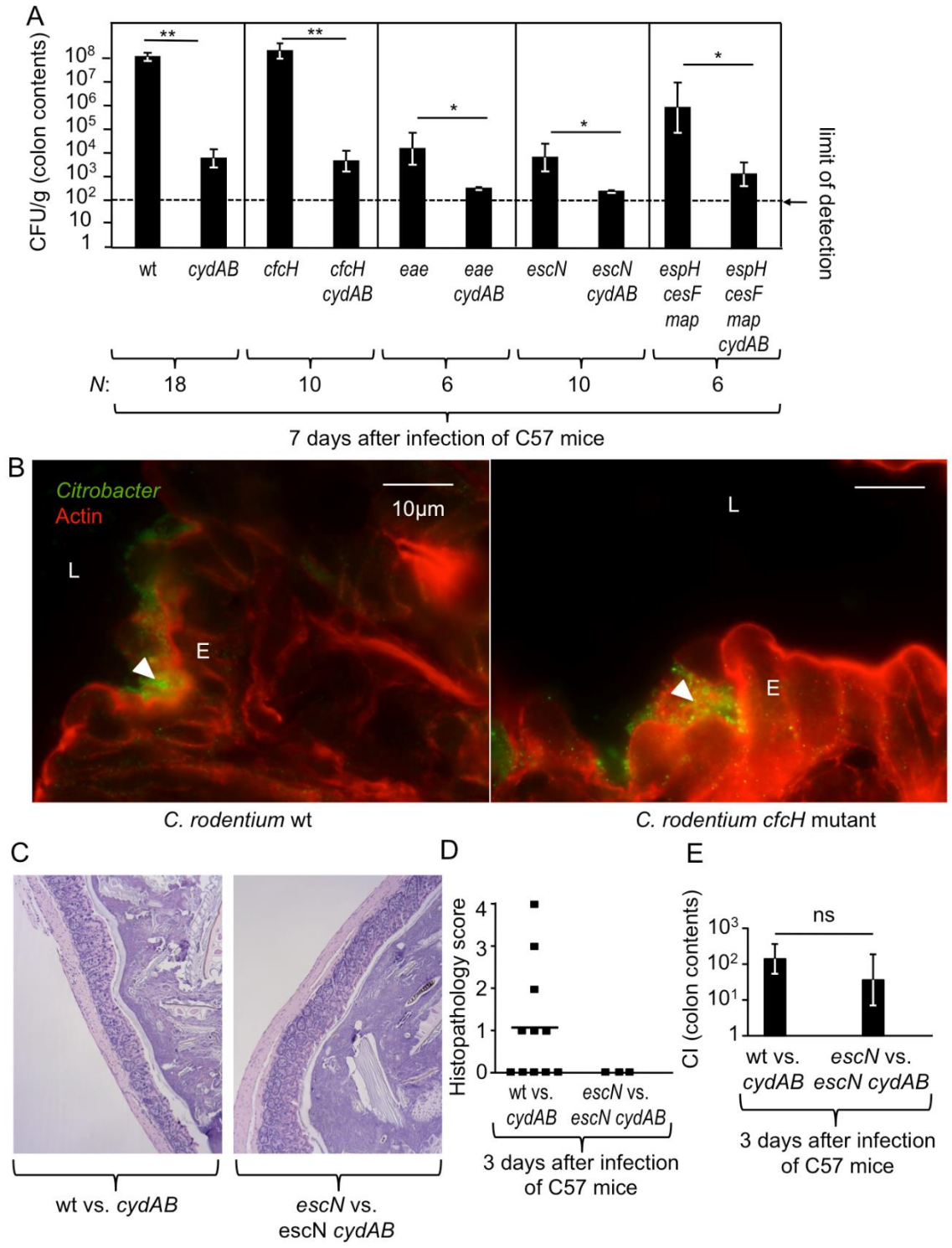

Figure S2.8: A *cydAB*-mediated *C. rodentium* expansion is T3SS-dependent.

Mice were infected with the indicated *C. rodentium* strain mixtures **(A, C, D and E)** or *C. rodentium* strains (**B**) and organs collected at three days (**C-D**) or seven days after infection (**A-B**). (**A**)

CFU for each strain was determined in colon contents. (B) Representative images of colonic sections from mice infected with the *C. rodentium* wild type (wt) or a *cfcH* mutant stained for detection of *Citrobacter* (arrow heads, green fluorescence) and actin (red fluorescence). **(C)** Representative images of H&E stained colonic sections for data shown in panel **D**. **(D)** Histopathology scores determined three days after infection. Each rectangle represents data from one animal. (**E**) Competitive index determined for the indicated strain mixture in colon contents. L, lumen; E, epithelium; *, $P < 0.05$; **, $P < 0.01$; ns, not statistically significantly different.

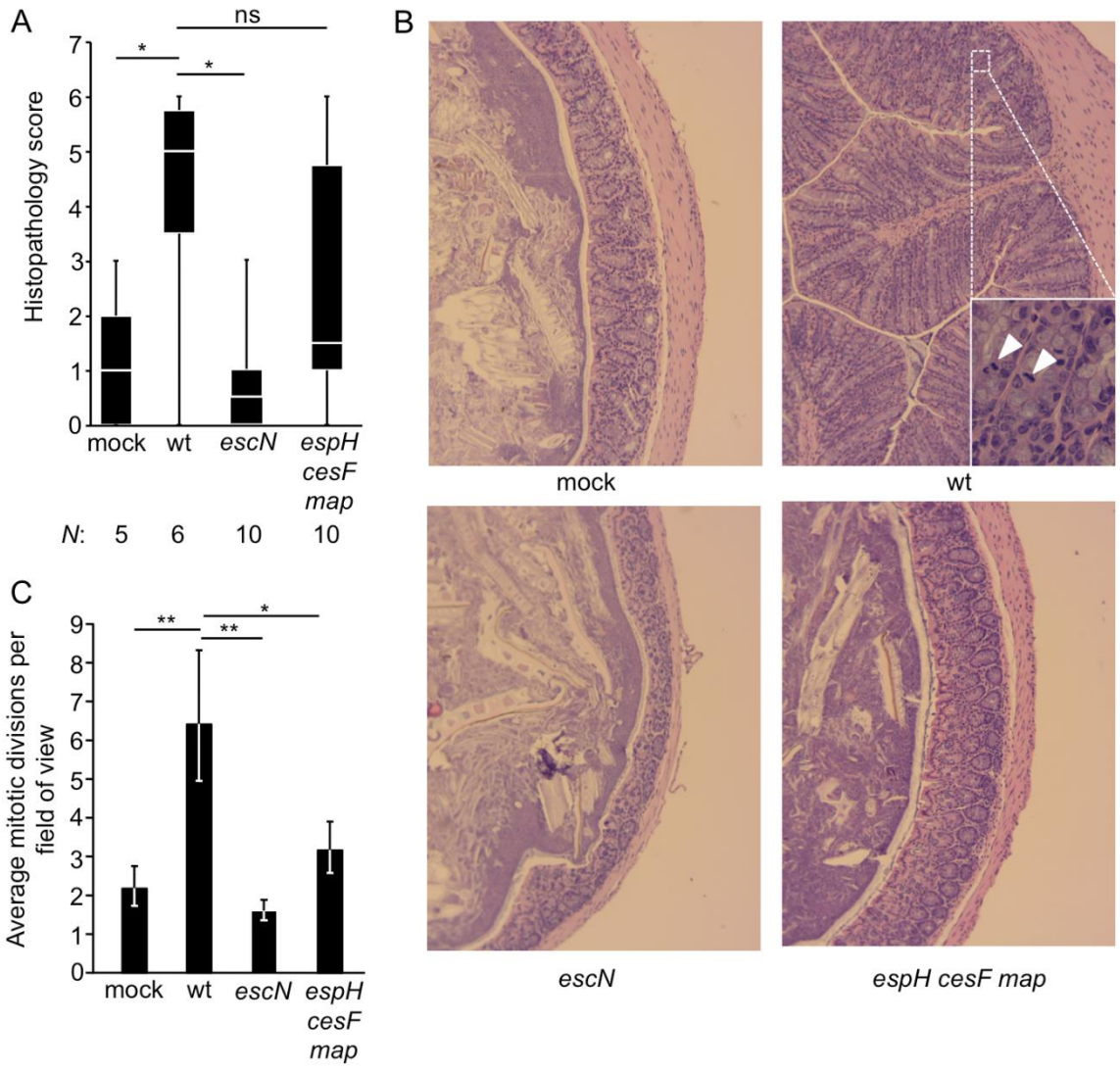

Fig. S2.9: Contribution of the T3SS to the development of histopathological changes during *C. rodentium* infection.

Mice (C57BL/6) were mock-infected or infected with the indicated *C. rodentium* strains and the colon collected for analysis seven days after infection. (**A**) The histopathology score was determined for colonic sections from the indicated numbers of animals. Boxes in Whisker plots represent the second and third quartiles of combined histopathology scores, while lines indicate the first and fourth quartiles. (**B**) Representative images of H&E stained colonic sections (taken with a 10x objective) for data shown in panel **A**. Arrowheads point to chromosomal condensation indicative of mitotic division, which was scored in

panel **C**. The insert in the top right panel was taken with a 40x objective. (**C**) The number of mitotic divisions in the epithelium per microscopic field was scored for sections form the indicated groups. *, $P < 0.05$; **, $P < 0.01$; ns, not statistically significantly different; wt, wild type.

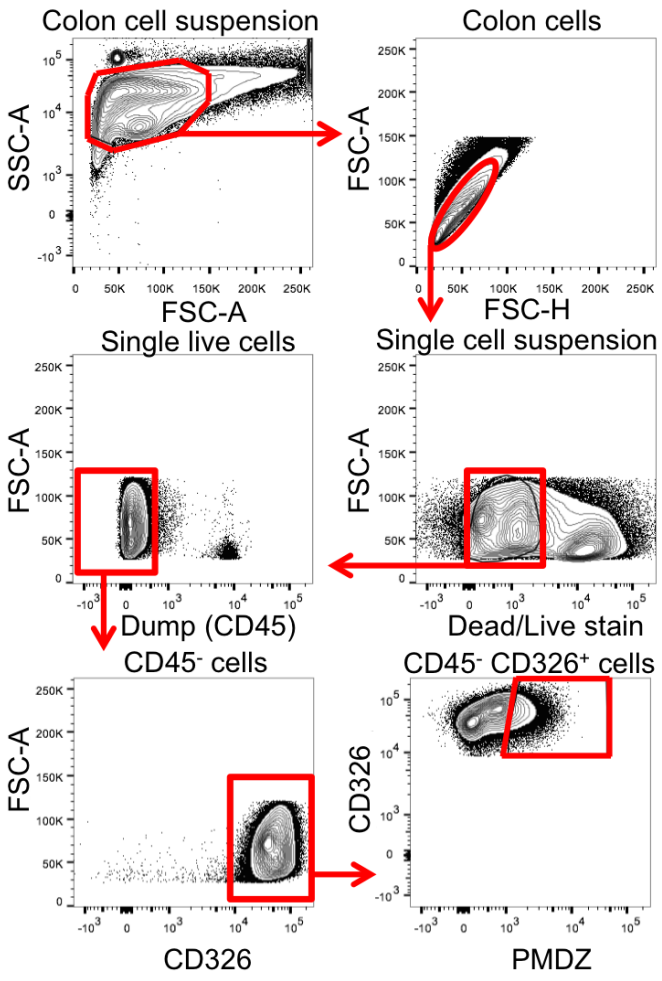

Fig. S2.10: Gating strategy for quantification of PMDZ$^+$ epithelial cells.

The epithelium was lifted from the colonic mucosa by EDTA treatment to prepare single cell preparations (top panels), which were stained with live/dead stain (middle right panel). Single live cells were stained with the lymphocyte marker CD45, which is expressed by intraepithelial lymphocytes (middle left panel) and gated for CD45$^-$ cells. CD45$^-$ cells were then gated for expression of the epithelial cell marker CD326 (also known as EpCAM)(bottom left panel), followed by gating for PMDZ$^+$ cells (bottom right panel).

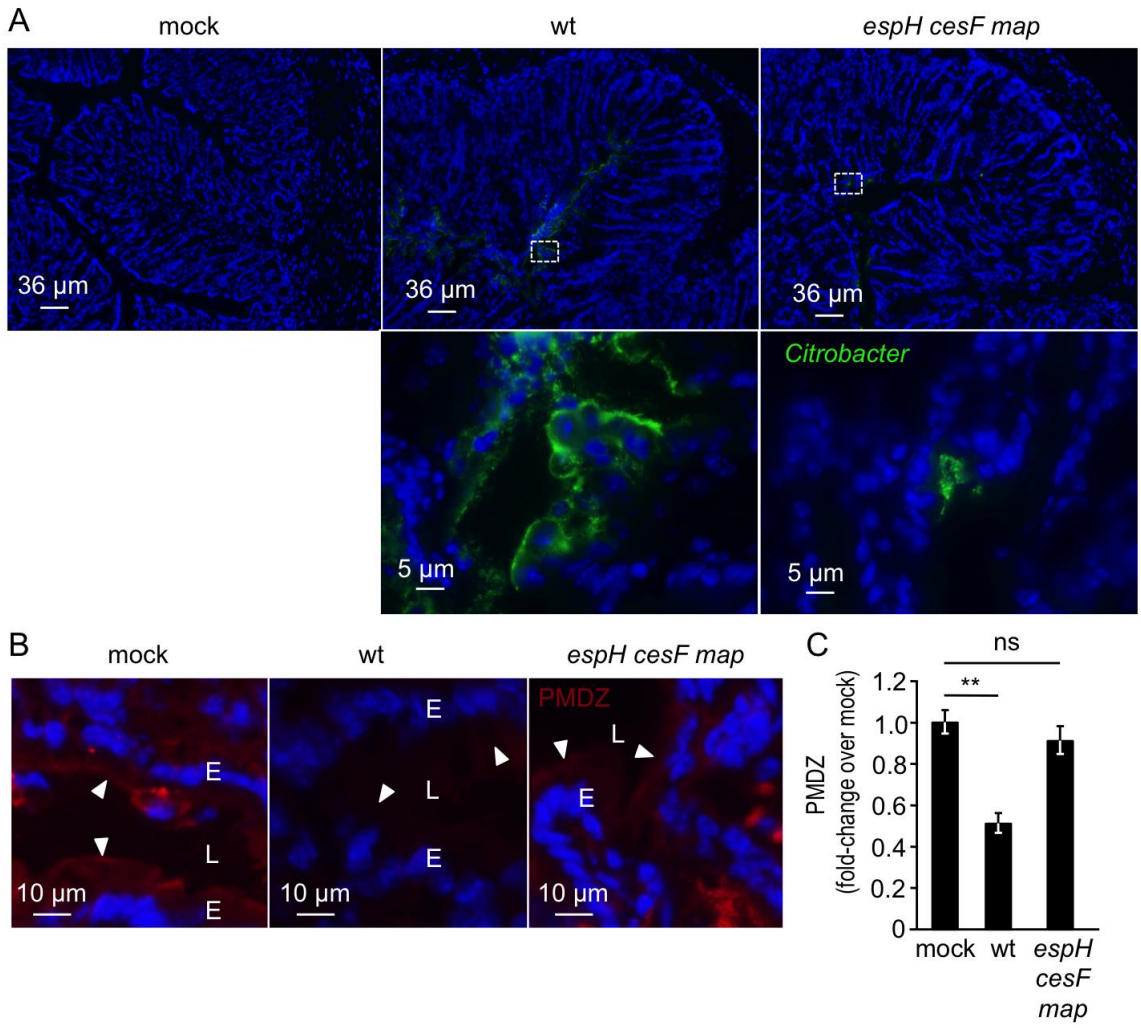

Fig. S2.11: The *C. rodentium* wild type, but not a *espH cesF map* mutant, reduces epithelial hypoxia during infection.

Mice were mock-infected (mock) or infected with the *C. rodentium* wild type (wt) or a *espH cesF map* mutant and the colon collected seven days after infection. (**A**) *C. rodentium* (green fluorescence) was detected in sections counterstained with DAPI nuclear stain (blue fluorescence). Representative images are shown. (**B**) Representative images of colonic sections stained to detect pimonidazole (PMDZ) hypoxia stain (red fluorescence) and counterstained with DAPI nuclear stain (blue fluorescence). Arrow heads point to the mucosal surface. E, epithelial cell; L, lumen. **(C)** Pimonidazole staining was quantified by image

analysis. Bars represent geometric mean ± standard error. **, $P < 0.01$; ns, not statistically significantly different.

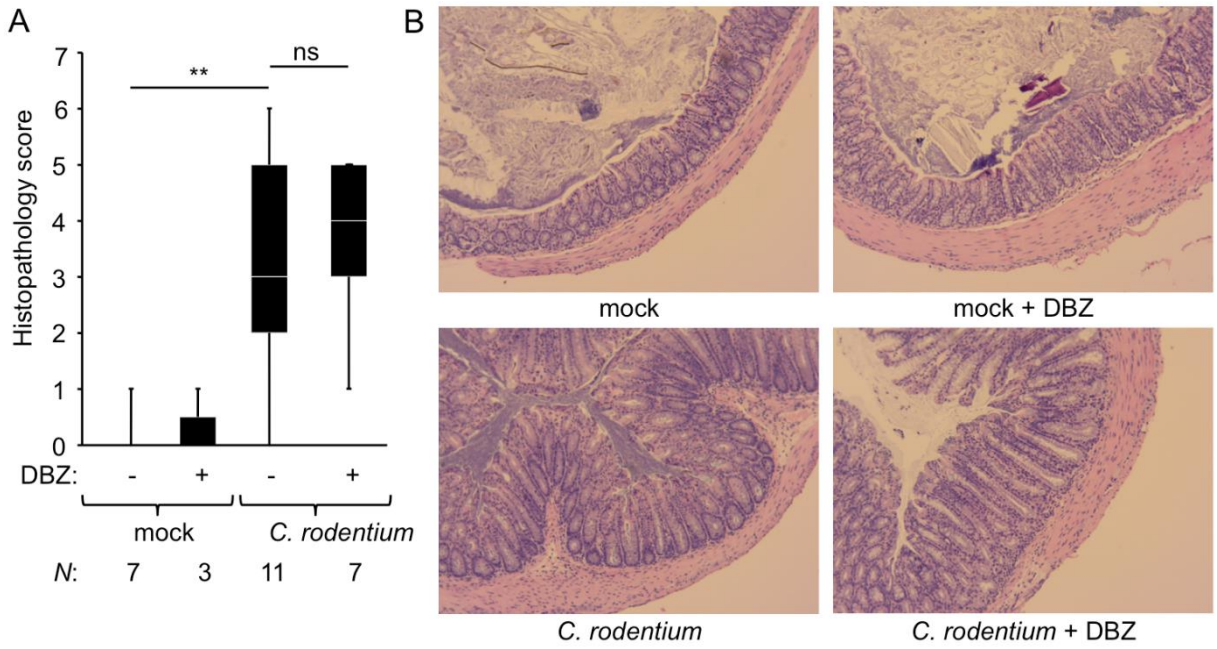

Fig. S2.12: DBZ treatment does not reduce the severity of histopathological changes during *C. rodentium* infection.

C57BL/6 mice were mock-infected (mock) or infected with the *C. rodentium* wild type (wt) or an *espH cesF map* mutant. Mice were either treated with dibenzazepine (DBZ) or with vehicle control. (**A**) The histopathology score was determined for colonic sections from the indicated numbers of animals. Boxes in Whisker plots represent the second and third quartiles of combined histopathology scores, while lines indicate the first and fourth quartiles. (**B**) Representative images of H&E stained colonic sections (taken with a 10x objective) for data shown in panel **A**. **, $P < 0.01$; ns, not statistically significantly different.

Table S2.1: Bacterial strains and plasmids used in this study

***Citrobacter rodentium* strains**

DBS100	wild type; ATCC 51459	(*45*)
CAL60	DBS100 Δ*napA*::Tet^R (pWSK129)	This study
CAL77	DBS100 Δ*napA* (pWSK129)	This study
CAL92	DBS100 Δ*napA* Δ*narZ*::Tet^R (pWSK129)	This study
CAL93	DBS100 Δ*napA* Δ*narZ*::Tet^R *narG*::pCAL6 (pWSK129)	This study
CAL142	DBS100 *moaA*::pCAL34	This study
CAL210	DBS100 Δ*fdnG*	This study
CAL247	DBS100 Δ*cydAB*::Kan^R	This study
CAL261	DBS100 Δ*fdoG*::Kan^R	This study
CAL267	DBS100 Δ*cydAB*	This study
CAL286	DBS100 *escN*::pCAL81	This study
CAL287	DBS100 Δ*cydAB*::Kan^R *escN*::pCAL81	This study
CAL290	DBS100 *eae*::Cm^R	This study

CAL291	DBS100 *eae*::Cm^R *cydAB*	This study
BMM11	DBS100 *cfcH*::pBMM1 *ΔcydAB*::Kan^R	This study
BMM12	DBS100 *cfcH*::pBMM1	This study
BMM30	DBS100 *ΔespH cesF map*	This study
BMM40	DBS100 *ΔespH cesF map ΔcydAB*::Kan^R	This study

***E. coli* strains**

DH5*α λpir*	F- *endA1 hsdR17* (r^-m^+) *supE44 thi-1 recA1 gyrA relA1 Δ(lacZYA-argF)$_{u189}$ Φ80lacZΔM15 λpir*	*(46)*
S17-1*λpir*	C600::RP4 2-(*tet::Mu*) (*kan::Tn7*) λpir *recA1 thi pro hsdR* (r^-m^+)	(*47*)
Top 10	Φ80lacZΔM15 *lacX74 recA1 araD139* Δ(*ara-leu*) 7697 *galU galK rpsL endA1 nupG*	Invitrogen

Plasmids

pWSK129	*ori*(pSC101) Kan^R	(*48*)
pCR2.1 cloning vector		Invitrogen

pGP704	oriR6K mobRP4 bla	(*49*)
pRDH10	*sacRB cat ori*R6K *mobRP4*, Tet^R	(*50*)
pUC4 KSAC	ori(pMB1) bla Kan^R	Pharmacia (GE Healthcare)
pEP185.2	oriR6K *mobRP4* Cm^R	(*51*)
pSW172	ori(R101) *repA*101ts $Carb^R$	(*12*)
pSPN23	pBluescriptII KS+, $Carb^R$, Tet^R	(*52*)
pCAL6	Intragenic *narG* region in pGP704	This study
pCAL7	pRDH10 with regions upstream and downstream of *napA*	This study
pCAL8	pRDH10 with regions upstream and downstream of *narZ*	This study
pCAL15	pRDH10 with regions upstream and downstream of *narZ* flanking a Tet^R cassette	This study
pCAL17	pRDH10 with regions upstream and downstream of *napA* flanking a Tet^R cassette	This study
pCAL34	Intragenic *moaA* region in pEP185.2	This study

pCAL52	pRDH10 with *phoN* gene from *S. enterica* serovar Typhimurium	This study
pCAL55	pCAL52 with regions upstream and downstream of *fdnG*	This study
pCAL59	pCAL52 with regions upstream and downstream of *cydAB*	This study
pCAL60	pCAL52 with regions upstream and downstream of *cydAB* flanking a Kan^R cassette	This study
pCAL72	pCAL52 with regions upstream and downstream of *fdoG*	This study
pCAL74	pCAL52 with regions upstream and downstream of *fdoG* flanking a Kan^R cassette	This study
pCAL81	Intragenic *escN* region in pEP185.2	This study
pBMM1	Intragenic *cfcH* region in pEP185.2	This study
pBMM3	pRDH10 with regions upstream of *espH* and downstream of *map*	This study

Table S2.2: PCR primers used in this study*

Gene	Organism	Sequence
napA	*C. rodentium*	5'-GCATGCGCACATTCTTAACCGC-3'
		5'-ACATCTAGAATGGCGTTTCCTCACC-3'
		5'-GGATCTAGAAGGTGTAAGCCATCATGTCC-3'
		5'-GCATGCTCGGTCAACGGAACGG-3'
narZ	*C. rodentium*	5'-CACTCTAGAGACATTTCTCCTGCTCC-3'
		5'-GCATGCTTACCTGTGTTCACCTTCC-3'
		5'-TATTCTAGATGGATGGTGAAGGTCGGG-3'
		5'-GCATGCTTCCAGTCCATCGCC-3'
narG	*C. rodentium*	5'-ACATCTAGAAAGACGCCGACAAAGC-3'
		5'-TCAGCATGCCAGGCGATAATGTAGC-3'
moaA	*C. rodentium*	5'-TACCCTCGAGATCCGCCAGATAGCCGTCAC-3'
		5'-TTAGGAGCTCGCCGATTTCACCCACATAGTC-3'
cydAB	*C. rodentium*	5'-ACCTGTCGACCCAAACCCTTCATTCACC-3'
		5'-GACATCTAGAGACTCCTTGCTCATCG-3'
		5'-ACTGTCTAGATTTCGCCTGGATTCTG-3'
		5'-TCAAGTCGACCGTGAAAACCATAGAGG-3'
fdnG	*C. rodentium*	5'-TTACGCATGCACGCAGACCATTATCGC-3'
		5'-GCGATCTAGAGGAAACTAACAGCAATACC-3'

		5’-CGATTCTAGATGACTCCAACTCGCAAACG-3’
		5’-CATAGCATGCGCCACCAGGAAGAAGC-3’
fdoG	*C. rodentium*	5’-TTATGCATGCTATTATCCTGCCATCAACC-3’
		5’-CGAATCTAGAGGAGTTGTGACAGAATACC-3’
		5’-AGTTTCTAGAGGTATTCCGATTCACTGG-3’
		5’-AGTGGCATGCTTATCATCTTCCTCTTGC-3’
escN	*C. rodentium*	5’-ACTAGTGGATCCCCCATTATTGTCCTTGCCCTTATC-3’
		5’-GAATTCCTGCAGCCCAAGAAAAAACACTCGGGG-3’
phoN	*S. Typhimurium*	5’-CGTCCTGCTTTTTTACCTG-3’
		5’-CACTTCCTTTCATTTGCTG-3’
espH	*C. rodentium*	5’-GCGACCACACCCGTCCTGTGCTACCATTCCCCCTTGTCGC-3’
cesF		5’-CCATCGGATTGAGCAGTGCGGTAAAGGAGT-3’
map		
		5’-CGCACTGCTCAATCCGATGGTGACGCTGTT-3’
		5’-ACGATGCGTCCGGCGTAGAGCGCACCTGGATGGACTGATT-3’

qRT-PCR

Gene	Organism	Sequence
Ifng	Mouse	5’-CAACAGCAAGGCGAAAAAGGATGC-3’
		5’-CCCCGAATCAGCAGCGACTCC-3’
Nos2	Mouse	5’-CCTCTTTCAGGTCACTTTGGTAGG-3’
		5’-TTGGGTCTTGTTCAGCCACGG-3’
Gapdh	Mouse	5’-TGTAGACCATGTAGTTGAGGTCA-3’
		5’-AGGTCGGTGTGAACGGATTTG-3’
sucA	*C. rodentium*	5’-TACCTGGTCGCCGTATCTCA-3’
		5’-AGTCGAACAGCTTCTCACCG-3’
16S rRNA	*Enterobacteriaceae*	5’-GTGCCAGCMGCCGCGGTAA-3’
		5’-GCCTCAAGGGCACAACCTCCAAG-3’

*Restriction sites underlined

Chapter 3

Anaerobic respiration of NOX1-derived hydrogen peroxide licenses bacterial growth at the colonic surface

Brittany M. Miller[1], Megan J. Liou[1], Lillian F. Zhang[1], Henry Nguyen[1], Yael Litvak[1,2], Eva-Magdalena Schorr[1], Kyung Ku Jang[1,3], Connor R. Tiffany[1], Brian P. Butler[4], Andreas J. Bäumler[1,*]

[1] Department of Medical Microbiology and Immunology, School of Medicine, University of California at Davis, One Shields Ave; Davis CA 95616, USA

[2] Department of Biological Chemistry, The Alexander Silberman Institute of Life Sciences, The Hebrew University of Jerusalem, Edmond J. Safra Campus Givat-Ram, Jerusalem 9190401, Israel

[3] Present address: Department of Microbiology, New York University School of Medicine, New York, NY 10016, USA

[4] Department of Pathobiology, School of Veterinary Medicine, St. George's University, Grenada, West Indies

Published in:

Miller BM, Liou MJ, Zhang LF, Nguyen H, Litvak Y, Schorr EM, et al. (2020) Anaerobic respiration of NOX1-derived hydrogen peroxide licenses bacterial growth at the colonic surface. Cell Host Microbe 28(6): 789-797. https://doi.org/10.1016/j.chom.2020.10.009

SUMMARY

The colonic microbiota exhibits cross-sectional heterogeneity, but the mechanisms that govern its spatial organization remain incompletely understood. Here we used *Citrobacter rodentium*, a pathogen that colonizes the colonic surface, to identify microbial traits that license growth and survival in this spatial niche. Previous work shows that during colonic crypt hyperplasia, type III secretion system (T3SS)-mediated intimate epithelial attachment provides *C. rodentium* with oxygen for aerobic respiration. However, prior to the development of colonic crypt hyperplasia, T3SS-mediated intimate attachment was not required for aerobic respiration, but for hydrogen peroxide (H_2O_2) respiration using cytochrome *c* peroxidase (Ccp). The epithelial NADPH oxidase NOX1 was the primary source of luminal H_2O_2 early after *C. rodentium* infection and was required for Ccp-dependent growth. Our results suggest that NOX1-derived H_2O_2 is a resource that governs bacterial growth and survival in close proximity to the mucosal surface during gut homeostasis.

INTRODUCTION

By supplying the habitat, the host wields a prominent influence over microbial growth at body surfaces (Byndloss et al., 2018; Foster et al., 2017). Host-derived resources that limit the range of successful traits within the microbiota can be viewed as habitat filters (Costello et al., 2012; Tiffany and Baumler, 2019). These host control mechanisms are important for shaping the size, species composition, and spatial organization of microbial communities (Litvak and Baumler, 2019), but in many cases their identity remains to be determined.

One habitat filter that shapes the microbiota composition in the large intestine is epithelial hypoxia, which selects for microbial traits that permit survival and growth by maintaining anaerobiosis, thereby driving the species composition towards a dominance of obligate anaerobic bacteria (Litvak et al., 2018; Litvak et al., 2017; Rigottier-Gois, 2013; Rivera-Chavez et al., 2017). The importance of this host control mechanism for maintaining the microbiota composition was first identified during studies investigating how enteric pathogens use their virulence factors to invade the gut ecosystem (Lopez et al., 2016; Rivera-Chavez et al., 2016). Type III secretion systems (T3SSs) of the facultative anaerobic pathogens *Salmonella enterica* and *Citrobacter rodentium* (phylum *Proteobacteria*) shift epithelial metabolism from oxidative phosphorylation in the mitochondria to aerobic glycolysis (the conversion of glucose into lactate even in the presence of oxygen), thereby abrogating epithelial hypoxia in the colon (Carson et al., 2019; Gillis et al., 2018; Gillis et al., 2019; Lopez et al., 2016; Rivera-Chavez et al., 2016). The consequent increase in epithelial oxygenation drives a luminal pathogen expansion through aerobic respiration (Lopez et al., 2016; Rivera-Chavez et al., 2016), thereby causing a dysbiotic shift in the microbiota composition from obligate to facultative anaerobes (Lupp et al., 2007; Stecher et al., 2007). These findings suggest that pathogens are useful tools for microbiome research, because their virulence factors target host-derived habitat filters that are important for balancing the microbiota (Spiga et al., 2017).

In addition to functions that shape the species composition, the large intestine features host control mechanisms that structure the spatial organization of microbial communities. The lumen of the large

intestine is not a homogenous environment, but the colonic microbiota exhibits cross-sectional heterogeneity in its spatial organization (Albenberg et al., 2014; Yasuda et al., 2015). The loose outer mucus layer is thought to be enriched in bacteria utilizing host-derived mucin, such as certain species belonging to the *Verrucomicrobia* and *Bacteroidetes* phyla (Berry et al., 2015; Li et al., 2015). Closer to the epithelium, host-derived oxygen radiates from the epithelial surface, which is thought to increase the proportion of "oxygen-tolerant" organisms of the *Proteobacteria* and *Actinobacteria* phyla (Albenberg et al., 2014), thereby helping to maintain an inner mucus layer that is largely devoid of bacteria (Johansson et al., 2008). However, our mechanistic understanding of the biogeography in the colon is still incomplete and it is likely that additional elements contributing to this process remain to be identified.

To elucidate spatial relationships between bacteria and their hosts, we used *C. rodentium*, a luminal pathogen that uses a T3SS to intimately attach to the epithelial surface in the cecum and colon of mice (Schauer and Falkow, 1993a, b). The T3SS is required for intestinal colonization by *C. rodentium*, suggesting that intimate attachment to the epithelial surface provides the pathogen with resources to compete with the gut microbiota (Kamada et al., 2012). The T3SS triggers a histopathological lesion, termed colonic crypt hyperplasia (Barthold et al., 1976), within a week after infection, thereby increasing epithelial oxygenation to enable the pathogen to respire oxygen using cytochrome *bd* oxidase (Lopez et al., 2016). However, prior to the development of intestinal lesions, the T3SS provides a growth advantage that is independent of cytochrome *bd* oxidase (Lopez et al., 2016). We reasoned that prior to the development of histopathological lesions, T3SS-mediated intimate attachment might provide *C. rodentium* access to unknown resources that license bacterial growth in close proximity to the epithelial surface. The goal of this study was to identify these resources.

RESULTS

The *C. rodentium* T3SS drives early growth using cytochrome *c* peroxidase

Salmonella enterica serovar (*S.*) Typhimurium uses its T3SSs to trigger intestinal inflammation (Tsolis et al., 1999), thereby orchestrating global changes in the environment inhabited by the microbiota (Rivera-Chavez et al., 2016; Winter et al., 2010). As a result, inflammation triggered by wild-type *S.* Typhimurium can rescue luminal growth of an avirulent *S.* Typhimurium mutant lacking both T3SSs (*invA spiB* mutant) when mice are inoculated with a mixture of both strains (**Fig. 3.1A**) (Stecher et al., 2007). In contrast, the T3SS system of *C. rodentium* provides the pathogen access to a spatial niche by mediating intimate attachment to the intestinal epithelium (Schauer and Falkow, 1993a, b). We reasoned that the T3SS might provide *C. rodentium* access to growth-limiting resources that are only available to bacteria that are intimately attached to the epithelial surface. However, these resources would no longer be accessible when intimate attachment is genetically ablated by inactivating *escN*, encoding a component of the T3SS. This hypothesis would predict that wild-type *C. rodentium* would not be able to rescue growth of an *escN* mutant when mice are inoculated with a mixture of both strains. To test this prediction, mice were inoculated with *C. rodentium* strain DSB100 (Barthold et al., 1976), an isogenic *escN* mutant (Lopez et al., 2016) or with a 1:1 mixture of both strains. Mice infected with the *C. rodentium* wild type shed the pathogen in significantly higher numbers than mice infected with the *escN* mutant (**Fig. 3.1B**), which was consistent with the idea that the T3SS is required for competing with the gut microbiota (Kamada et al., 2012). However, the *C. rodentium* wild type did not rescue the growth of an *escN* mutant when mice were infected with a 1:1 mixture of both strains (**Fig. 3.1B and S3.1A**), thus supporting the idea that the T3SS provided access to a spatial niche in close proximity to the epithelium.

The marked differences in colony-forming units (CFU) recovered from colon contents of mice infected with the *escN* mutant compared to mice infected with *C. rodentium* wild type (**Fig. 3.1B**) prevent comparing the spatial localization of both strains. However, inoculation of germ-free mice results in similar recovery of wild-type and T3SS-deficient *C. rodentium* strains from colon contents (Kamada et al., 2012). To validate that inactivation of T3SS-mediated intimate attachment to epithelial cells by a mutation in *escN* would alter the spatial distribution of *C. rodentium*, germ-free mice were inoculated with either the *C.*

rodentium wild type or an isogenic *escN* mutant. Whereas the *C. rodentium* wild type was detected in close proximity to the mucosal surface, the *escN* mutant did not colonize this niche (**Fig. S3.1B**), although both strains were recovered in similar numbers from colon contents (**Fig. S3.1C**). These data confirmed previous reports that the T3SS system provides *C. rodentium* access to a spatial niche in close proximity to the intestinal epithelium (Kamada et al., 2012).

Conventional wisdom holds that during gut homeostasis, an oxygen-gradient contributes to the cross-sectional heterogeneity in the spatial organization of the colonic microbiota (Donaldson et al., 2016; Tropini et al., 2017). Consistent with this idea, the presence of a functional T3SS enhances the growth advantage conferred by cytochrome *bd* oxidase at seven days after infection (i.e. after mice develop colonic crypt hyperplasia) (Lopez et al., 2016). However, prior to the development of colonic crypt hyperplasia (i.e. at three days after infection), cytochrome *bd* oxidase-mediated growth is T3SS-independent (Lopez et al., 2016), despite the fact that a functional T3SS provided a marked growth advantage at this time point (**Fig. S3.1A**). One possible explanation for this observation was that the spatial niche *C. rodentium* occupies provides access to oxygen, but the pathogen uses a different enzyme to respire oxygen prior to the development of colonic crypt hyperplasia. The *C. rodentium* genome does not contain the *appBC* genes, which encode a cytochrome *bd*-II oxidase present in *Escherichia coli* and *Salmonella enterica* (Dassa et al., 1991). In addition to the *cydAB* genes, which encode cytochrome *bd* oxidase, the *C. rodentium* genome contains the *cyxAB* genes, which encode a cytochrome *bd*-II oxidase that is predicted to enable the pathogen to respire oxygen under microaerophilic conditions (**Fig. 3.1C**). However, the *cyxAB* genes did not markedly enhance growth in the gut, as infection of mice with a 1:1 mixture of the *C. rodentium* wild type and a *cyxAB* mutant (Lopez et al., 2016) revealed only a small fitness advantage three days after infection (**Fig. 3.1D**). We thus entertained the idea that the spatial niche *C. rodentium* occupies provides access to a growth-limiting resource that is distinct from oxygen.

The conclusion that bacterial populations in close proximity to the epithelial surface are enriched in “oxygen tolerant” species is based on transcriptional profiling, which reveals an elevated expression of

genes encoding catalase activity (Albenberg et al., 2014). However, catalase confers resistance to hydrogen peroxide (H_2O_2), which could also be responsible for the observed enrichment in "oxygen-tolerant" organisms. The *C. rodentium* genome encodes two catalases that confer "oxygen-tolerance" (Petty et al., 2010). In addition, the *C. rodentium* genome contains the *ccp* gene, which encodes a cytochrome *c* peroxidase (**Fig. 3.1C**). In *E. coli*, cytochrome *c* peroxidase transfers electrons from the quinone pool to H_2O_2 as an electron acceptor for anaerobic respiration (Khademian and Imlay, 2017). The *ccp* gene conferred a fitness advantage, because the *C. rodentium* wild type was recovered in approximately 20-fold higher numbers than a *ccp* mutant when mice were infected with a 1:1 mixture of both strains (**Fig. 3.1D**). Growth of the *ccp* mutant could be restored by introducing the cloned *ccp* gene on a plasmid (**Fig. S3.2A**). Notably, at three days after infection the growth advantage conferred by cytochrome *c* peroxidase required a functional T3SS, as it was no longer observed when mice were infected with a 1:1 mixture of an *escN* mutant and an *escN ccp* mutant (**Fig. 3.2A and S3.2B**). In stark contrast, a *cydAB*-mediated growth advantage was T3SS-independent at three days after infection, because it was still observed when mice were infected with a 1:1 mixture of an *escN* mutant and an *escN cydAB* mutant (**Fig. 3.2A and S3.2B**). These results suggested that prior to the development of colonic crypt hyperplasia, the T3SS systems provides a fitness advantage by providing access to H_2O_2, not oxygen.

NOX1-derived H_2O_2 promotes *ccp*-dependent growth prior to colonic inflammation

The *ccp* gene appeared to be more important for growth in conventional mice compared to growth in gnotobiotic mice, as indicated by decreased competitive index when gnotobiotic mice were inoculated with a 1:1 mixture of wild type and *ccp* mutant (**Fig. 3.2B**), indicative of *ccp* contributing to competition with the microbiota. A *cydAB*-dependent growth of *C. rodentium* in the intestinal lumen involves the tricarboxylic acid (TCA) cycle (Lopez et al., 2016), a metabolism that triggers endogenous production of H_2O_2 as a by-product in *E. coli* (Iuchi and Weiner, 1996). To test the possibility that *ccp* is required for growth in the mouse intestine because it detoxifies endogenous H_2O_2 generated as a byproduct of *cydAB*-

mediated aerobic metabolism in the bacterial cytosol, mice were infected with a 1:1 mixture of a *cydAB* mutant and a *cydAB ccp* mutant. Notably, the growth advantage conferred by *ccp* was still observed when cytochrome *bd* oxidase-mediated aerobic respiration was genetically ablated (**Fig. 3.2C**), suggesting that the fitness advantage conferred by cytochrome *c* peroxidase was due to an exogenous source of H_2O_2. To determine whether host-derived H_2O_2 contributes to *ccp*-dependent growth, we inhibited host NADPH oxidase activity using apocynin (Kim et al., 2012). Apocynin treatment reduced the fitness advantage conferred by *ccp* (**Fig. 3.2D**), suggesting that the nutrient-niche *C. rodentium* occupies in the gut exposes the pathogen to H_2O_2 derived from host NADPH oxidases.

Next, we investigated possible cellular sources of H_2O_2. One source of H_2O_2 in the gut is the phagocyte NADPH oxidase (NOX2), as neutrophils migrating into the intestinal lumen clear *C. rodentium* between day 7 and day 14 after infection of mice (Kamada et al., 2015). Infection of mice with the *C. rodentium* wild type or a *ccp* mutant induced marked expression of inflammatory markers in the intestinal mucosa by day seven after infection, but not at three days after infection (**Fig. 3.3A**). Whereas no pathological changes were observed in sections of the cecal mucosa collected three days after infection with the *C. rodentium* wild type or a *ccp* mutant, colonic crypt hyperplasia and inflammatory infiltrates were observed by day seven after infection (**Fig. 3.3B and C**). Consistent with the idea that phagocytes alter the luminal environment by day seven after infection, the *ccp*-mediated growth advantage was reduced in mice lacking *Cybb*, a gene encoding a subunit of the phagocyte NADPH oxidase NOX2 (**Fig. 3.3D**). At 7 days after infection, concentrations of H_2O_2 were lower in colon contents of *Cybb*-deficient mice compared to congenic wild type mice (C57BL/6J) (**Fig. 3.3E**). However, at three days after infection, prior to the development of histopathological lesions (**Fig. 3.3C**), NOX2 did not contribute to cytochrome *c* peroxidase-mediated growth, as the fitness advantage conferred by *ccp* was not diminished in *Cybb*-deficient mice at this time point (**Fig. 3.3D**). Thus, in the absence of overt signs of inflammation (**Fig. 3.3B and C**), phagocyte NOX2 was not an important source of *ccp*-mediated *C. rodentium* growth.

We then considered the epithelial surface as a possible source of H_2O_2 production at three days after *C. rodentium* infection. The *Nox1* gene, encoding an epithelial NADPH oxidase, is expressed constitutively at high levels in the colonic epithelium and at lower levels in the ileal epithelium, but not in epithelial cells of the upper gastrointestinal tract (Matziouridou et al., 2018). We therefore investigated whether H_2O_2 produced by NOX1 was a factor influencing the growth of *C. rodentium* at three days after infection. Consistent with a constitutive expression of *Nox1* in the colon (Matziouridou et al., 2018), *Nox1*-deficient mice had significantly lower concentrations of H_2O_2 in their colon contents compared to congenic wild type mice (C57BL/6J) (**Fig. 3.4A**). Infection with *C. rodentium* did not alter H_2O_2 levels in colon contents in wild type or *Nox1*-deficient mice (**Fig. 3.4A**). These data suggested that NOX1 was a significant source of colonic H_2O_2 under homeostasis. To determine whether NOX1 contributed to cytochrome *c* peroxidase-dependent fitness advantage early after infection, *Nox1*-deficient mice and congenic wild type mice (C57BL/6) were infected with a 1:1 mixture of the *C. rodentium* wild type and a *ccp* mutant. Notably, the fitness advantage conferred by cytochrome *c* peroxidase was no longer observed in mice lacking NOX1 (**Fig. 3.4B**).

Mice lacking the NOX dimerization partner CYBA exhibit lower *C. rodentium* colonization levels and an increased abundance of *Lactobacillus* species in their microbiota (Pircalabioru et al., 2016). Based on the observation that *C. rodentium* growth in the test tube can be inhibited by a cell-free culture supernatant of *Lactobacillus reuteri* it was postulated that increased H_2O_2 production by *Lactobacillus* species decreases growth of *C. rodentium* in *Cyba*-deficient mice (Pircalabioru et al., 2016). However, in a subsequent study the authors did not observe an expansion of *Lactobacillus* species in *Cyba*-deficient mice (Aviello et al., 2019). Similarly, microbiota analysis by 16S rRNA gene amplicon sequencing (microbiota profiling) did not reveal an elevated abundance of *Lactobacillus* species in the cecal microbiota of *Nox1*-deficient mice compared to wild type controls (**Fig. 3.4C and 3.4D**). The main differences in the microbiota composition were an increased abundance of the genera *Bacteroides* and *Parasuterella* in *Nox1*-deficient mice and an increased abundance of the genus *Anaeroplasma* in wild type (C57BL/6) mice (**Fig. 3.4C**).

These data were consistent with the idea that the *Nox1* genotype, rather than the abundance of *Lactobacilli*, governed H_2O_2 levels in the colon (**Fig. 3.4A and 3.4D**). To distinguish whether the *ccp*-mediated fitness advantage was caused by differences in the mouse genotype (*Nox1*-deficiency versus wild type) or by differences in the microbiota composition between mouse strains, germ-free mice received a fecal microbiota transplant from either *Nox1*-deficient mice or congenic wild type mice (**Fig. S3.3A**). Mice were then challenged with a 1:1 mixture of the *C. rodentium* wild type and a *ccp* mutant. Similar H_2O_2 levels were detected in colon contents of gnotobiotic mice receiving a fecal microbiota transplant from either *Nox1*-deficient mice or congenic wild type mice (**Fig. S3.3B**), suggesting that differences in the microbiota composition were not responsible for changes in H_2O_2 levels. Notably, engrafting germ-free mice with microbiota from *Nox1*-deficient mice did not abrogate the fitness advantage conferred by cytochrome *c* peroxidase (**Fig. 3.4E**), whereas the *ccp*-mediated fitness advantage was abrogated during infection of *Nox1*-deficient mice (**Fig. 3.4B**). Collectively, these data suggested that the *ccp*-mediated fitness advantage observed prior to development of colonic crypt hyperplasia was due to the constitutively synthesized epithelial NADPH oxidase NOX1.

Ccp promotes growth through anaerobic H_2O_2 respiration

A previous study suggests that reduced *C. rodentium* numbers recovered from *Cyba*-deficient mice were due to increased H_2O_2-mediated killing of the pathogen by *Lactobacillus* species (Pircalabioru et al., 2016). However, the hypothesis that H_2O_2-mediated killing was responsible for reducing *C. rodentium* numbers was not consistent with the finding that H_2O_2 levels were decreased, rather than increased, by *Nox1*-deficiency (**Fig. 3.4A**). Furthermore, in *E. coli*, cytochrome *c* peroxidase is ineffective as an enzyme defending against H_2O_2 toxicity, but it enables *bacteria* to respire using H_2O_2 as an anaerobic electron acceptor (Khademian and Imlay, 2017). To verify this conclusion, we investigated whether a mutation in *ccp* increases the susceptibility of *C. rodentium* to H_2O_2. *C. rodentium* was able to tolerate mM concentrations of H_2O_2 (**Fig. 3.5A**), presumably because its genome encodes catalase activity (Petty et al.,

2010). However, we did not detect differences between the *C. rodentium* wild type and a *ccp* mutant in their ability to survive exposure to H_2O_2 under anaerobic or aerobic laboratory growth (**Fig. 3.5A**). The fact that H_2O_2 tolerance remained unchanged by genetic ablation of *ccp* might be due in part to a compensatory increase in expression of *katG*, encoding the periplasmic katalase (**Fig. 3.5B**). Nonetheless, these data were consistent with the idea that the *ccp*-mediated fitness advantage was not attributable to increased susceptibility to H_2O_2-mediated killing. Next. we wanted to investigate whether the fitness defect of a *ccp* mutant was due to reduced growth or enhanced killing *in vivo* when mice are infected with a single bacterial strain. We reasoned that *Nox1*-deficiency would increase numbers of a *ccp* mutant to levels of the *C. rodentium* wild type in case cytochrome *c* peroxidase functions in detoxifying H_2O_2. In contrast, *Nox1*-deficiency would be expected to lower the numbers of the *C. rodentium* wild type to those of the *ccp* mutant in case cytochrome *c* peroxidase enhances growth by using H_2O_2 for anaerobic respiration. Genetic ablation of cytochrome *c* peroxidase significantly reduced bacterial recovery from the feces of mice (C57BL/6) infected with a *ccp* mutant compared to mice infected with the *C. rodentium* wild type (**Fig. 3.5C**). Notably, *Nox1*-deficiency lowered the numbers of the *C. rodentium* wild type to those of the *ccp* mutant (**Fig. 3.5C**), thus providing additional support for the idea that cytochrome *c* peroxidase promotes growth through anaerobic H_2O_2 respiration rather than by preventing H_2O_2-mediated killing.

DISCUSSION

An expansion of facultative anaerobic bacteria in the colon can be driven by elevated oxygen levels, which can arise because epithelial oxygenation is increased (Byndloss et al., 2017; Cevallos et al., 2019; Rivera-Chavez et al., 2016) or because mice are exposed to high atmospheric oxygen levels in a hyperbaric chamber (Albenberg et al., 2014). For example, respiration of oxygen by cytochrome *bd* oxidase contributes to T3SS-mediated growth of *C. rodentium* after mice develop colonic crypt hyperplasia, a lesion that leads to elevated epithelial oxygenation (Lopez et al., 2016). However, during conditions of homeostasis, the

epithelial surface in the colon is hypoxic (<1% oxygen), which severely limits the amount of oxygen diffusing into the gut lumen (Zheng et al., 2015).

The idea that an oxygen gradient generates heterogeneity in the spatial organization of the colonic microbiota during homeostasis (Donaldson et al., 2016; Tropini et al., 2017) is supported by correlative evidence between the presence of an oxygen gradient and an increased proportion of "oxygen-tolerant" species in close proximity to the mucosal surface (Albenberg et al., 2014). This correlation assumes that genes encoding catalase activity make species "oxygen-tolerant" (Albenberg et al., 2014), rather than conferring resistance to H_2O_2 in the gut. However, constitutive synthesis of NOX1 in the epithelium of the large intestine (Matziouridou et al., 2018) supports an alternative explanation for the observed increased proportion of "oxygen-tolerant" species close to the epithelial surface (Albenberg et al., 2014). Rather than protecting bacteria from oxygen, catalases may protect bacteria from H_2O_2 produced by epithelial NOX1. The presence of catalase genes (Petty et al., 2010) likely accounts for the ability of *C. rodentium* to tolerate mM concentrations of H_2O_2. Thus, NOX1-derived H_2O_2 might exclude bacteria from the mucosal surface that lack required traits, such as catalase activity. Consistent with a spatial role of NOX1-derived H_2O_2 prior to the development of colonic crypt hyperplasia, T3SS-mediated intimate attachment provided *C. rodentium* with a *ccp*-dependent fitness advantage, by enabling the pathogen to access NOX1-derived H_2O_2 for growth by anaerobic H_2O_2 respiration. These findings provided experimental support for the idea that during homeostasis, H_2O_2 shapes bacterial growth in close proximity to the epithelial surface.

The picture emerging from these studies is that NOX1-derived H_2O_2 might serve as a habitat filter that shapes the spatial organization of the colonic microbiota. Since obligate anaerobic bacteria, which dominate the colonic microbiota, are generally sensitive to H_2O_2, this habitat filter might contribute to the inner mucus layer being largely devoid of bacteria (Johansson et al., 2008). Consistent with this idea, a variant of the NOX dimerization partner CYBA that generates reduced amounts of H_2O_2 exhibits profound mucus layer disruption with bacterial penetration into crypts (Aviello et al., 2019), despite the fact that NOX1-deficiency increases goblet cell differentiation and mucus production (Coant et al., 2010). An

inability to keep the microbiota at a distance to the epithelial surface might thus contribute to early onset inflammatory bowel disease, which is observed in humans with *NOX1*-deficiency (Schwerd et al., 2018). However, additional work is needed to test whether and to which extend this habitat filter contributes to maintenance of a 'demilitarized zone' that protects the epithelial surface from the large community of obligate anaerobic bacteria in the colon.

ACKNOWLEDGEMENTS

We would like to thank the UNC National Gnotobiotic Rodent Resource Center for kindly providing germ-free C57BL/6J mice.

Y.L. was supported by Vaadia-BARD Postdoctoral Fellowship FI-505-2014. Work in A.J.B.'s lab was supported by USDA/NIFA award 2015-67015-22930 (A.J.B), Crohn's and Colitis Foundation of America Senior Investigator Award # 650976 and by Public Health Service Grants AI36309 (L.F.Z.), AI044170 (A.J.B.), AI096528 (A.J.B.), AI112445 (A.J.B.), AI146432 (A.J.B.) and AI112949 (A.J.B.).

AUTHOR CONTRIBUTIONS

Conceptualization, B.M.M. and A.J.B. Methodology, B.M.M., L.F.Z., M.J.L., H.N., Y.L., K.K.J., E.M.S., C.R.T., B.P.B. and A.J.B.; Investigation, B.M.M., L.F.Z., M.J.L., H.N., Y.L., K.K.J., C.R.T., B.P.B. and A.J.B.; Resources, A.J.B.. Funding Acquisition, Y.L., L.F.Z. and A.J.B.; Writing – Original Draft, B.M.M. and A.J.B.; Writing – Review & Editing, B.M.M., Y.L., K.K.J., B.P.B. and A.J.B.; Supervision, B.M.M., Y.L. and A.J.B.

DECLARATION OF INTERESTS

The authors declare no competing interests.

Figures

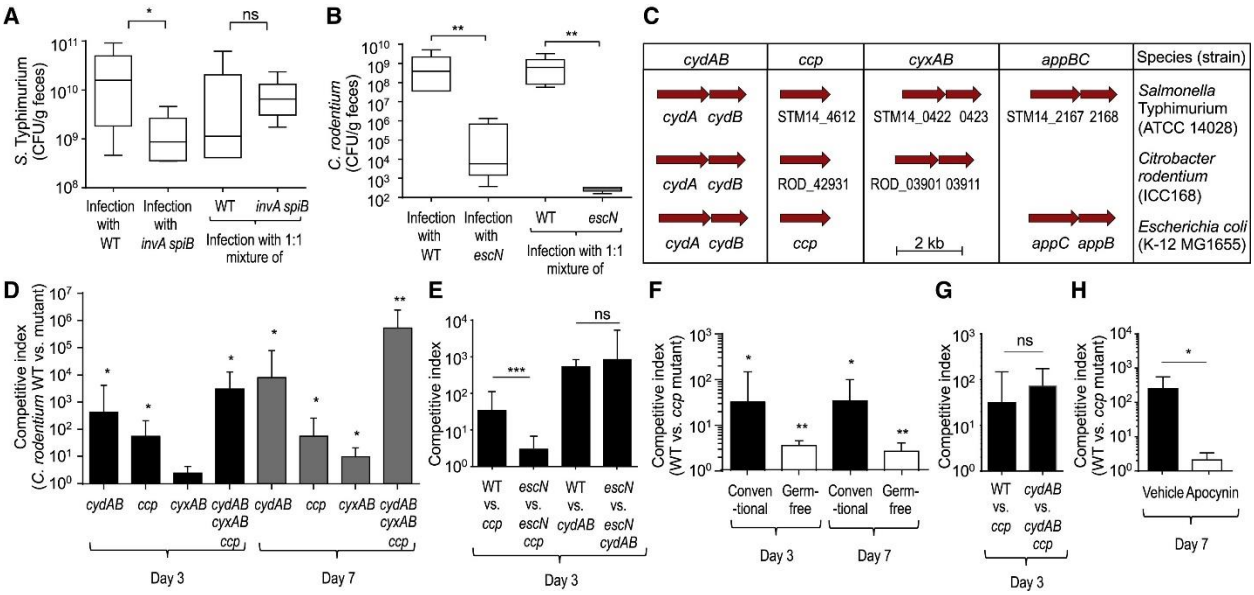

Figure 3.1: (A) Mice (C57BL/6J, *N* = 6) were infected intragastrically with *S.* Typhimurium wild type (WT) (Kingsley et al., 2003), an *invA spiB* mutant (Faber et al., 2016) or with a 1:1 mixture of both strains. The graph shows recovery from the feces at 5 days after infection. (B) Mice (C57BL/6J, *N* = 6) were infected intragastrically with *C. rodentium* wild type (WT), an *escN* mutant or with a 1:1 mixture of both strains. The graph shows recovery from the feces at 7 days after infection. (C) Schematic showing the presence of select respiratory enzymes in the genomes of *C. rodentium*, *E. coli* or *S. enterica* serovar Typhimurium. (D) Mice (C57BL/6J, *N* = 4) were infected intragastrically with a 1:1 mixture of the *C. rodentium* wild type (WT) and one of the indicated mutant strains. The competitive index (ratio of WT to mutant) in the feces was determined at the indicated time points. Statistical analysis indicates whether the competitive index was significantly different from 1. *, $P < 0.05$; **, $P < 0.01$; ns, $P > 0.05$.

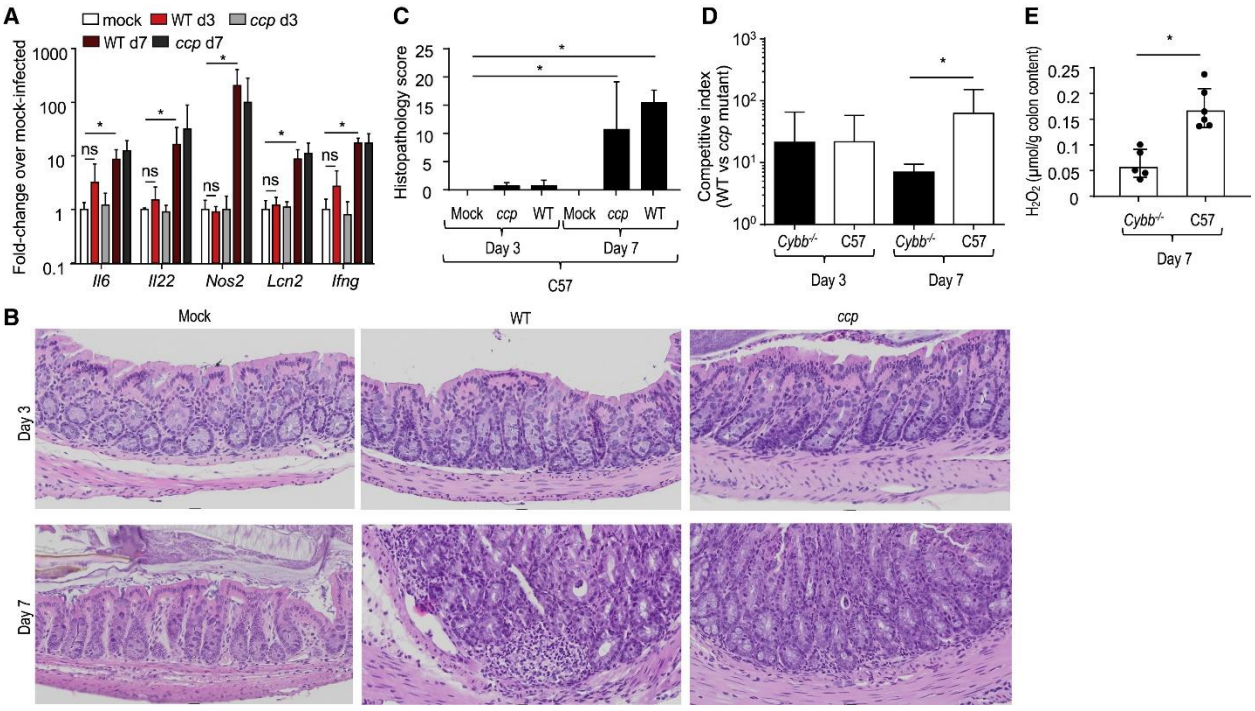

Figure 3.2: (A–C) Conventional mice (C57BL/6J, N = 6) were mock-infected or infected with the *C. rodentium* wild type (WT) or with a *ccp* mutant. (A) Expression of the indicated inflammatory genes was quantified by real-time PCR in RNA isolated from the colonic mucosa on days 3 (d3) and 7 (d7) after infection. (B and C) The severity of intestinal lesions was scored by a veterinary pathologist in blinded sections from the colon. (B) representative images are shown. (C) Combined histopathology score. (D-E) C57BL/6 mice (C57, N = 6) and congenic *Cybb*-deficient mice (*Cybb*−/−, N = 6) were infected with a 1:1 mixture of the *C. rodentium wild* type (WT) or with a *ccp* mutant. (D) The competitive index (ratio of WT to mutant) in the feces was determined at the indicated time points. (E) Hydrogen peroxide was measured in the supernatant of colon contents using Amplex Red and horseradish peroxidase on day 7 after infection. $*p < 0.05$.

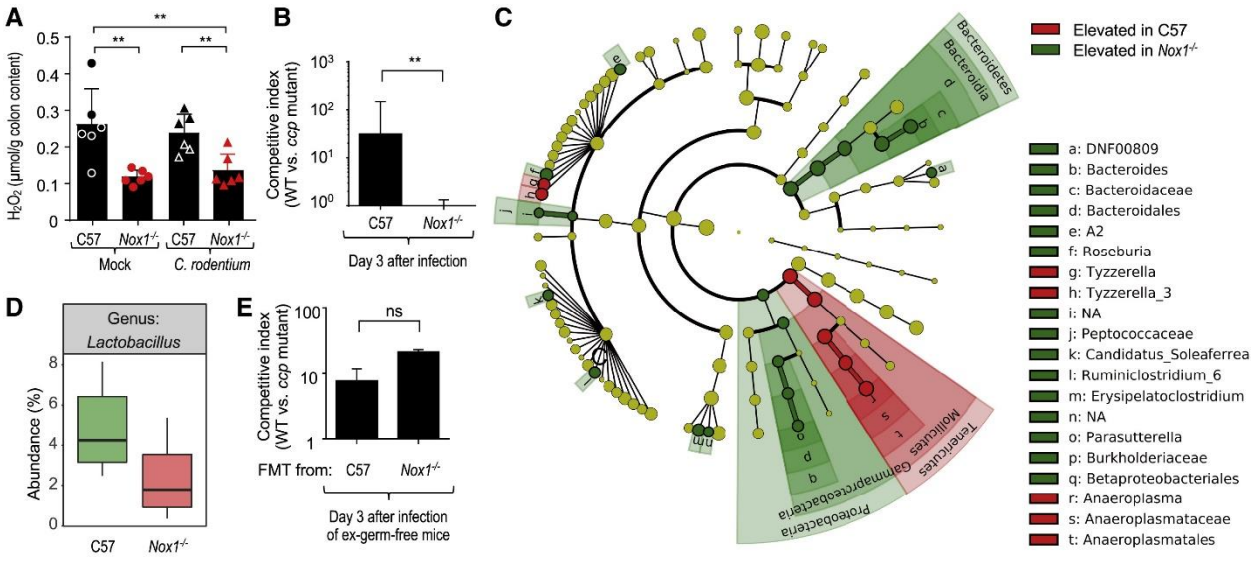

Figure 3.3: (A-C) Conventional mice (C57BL/6J, N = 6) were mock-infected or infected with the *C. rodentium* wild type (WT) or with a *ccp* mutant. (A) Expression of the indicated inflammatory genes was quantified by real-time PCR in RNA isolated from the colonic mucosa on days 3 (d3) and 7 (d7) after infection. (B-C) The severity of intestinal lesions was scored by a veterinary pathologist in blinded sections from the colon. (B) representative images are shown. (C) Combined histopathology score. (D-E) C57BL/6 mice (C57, N = 6) and congenic *Cybb*-deficient mice (*Cybb*$^{-/-}$, N = 6) were infected with a 1:1 mixture of the *C. rodentium* wild type (WT) or with a *ccp* mutant. (D) The competitive index (ratio of WT to mutant) in the feces was determined at the indicated time points. (E) Hydrogen peroxide was measured in the supernatant of colon contents using Amplex Red and horseradish peroxidase on day 7 after infection. *, $P < 0.05$.

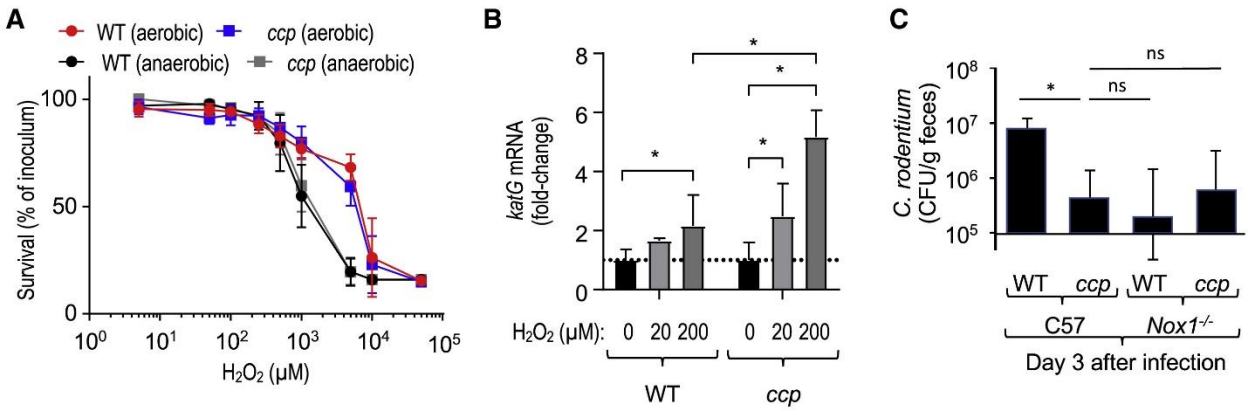

Figure 3.4: (A) C57BL/6 mice (C57, *N* = 6) and congenic *Nox1*-deficient mice (*Nox1*$^{-/-}$, *N* = 6) were mock-infected or infected with *C. rodentium* wild type. Hydrogen peroxide was measured in the supernatant of colon contents using Amplex Red and horseradish peroxidase on day 3 after infection. (B) C57BL/6 mice (C57, *N* = 6) and congenic *Nox1*-deficient mice (*Nox1*$^{-/-}$, *N* = 6) were infected with a 1:1 mixture of the *C. rodentium* wild type (WT) and a *ccp* mutant. The competitive index (ratio of WT to mutant) in the feces was determined at the indicated time point. (C and D) DNA was isolated from fecal contents of C57BL/6 mice (C57, *N* = 6) or congenic *Nox1*-deficient mice (*Nox1*$^{-/-}$, *N* = 6) and the microbiota composition analyzed by 16S rRNA gene amplicon sequencing. (C) Results of a linear discriminant analysis of microbiota composition in C57BL/6 mice compared to *Nox1*-deficient mice are displayed as a cladogram, highlighting differences in the abundance of taxa (red and green highlighting) determined by 16S rRNA gene amplicon sequencing. Taxa are arranged on a circular phylogenetic tree. Green, taxa elevated in *Nox1*-deficient mice compared to C57BL/6 mice; Red, taxa reduced in *Nox1*-deficient mice compared to C57BL/6 mice. (D) Relative abundance of *Lactobacillus* species. (E) Germ-free mice (Swiss Webster, *N* = 4) received a fecal microbiota transplant from conventional mice (C57) or congenic *Nox1*-deficient mice (*Nox1*$^{-/-}$) and seven days later mice were challenged with a 1:1 mixture of the *C. rodentium* wild type (WT) and a *ccp* mutant. The competitive index (ratio of WT to mutant) in the feces was determined at the indicated time point. **, $P < 0.01$; ns, $P > 0.05$.

Figure 3.5: (A) Survival of the *C. rodentium* wild type (WT) and a *ccp* mutant was determined under aerobic or anaerobic conditions in the presence of the indicated H_2O_2 concentrations. (B) The *C. rodentium* wild type (WT) and an isogenic *ccp* mutant (*ccp*) were exposed to the indicated concentrations of H_2O_2 and *katG* expression determined by real-time PCR. (C) C57BL/6 mice (C57, $N = 6$) or congenic *Nox1*-deficient mice (*Nox1,* $N = 6$) were infected with the *C. rodentium* wild type (WT) or with a *C. rodentium ccp* mutant. Colony-forming units (CFU) of *C. rodentium* were determined in the feces at the indicated time point. *, $P < 0.05$; ns, $P > 0.05$.

STAR METHODS

Resource Availability

Lead Contact. Andreas J. Bäumler (ajbaumler@ucdavis.edu).

***Materials Availability*.** The study did not create new unique reagents. Further information and requests for resources and reagents should be directed to and will be fulfilled by the Lead Contact.

***Data and Code Availability*:** The 16S rRNA gene amplicon sequencing data is available under BioProject accession numbers PRJNA660475 (gnotobiotic mice) and PRJNA607193 (conventional C57BL/6J and *Nox1*-deficient mice) through the NCBI BioProject database (https://www.ncbi.nlm.nih.gov/bioproject/).

Experimental model and subject details

Animal experiments

The Institutional Animal Care and Use Committee at the University of California, Davis, approved all animal experiments. For experiments involving mice colonized with conventional specific pathogen free microbiota, female C57BL/6J, B6.129X1-*Nox1*^{tm1Kkr}/J (Nox1$^{-/-}$), or B6.129S-*Cybb*^{tm1Din}/J (gp91phox-) strains (Jackson Laboratories) aged 5–7 weeks were inoculated with 1×10^9 colony forming units (CFU) per mouse of a single *C. rodentium* strain in LB broth intragastrically, or 0.1 ml sterile LB broth as mock infection. In competitive infections, a 1:1 ratio of two *C. rodentium* strains were given intragastrically at a combined final concentration of 1×10^9 CFU/mouse. Fecal pellets were collected on days 3 or 7, and mice were sacrificed between 3 and 7 days after infection. Colon contents were stored in phosphate-buffered saline (PBS) on ice. Colon tissue for histopathology was fixed in 10% buffered formalin phosphate overnight, while colon sections for murine RNA analysis were flash frozen and stored at −80°C. *C. rodentium* from feces and colon contents were enumerated by plating serial ten-fold dilutions of samples

on MacConkey agar (BD Biosciences) containing the appropriate antibiotics based on the resistance markers listed for each strain in **Table S3.1**. Plates were incubated overnight at 37°C under atmospheric oxygen conditions. For competitive infections, the output ratio of recovered bacteria strains was divided by the input ratio of the inoculum to determine competitive index.

For infection of mice with *S.* Typhimurium, mice were pre-treated with an intragastric dose of 20 mg streptomycin 24 hours prior to infection. For single infections, mice were inoculated intragastrically with 1×10^9 CFU of the indicated *S.* Typhimurium strains. For competitive infection, mice were inoculated with 1×10^9 CFU of a 1:1 mixture of the indicated strains. Mice were euthanized 4 days after infection, and cecal contents were collected for enumeration of bacterial numbers. Bacterial numbers were determined by standard plate count on LB agar (BD Biosciences) containing the appropriate antibiotics. The ratio of recovered wild-type and mutant bacteria were normalized by the ratio of the inoculum to calculate the competitive index.

Germ-free Swiss Webster mice were bred and housed at the Teaching and Research Animal Care Services facilities at UC Davis. Male and female mice aged 5-7 weeks were used, and were infected and euthanized as described above.

To inhibit NADPH oxidase *in vivo*, mice were first mock infected or infected with a 1:1 mixture of the indicated *C. rodentium* strains as described above. Apocynin (Sigma) was initially dissolved in 100% ethanol and then further diluted in dPBS (Gibco). Mice given were 80 μg/ml of apocynin or ethanol vehicle control in sterile drinking water starting at day of infection. Fresh water containing apocynin and vehicle control were made daily continuing up to day 7 post-infection. Water intake was monitored, and no significant difference between consumption of apocynin and vehicle water was noted.

Bacterial strains and culture conditions

For the *C. rodentium*, *E. coli* and *S.* Typhimurium strains used in this study, see **Table S3.1**. Strains were grown routinely in Luria-Bertani (LB) broth (BD Biosciences #244620) or on LB plates unless otherwise indicated. Antibiotics were used at the following concentrations when required: carbenicillin (Carb), 0.1 mg/ml; chloramphenicol (Cm), 0.015 mg/ml; kanamycin (Kan), 0.1 mg/ml; tetracycline (Tet), 0.02 mg/ml; spectinomycin (Spec), 0.1 mg/ml.

Method details

Specific-pathogen free mouse husbandry

Prior to transport, mice at Jackson were fed LabDiet 5K52 formulation (6% fat). Upon arrival, mice from each cohort were randomly assigned into individually ventilated cages on one rack at a housing density of 3 to 4 animals per cage and allowed to acclimate in our vivarium for at least a week undisturbed. Feed was switched to irradiated TEKLAD GLOBAL 18% protein rodent diet 2918 (Envigo) and no breeding was performed. 70% ethanol was used to disinfect surfaces and gloves between groups. Clean (but not sterile) paper towels were utilized for fecal sample collections.

Hydrogen peroxide killing assay

Bacterial cultures were grown overnight at 37°C in LB broth under aerobic (atmospheric oxygen) conditions or in an anaerobic chamber (Coy Laboratories) with an environment of 5% CO_2, 5% H_2, and 90% N_2. 10^5 bacterial cells were inoculated into PBS containing hydrogen peroxide of concentrations from 0 to 100 millimolar. The assay was allowed to run for 30 minutes at 37°C in aerobic or anaerobic conditions as stated above, after which each condition was plated on LB plates and enumerated by standard plate counting. Each condition was repeated in triplicate.

Construction of C. rodentium mutants

To construct an *escN* mutant, regions of approximately 500 bp in length flanking the *escN* gene were amplified via PCR using Q5 High Fidelity 2X Master Mix (NEB) and primers listed in **Table S3.1**, run on an agarose gel, and purified using the Zymoclean Gel DNA Recovery kit (Zymo Research). The kanamycin (KSAC) cassette from pUC4 (Lopez et al., 2016) was amplified, and this along with the *escN* flanking regions were ligated into pRDH10 (Kingsley et al., 1999) via the Gibson Assembly (NEB). The plasmid, named pBMM6, was propagated in *E. coli* DH5*α λpir* (Pal et al., 2005). pBMM6 was then transformed into *E. coli* S17-1 *λpir* (Simon et al., 1983), and this strain was conjugated with DBS100 (pSW172) (Spees et al., 2013). Double crossover events were selected via sucrose selection, and mutants were screened for kanamycin and carbenicillin resistance and loss of chloramphenicol resistance. PCR was used to confirm the deletion, and the temperature sensitive plasmid was cured after growth overnight at 40°C. The strain was then named BMM39.

To construct a *ccp* mutation, primers (**Tab. S3.2**) were designed that overlapped the 70 flanking base pairs on both ends of the *C. rodentium ccp* gene (ROD_42931) and 20 base pairs of the chloramphenicol cassette from pEP185.2 (Kinder et al., 1993). PCR was used to amplify the fragment with Q5 High Fidelity 2X Master Mix (NEB), run on an agarose gel, and gel purified via the Zymoclean Gel DNA Recovery kit (Zymo Research). The fragment was desalted via drop dialysis using nitrocellulose membrane filters (Millipore), and subsequently DpnI (NEB) treated. *C. rodentium* was electroporated with the temperature sensitive inducible lambda red recombinase plasmid pKD46 (Datsenko and Wanner, 2000) in which the ampicillin cassette has been replaced with a spectinomycin cassette. DBS100 (pKD46) was grown overnight at 30°C, and subcultured the next morning, and the plasmid recombinase was induced with 10 mM arabinose. DBS100 (pKD46) was then washed with distilled water, and the fragment was electroporated into DBS100 (pKD46). Mutants were selected via chloramphenicol resistance and confirmed for loss of pKD46 by loss of spectinomycin resistance. The mutant was verified via PCR screening, and then named BMM87.

To construct a *cyxA* mutant, primers (**Tab. S3.2**) were designed that overlapped the 70 flanking base pairs on both ends of the *C. rodentium cyxA* gene (ROD_03901) and 20 base pairs of the tetracycline cassette from pSPN23 (Raffatellu et al., 2009). Q5 High Fidelity 2X Master Mix (NEB) was used to amplify the fragment via PCR, the product was run on an agarose gel, and was gel purified using the Zymoclean Gel DNA Recovery kit (Zymo Research). The fragment was then prepared as described above. DBS100 (pKD46) was prepared as described above, followed by electroporation with the *cyxA* fragment. Mutants were selected via tetracycline resistance and confirmed for loss of pKD46 by loss of spectinomycin resistance. The mutant was verified via PCR screening, and was named BMM101.

To construct an *escN ccp* mutant, BMM39 was electroporated with the pKD46 plasmid and lambda red recombination was used as described above, using the *ccp* fragment. Mutants were selected via chloramphenicol and kanamycin resistance. Loss of pKD46 was confirmed via loss of spectinomycin resistance. The mutant was verified by PCR, and then named BMM109.

To construct a *cydAB ccp* mutant, lambda red recombination was used to introduce the *ccp* mutation into BMM86 as described above. Mutants were selected for kanamycin and chloramphenicol resistance, and were then screened via PCR. Loss of pKD46 was confirmed via loss of spectinomycin resistance. The mutant was named BMM88.

To construct a *cydAB cyxAB ccp* triple mutant, the pKD46 plasmid was introduced into BMM88. Lambda red recombination was used as described above to introduce the *cyxA* mutation. Mutants were selected for kanamycin, chloramphenicol, and tetracycline resistance. Loss of pKD46 was confirmed by loss of spectinomycin resistance. The mutant was screened via PCR and named BMM104.

To generate a plasmid for complementing the *ccp* mutation, primer pair ccpcomp Fwd (5′-ggtatcgataagcttgatTTTCCCGTTATCCCCTTTTTTAC-3′) and ccpcomp Rev (5′-gctgcaggaattcgatTTACTTGCCCTGCATATAAG-3′) was used to amplify the region containing coding sequence and 500 bp upstream of the *C. rodentium ccp* gene. The resulting PCR product was run on an

agarose gel and gel purified using Zymoclean Gel DNA Recovery kit (Zymo Research). The fragment was then cloned into the EcoRV restriction site of the low copy number plasmid pWSK129 (Wang and Kushner, 1991) to generate the plasmid pBMM18 via Gibson Assembly Master Mix (NEB). The insert was confirmed via PCR. The plasmid was propagated in *E. coli* DH5*α λpir* and was then electroporated into BMM87.

Hydrogen peroxide measurements

Colonic contents and mucus scrapings were collected from infected mice for analysis. During necropsy, the middle 2-3cm of the colon was removed and cut longitudinally. Contents were removed carefully and stored in distilled H_2O on ice. Forceps were then used to gently scrape the mucus layer from the underlying tissue, which was also stored in distilled H_2O on ice. Samples were homogenized, centrifuged, and the supernatant was used for analysis. The Amplex Red/Horseradish Peroxidase assay kit was used (Thermofisher) according to manufacturer's instructions. The absorbance was read on a microplate reader (BioRad) at 550nm.

Histopathology

Colon tissues were fixed by immersion in 10% neutral buffered formalin, embedded in paraffin, sectioned at 4 um, stained with hematoxylin & eosin (HE) using standard histologic techniques and examined by light microscopy. A board-certified veterinary pathologist scored histopathological changes of blinded samples. Inflammatory lesions were scored based on the degree of leukocyte infiltration, edema, crypt abscessation and accumulation of luminal exudate. Architectural changes to the colonic mucosa were scored based on the degree of mucosal epithelial hyperplasia, surface erosion, goblet cell depletion and extent of brush border bacterial colonization. Quantitative and semi-quantitative histopathological analyses of colonic lesions were completed using a defined set of scoring criteria listed in **Table S3.2**.

RNA isolation and quantitative real-time PCR

Murine colon tissue samples were homogenized in TRI Reagent (Molecular Research Center, Inc.) using a Mini-Beadbeater (BioSpec Products) and RNA was isolated following the manufacturer's protocol. RNA was eluted in DNAse buffer and contaminating DNA was removed using the DNA-free kit (Applied Biosystems), and RNA was stored at −80°C.

RNA concentration and quality were measured spectrophotometrically using a Nanodrop (ND-1000, Nanodrop Technologies). Isolated RNA from murine samples was reverse transcribed using random hexamers and MuLV reverse transcriptase (Applied Biosystems). Quantitative real-time PCR (qPCR) was performed using SYBR green PCR mix (Applied Biosystems) and the primer sets listed in **Table S3.1** to a concentration of 0.25 mM. Delta delta Ct was used to calculate fold change between groups.

Bacterial catalase expression

For *in vitro* measurements of catalase expression of *C. rodentium*, wild type and *ccp* mutant were grown overnight in 5mL LB under shaking conditions at 37°C. 10^9 bacteria were spun down in a microcentrifuge tube, washed with PBS twice, before being resuspended in PBS containing either: 0, 20, or 200 μM H2O2 in a 96 well plate. Bacteria were incubated at 37°C for 30 minutes, before being collected and washed twice in PBS as described above. The bacterial cell pellet was then resuspended in TRI Reagent. RNA was isolated and qPCR was conducted as described above.

Imaging of murine colon

For imaging of germ-free C57BL/6J mouse colons, sections of mid-colon were collected and fixed in 4% PFA overnight before being submerged in 40% sterile sucrose for 48 hours. Sections were then

moved to Optimal Cutting Temperature (OCT) compound (Fisher HealthCare), and OCT was allowed to penetrate the sections for 3 hours, before sections were moved to molds and frozen in OCT on dry ice. Sections were cut in transverse orientation at a thickness of 7 µm. Slides were brought to room temperature, fixed with 4% PFA, and permeabilized with 0.2% Triton-X 100. *C. rodentium* were stained with rabbit anti-O152 primary antibody (Abcam ab78978), and a goat anti-rabbit Alexafluor 647 conjugate (Abcam ab 150079). Actin was stained with phalloidin-tetramethylrhodamine B isothiocyanate (Sigma Aldrich P1951), and nuclei were visualized with DAPI (Sigma Aldrich D9542). Sections were mounted with SlowFade Gold mounting media (Invitrogen S36938) and imaged.

16S rRNA gene amplicon sequencing sample preparation, library preparation, and sequencing

Nucleic acid extraction was done using the Powersoil kit from Qiagen following kit instructions. DNA concentration was recorded using Qubit a 2.0 flourometer. Samples were normalized to 20 ng/uL before library prep.

Primers 319F (TCGTCGGCAGCGTCAGATGTGTATAAGAGACAG(spacer)GTACTCCTACGGGAGGCAGCAGT) and 806R (GTCTCGTGGGCTCGGAGATGTGTATAAGAGACAG(spacer)CCGGACTACNVGGGTWTCTAAT) were used to amplify the V3-V4 domain of the 16S rRNA using a two-step PCR procedure. In step one of the amplification procedure, both forward and reverse primers contained an Illumina tag sequence (bold), a variable length spacer (no spacer, C, TC, or ATC for 319F; no spacer, G, TG, ATG for 806R) to increase diversity and improve the quality of the sequencing run, a linker sequence (italicized), and the 16S target sequence (underlined). Each 25 µl PCR reaction contained 1 Unit Kapa2G Robust Hot Start Polymerase (Kapa Biosystems), 1.5 mM MgCl2, 0.2 mM final concentration dNTP mix, 0.2 µM final concentration of each primer and 1ul of DNA for each sample. PCR conditions were: an initial incubation at 95°C for 3 min,

followed by 25 cycles of 95°C for 45 s, 50°C for 30 s, 72°C for 30 s and a final extension of 72°C for 3 min. In step two, each sample was barcoded with a unique forward and reverse barcode combination using forward primers (AATGATACGGCGACCACCGAGATCTACACNNNNNNNNTCGTCGGCAGCGTC) with an Illumina P5 adapter sequence (bold), a unique 8 nt barcode (N), a partial matching sequence of the forward adapter used in step one (underlined), and reverse primers (CAAGCAGAAGACGGCATACGAGATNNNNNNNNGTCTCGTGGGCTCGG)) with an Illumina P7 adapter sequence (bold), unique 8 nt barcode (N), and a partial matching sequence of the reverse adapter used in step one (underlined). The PCR reaction in step two contained 1 Unit Kapa2G Robust Hot Start Polymerase (Kapa Biosystems), 1.5 mM MgCl2, 0.2 mM final concentration dNTP mix, 0.2 μM final concentration of each uniquely barcoded primer and 1ul of the product from the PCR reaction in step one diluted at a 10:1 ratio in water. PCR conditions were: an initial incubation at 95°C for 3 min, followed by 9 cycles of 95°C for 30 s, 58°C for 30 s, 72°C for 30 s and a final extension of 72°C for 3 min.

The final product was quantified on the Qubit instrument using the Qubit Broad Range DNA kit (Invitrogen) and individual amplicons were pooled in equal concentrations. The pooled library was cleaned utilizing Ampure XP beads (Beckman Coulter) then the band of interest was further subjected to isolation via gel electrophoresis on a 1.5% Blue Pippin HT gel (Sage Science). The library was quantified via qPCR followed by 300-bp paired-end sequencing using an Illumina MiSeq instrument in the Genome Center DNA Technologies Core, University of California, Davis.

16S rRNA gene amplicon sequencing analysis

Sequencing reads were demultiplexed using QIIME 1.8 (Caporaso et al., 2010), and non-biological nucleotides were trimmed using Trimmomatic (Bolger et al., 2014). 16S rRNA sequencing reads were subsequently processed and assembled into amplicon sequence variants (ASV) using dada2 (Callahan et

al., 2016) in R. First, reads with more than 2 expected errors were removed. Dereplication and sample inference were then performed on forward and reverse reads, prior to merging. A sequence table was constructed from merged reads, and chimeric reads were subsequently removed. Taxonomy was assigned to reads to the genus level using the dada2 formatted rdp training dataset 14 found here https://zenodo.org/record/158955#.XJqlnxNKjUI. The R package phyloseq (McMurdie and Holmes, 2013) was then used in downstream analysis of the data, including the generation of a phyloseq object, relative abundance bar plots, and the principle coordinate analysis plot. For the weighted unifrac analysis, the R package msa (Bodenhofer et al., 2015) was used to generate a multiple sequence alignment from the assembled reads with the following parameters: method="ClustalW", type="dna", order="input". For linear discriminant analysis, data were reformatted in R, written to a tab separated text file, and then uploaded to the LEfSe galaxy server (Segata et al., 2011) where the default statistical parameters were used in the analysis to generate LDA scores and the LDA cladogram. Differential abundance analysis of taxa was performed using the R package deseq2 [25516281] with the parameters: test="Wald", fitType="parametric", cooksCutoff = FALSE.

The data have been deposited with links to BioProject accession numbers PRJNA660475 (gnotobiotic mice) and PRJNA607193 (conventional C57BL/6J and *Nox1*-deficient mice) in the NCBI BioProject database (https://www.ncbi.nlm.nih.gov/bioproject/).

Statistical analysis

Data for all experiments displayed as bar graphs represent the geometric mean and the standard error of the mean. For most experiments, data points were first log transformed and differences between experimental groups were determined on the transformed data using a Student's T-test (for comparing two groups) or ANOVA followed by Fisher's LSD post hoc test (for comparison of more than two groups). A P-value of less than 0.05 was considered significant.

REFERENCES

Albenberg, L., Esipova, T.V., Judge, C.P., Bittinger, K., Chen, J., Laughlin, A., Grunberg, S., Baldassano, R.N., Lewis, J.D., Li, H.*, et al.* (2014). Correlation between intraluminal oxygen gradient and radial partitioning of intestinal microbiota. Gastroenterology *147*, 1055-1063 e1058.

Aviello, G., Singh, A.K., O'Neill, S., Conroy, E., Gallagher, W., D'Agostino, G., Walker, A.W., Bourke, B., Scholz, D., and Knaus, U.G. (2019). Colitis susceptibility in mice with reactive oxygen species deficiency is mediated by mucus barrier and immune defense defects. Mucosal Immunol *12*, 1316-1326.

Barthold, S.W., Coleman, G.L., Bhatt, P.N., Osbaldiston, G.W., and Jonas, A.M. (1976). The etiology of transmissible murine colonic hyperplasia. Lab Anim Sci *26*, 889-894.

Berry, D., Mader, E., Lee, T.K., Woebken, D., Wang, Y., Zhu, D., Palatinszky, M., Schintlmeister, A., Schmid, M.C., Hanson, B.T.*, et al.* (2015). Tracking heavy water (D2O) incorporation for identifying and sorting active microbial cells. Proc Natl Acad Sci U S A *112*, E194-203.

Bodenhofer, U., Bonatesta, E., Horejs-Kainrath, C., and Hochreiter, S. (2015). msa: an R package for multiple sequence alignment. Bioinformatics *31*, 3997-3999.

Bolger, A.M., Lohse, M., and Usadel, B. (2014). Trimmomatic: a flexible trimmer for Illumina sequence data. Bioinformatics *30*, 2114-2120.

Byndloss, M.X., Olsan, E.E., Rivera-Chavez, F., Tiffany, C.R., Cevallos, S.A., Lokken, K.L., Torres, T.P., Byndloss, A.J., Faber, F., Gao, Y.*, et al.* (2017). Microbiota-activated PPAR-gamma signaling inhibits dysbiotic Enterobacteriaceae expansion. Science *357*, 570-575.

Byndloss, M.X., Pernitzsch, S.R., and Baumler, A.J. (2018). Healthy hosts rule within: ecological forces shaping the gut microbiota. Mucosal Immunol *11*, 1299-1305.

Callahan, B.J., McMurdie, P.J., Rosen, M.J., Han, A.W., Johnson, A.J., and Holmes, S.P. (2016). DADA2: High-resolution sample inference from Illumina amplicon data. Nat Methods *13*, 581-583.

Caporaso, J.G., Kuczynski, J., Stombaugh, J., Bittinger, K., Bushman, F.D., Costello, E.K., Fierer, N., Pena, A.G., Goodrich, J.K., Gordon, J.I.*, et al.* (2010). QIIME allows analysis of high-throughput community sequencing data. Nat Methods *7*, 335-336.

Carson, D., Barry, R., Hopkins, E.G.D., Roumeliotis, T.I., Garcia-Weber, D., Mullineaux-Sanders, C., Elinav, E., Arrieumerlou, C., Choudhary, J.S., and Frankel, G. (2019). Citrobacter rodentium induces rapid and unique metabolic and inflammatory responses in mice suffering from severe disease. Cell Microbiol, e13126.

Cevallos, S.A., Lee, J.Y., Tiffany, C.R., Byndloss, A.J., Johnston, L., Byndloss, M.X., and Baumler, A.J. (2019). Increased Epithelial Oxygenation Links Colitis to an Expansion of Tumorigenic Bacteria. MBio *10*.

Coant, N., Ben Mkaddem, S., Pedruzzi, E., Guichard, C., Treton, X., Ducroc, R., Freund, J.N., Cazals-Hatem, D., Bouhnik, Y., Woerther, P.L.*, et al.* (2010). NADPH oxidase 1 modulates WNT and NOTCH1 signaling to control the fate of proliferative progenitor cells in the colon. Mol Cell Biol *30*, 2636-2650.

Costello, E.K., Stagaman, K., Dethlefsen, L., Bohannan, B.J., and Relman, D.A. (2012). The application of ecological theory toward an understanding of the human microbiome. Science *336*, 1255-1262.

Dassa, J., Fsihi, H., Marck, C., Dion, M., Kieffer-Bontemps, M., and Boquet, P.L. (1991). A new oxygen-regulated operon in Escherichia coli comprises the genes for a putative third cytochrome oxidase and for pH 2.5 acid phosphatase (appA). Mol Gen Genet *229*, 341-352.

Datsenko, K.A., and Wanner, B.L. (2000). One-step inactivation of chromosomal genes in Escherichia coli K-12 using PCR products. Proc Natl Acad Sci U S A *97*, 6640-6645.

Donaldson, G.P., Lee, S.M., and Mazmanian, S.K. (2016). Gut biogeography of the bacterial microbiota. Nat Rev Microbiol *14*, 20-32.

Faber, F., Tran, L., Byndloss, M.X., Lopez, C.A., Velazquez, E.M., Kerrinnes, T., Nuccio, S.P., Wangdi, T., Fiehn, O., Tsolis, R.M.*, et al.* (2016). Host-mediated sugar oxidation promotes post-antibiotic pathogen expansion. Nature *534*, 697-699.

Foster, K.R., Schluter, J., Coyte, K.Z., and Rakoff-Nahoum, S. (2017). The evolution of the host microbiome as an ecosystem on a leash. Nature *548*, 43-51.

Gillis, C.C., Hughes, E.R., Spiga, L., Winter, M.G., Zhu, W., Furtado de Carvalho, T., Chanin, R.B., Behrendt, C.L., Hooper, L.V., Santos, R.L.*, et al.* (2018). Dysbiosis-Associated Change in Host Metabolism Generates Lactate to Support Salmonella Growth. Cell Host Microbe *23*, 54-64 e56.

Gillis, C.C., Winter, M.G., Chanin, R.B., Zhu, W., Spiga, L., and Winter, S.E. (2019). Host-Derived Metabolites Modulate Transcription of Salmonella Genes Involved in l-Lactate Utilization during Gut Colonization. Infect Immun *87*.

Iuchi, S., and Weiner, L. (1996). Cellular and molecular physiology of Escherichia coli in the adaptation to aerobic environments. J Biochem *120*, 1055-1063.

Johansson, M.E., Phillipson, M., Petersson, J., Velcich, A., Holm, L., and Hansson, G.C. (2008). The inner of the two Muc2 mucin-dependent mucus layers in colon is devoid of bacteria. Proc Natl Acad Sci U S A *105*, 15064-15069.

Kamada, N., Kim, Y.G., Sham, H.P., Vallance, B.A., Puente, J.L., Martens, E.C., and Nunez, G. (2012). Regulated virulence controls the ability of a pathogen to compete with the gut microbiota. Science *336*, 1325-1329.

Kamada, N., Sakamoto, K., Seo, S.U., Zeng, M.Y., Kim, Y.G., Cascalho, M., Vallance, B.A., Puente, J.L., and Nunez, G. (2015). Humoral Immunity in the Gut Selectively Targets Phenotypically Virulent Attaching-and-Effacing Bacteria for Intraluminal Elimination. Cell Host Microbe *17*, 617-627.

Khademian, M., and Imlay, J.A. (2017). Escherichia coli cytochrome c peroxidase is a respiratory oxidase that enables the use of hydrogen peroxide as a terminal electron acceptor. Proc Natl Acad Sci U S A *114*, E6922-E6931.

Kim, S.Y., Moon, K.A., Jo, H.Y., Jeong, S., Seon, S.H., Jung, E., Cho, Y.S., Chun, E., and Lee, K.Y. (2012). Anti-inflammatory effects of apocynin, an inhibitor of NADPH oxidase, in airway inflammation. Immunol Cell Biol *90*, 441-448.

Kinder, S.A., Badger, J.L., Bryant, G.O., Pepe, J.C., and Miller, V.L. (1993). Cloning of the *YenI* restriction endonuclease and methyltransferase from *Yersinia enterocolitica* serotype O:8 and construction of a transformable R-M+ mutant. Gene *136*, 271-275.

Kingsley, R.A., Humphries, A.D., Weening, E.H., De Zoete, M.R., Winter, S., Papaconstantinopoulou, A., Dougan, G., and Baumler, A.J. (2003). Molecular and phenotypic analysis of the CS54 island of Salmonella enterica serotype typhimurium: identification of intestinal colonization and persistence determinants. Infect Immun *71*, 629-640.

Kingsley, R.A., Reissbrodt, R., Rabsch, W., Ketley, J.M., Tsolis, R.M., Everest, P., Dougan, G., Baumler, A.J., Roberts, M., and Williams, P.H. (1999). Ferrioxamine-mediated Iron(III) utilization by Salmonella enterica. Appl Environ Microbiol *65*, 1610-1618.

Li, H., Limenitakis, J.P., Fuhrer, T., Geuking, M.B., Lawson, M.A., Wyss, M., Brugiroux, S., Keller, I., Macpherson, J.A., Rupp, S.*, et al.* (2015). The outer mucus layer hosts a distinct intestinal microbial niche. Nat Commun *6*, 8292.

Litvak, Y., and Baumler, A.J. (2019). Microbiota-Nourishing Immunity: A Guide to Understanding Our Microbial Self. Immunity *51*, 214-224.

Litvak, Y., Byndloss, M.X., and Baumler, A.J. (2018). Colonocyte metabolism shapes the gut microbiota. Science *362*.

Litvak, Y., Byndloss, M.X., Tsolis, R.M., and Baumler, A.J. (2017). Dysbiotic Proteobacteria expansion: a microbial signature of epithelial dysfunction. Curr Opin Microbiol *39*, 1-6.

Lopez, C.A., Miller, B.M., Rivera-Chavez, F., Velazquez, E.M., Byndloss, M.X., Chavez-Arroyo, A., Lokken, K.L., Tsolis, R.M., Winter, S.E., and Baumler, A.J. (2016). Virulence factors enhance Citrobacter rodentium expansion through aerobic respiration. Science *353*, 1249-1253.

Lupp, C., Robertson, M.L., Wickham, M.E., Sekirov, I., Champion, O.L., Gaynor, E.C., and Finlay, B.B. (2007). Host-mediated inflammation disrupts the intestinal microbiota and promotes the overgrowth of Enterobacteriaceae. Cell host & microbe *2*, 119-129.

Matziouridou, C., Rocha, S.D.C., Haabeth, O.A., Rudi, K., Carlsen, H., and Kielland, A. (2018). iNOS- and NOX1-dependent ROS production maintains bacterial homeostasis in the ileum of mice. Mucosal Immunol *11*, 774-784.

McMurdie, P.J., and Holmes, S. (2013). phyloseq: an R package for reproducible interactive analysis and graphics of microbiome census data. PLoS One *8*, e61217.

Pal, D., Venkova-Canova, T., Srivastava, P., and Chattoraj, D.K. (2005). Multipartite regulation of rctB, the replication initiator gene of Vibrio cholerae chromosome II. Journal of bacteriology *187*, 7167-7175.

Petty, N.K., Bulgin, R., Crepin, V.F., Cerdeno-Tarraga, A.M., Schroeder, G.N., Quail, M.A., Lennard, N., Corton, C., Barron, A., Clark, L.*, et al.* (2010). The Citrobacter rodentium genome sequence reveals convergent evolution with human pathogenic Escherichia coli. Journal of bacteriology *192*, 525-538.

Pircalabioru, G., Aviello, G., Kubica, M., Zhdanov, A., Paclet, M.H., Brennan, L., Hertzberger, R., Papkovsky, D., Bourke, B., and Knaus, U.G. (2016). Defensive Mutualism Rescues NADPH Oxidase Inactivation in Gut Infection. Cell Host Microbe *19*, 651-663.

Raffatellu, M., George, M.D., Akiyama, Y., Hornsby, M.J., Nuccio, S.P., Paixao, T.A., Butler, B.P., Chu, H., Santos, R.L., Berger, T.*, et al.* (2009). Lipocalin-2 resistance confers an advantage to Salmonella enterica serotype Typhimurium for growth and survival in the inflamed intestine. Cell Host Microbe *5*, 476-486.

Rigottier-Gois, L. (2013). Dysbiosis in inflammatory bowel diseases: the oxygen hypothesis. ISME J *7*, 1256-1261.

Rivera-Chavez, F., Lopez, C.A., and Baumler, A.J. (2017). Oxygen as a driver of gut dysbiosis. Free Radic Biol Med *105*, 93-101.

Rivera-Chavez, F., Zhang, L.F., Faber, F., Lopez, C.A., Byndloss, M.X., Olsan, E.E., Xu, G., Velazquez, E.M., Lebrilla, C.B., Winter, S.E.*, et al.* (2016). Depletion of Butyrate-Producing Clostridia from the Gut Microbiota Drives an Aerobic Luminal Expansion of Salmonella. Cell Host Microbe *19*, 443-454.

Schauer, D.B., and Falkow, S. (1993a). Attaching and effacing locus of a Citrobacter freundii biotype that causes transmissible murine colonic hyperplasia. Infect Immun *61*, 2486-2492.

Schauer, D.B., and Falkow, S. (1993b). The eae gene of Citrobacter freundii biotype 4280 is necessary for colonization in transmissible murine colonic hyperplasia. Infect Immun *61*, 4654-4661.

Schwerd, T., Bryant, R.V., Pandey, S., Capitani, M., Meran, L., Cazier, J.B., Jung, J., Mondal, K., Parkes, M., Mathew, C.G.*, et al.* (2018). NOX1 loss-of-function genetic variants in patients with inflammatory bowel disease. Mucosal Immunol *11*, 562-574.

Segata, N., Izard, J., Waldron, L., Gevers, D., Miropolsky, L., Garrett, W.S., and Huttenhower, C. (2011). Metagenomic biomarker discovery and explanation. Genome Biol *12*, R60.

Simon, R., Priefer, U., and Puhler, A. (1983). A broad host range mobilization system for in vivo genetic engineering: transposon mutagenesis in Gram-negative bacteria. Bio/Technology *1*, 784-791.

Spees, A.M., Wangdi, T., Lopez, C.A., Kingsbury, D.D., Xavier, M.N., Winter, S.E., Tsolis, R.M., and Baumler, A.J. (2013). Streptomycin-induced inflammation enhances Escherichia coli gut colonization through nitrate respiration. mBio *4*.

Spiga, L., Winter, M.G., Furtado de Carvalho, T., Zhu, W., Hughes, E.R., Gillis, C.C., Behrendt, C.L., Kim, J., Chessa, D., Andrews-Polymenis, H.L.*, et al.* (2017). An Oxidative Central Metabolism Enables Salmonella to Utilize Microbiota-Derived Succinate. Cell Host Microbe *22*, 291-301 e296.

Stecher, B., Robbiani, R., Walker, A.W., Westendorf, A.M., Barthel, M., Kremer, M., Chaffron, S., Macpherson, A.J., Buer, J., Parkhill, J.*, et al.* (2007). Salmonella enterica serovar

typhimurium exploits inflammation to compete with the intestinal microbiota. PLoS biology *5*, 2177-2189.

Tiffany, C.R., and Baumler, A.J. (2019). Dysbiosis: from fiction to function. Am J Physiol Gastrointest Liver Physiol *317*, G602-G608.

Tropini, C., Earle, K.A., Huang, K.C., and Sonnenburg, J.L. (2017). The Gut Microbiome: Connecting Spatial Organization to Function. Cell Host Microbe *21*, 433-442.

Tsolis, R.M., Adams, L.G., Ficht, T.A., and Baumler, A.J. (1999). Contribution of Salmonella typhimurium virulence factors to diarrheal disease in calves. Infect Immun *67*, 4879-4885.

Wang, R.F., and Kushner, S.R. (1991). Construction of versatile low-copy-number vectors for cloning, sequencing and gene expression in Escherichia coli. Gene *100*, 195-199.

Winter, S.E., Thiennimitr, P., Winter, M.G., Butler, B.P., Huseby, D.L., Crawford, R.W., Russell, J.M., Bevins, C.L., Adams, L.G., Tsolis, R.M.*, et al.* (2010). Gut inflammation provides a respiratory electron acceptor for Salmonella. Nature *467*, 426-429.

Yasuda, K., Oh, K., Ren, B., Tickle, T.L., Franzosa, E.A., Wachtman, L.M., Miller, A.D., Westmoreland, S.V., Mansfield, K.G., Vallender, E.J.*, et al.* (2015). Biogeography of the intestinal mucosal and lumenal microbiome in the rhesus macaque. Cell Host Microbe *17*, 385-391.

Zheng, L., Kelly, C.J., and Colgan, S.P. (2015). Physiologic hypoxia and oxygen homeostasis in the healthy intestine. A Review in the Theme: Cellular Responses to Hypoxia. Am J Physiol Cell Physiol *309*, C350-360.

SUPPLEMENTARY DATA

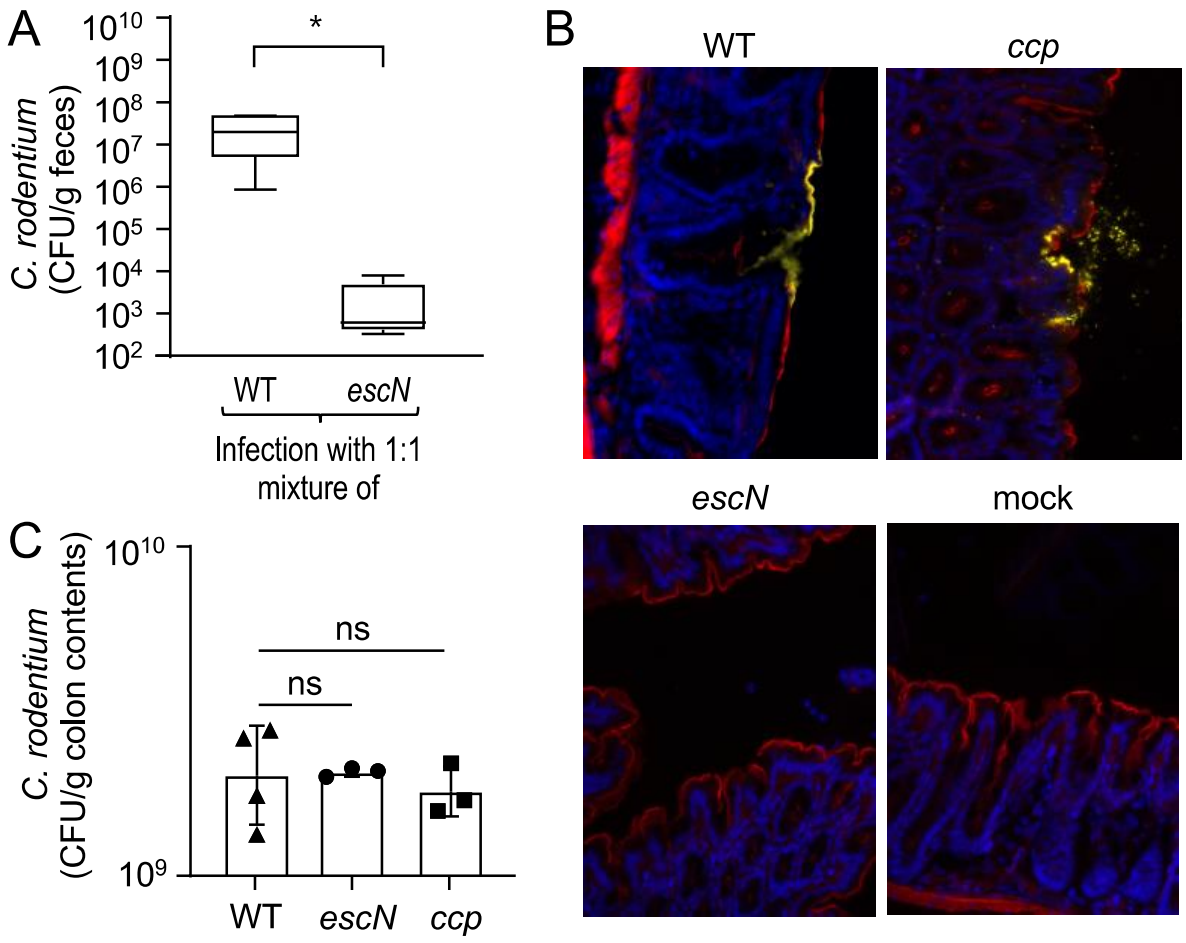

Figure S3.1: Related to Figure 3.1. The T3SS provides *C. rodentium* access to a spatial niche in close proximity to the mucosal surface.

(A) Mice (C57BL/6J, $N = 6$) were infected intragastrically with a 1:1 mixture of the *C. rodentium* wild type (WT) and an *escN* mutant. The graph shows recovery from the feces at 3 days after infection. (B and C) Germ-free mice (N is indicated in panel C) were mock inoculated or inoculated with the *C. rodentium* wild type (WT), a *ccp* mutant or an *escN* mutant. (B) *C. rodentium* (yellow fluorescence) was detected 5 days after infection in sections of the colon counterstained with DAPI nuclear stain (blue fluorescence). Actin was labelled with phalloidin-tetramethylrhodamine B isothiocyanate (red Fluorescence). (C) Colony-forming units (CFU) recovered from colon contents were enumerated. *, $P < 0.05$; ns, $P > 0.05$.

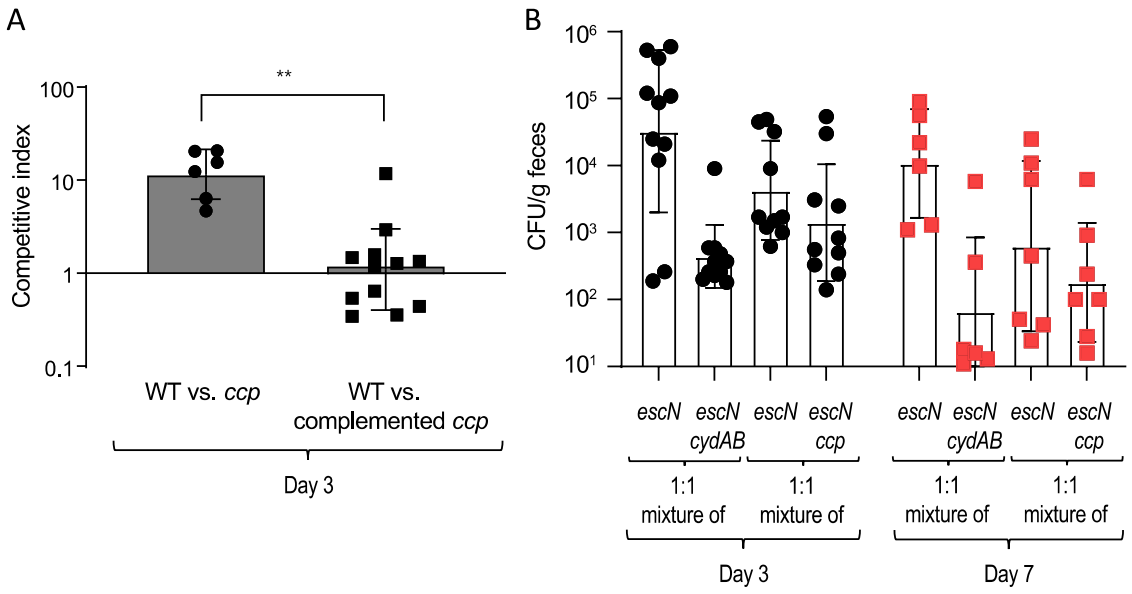

Figure S3.2: Related to Figure 3.1. Characterization of the growth advantage mediated by *ccp*

(A) Complementation of the *ccp* mutation (complemented *ccp* mutant) restored growth in the gut. Conventional mice (C57BL/6J) were infected intragastrically with a 1:1 mixture of the *C. rodentium* wild type (WT) and a *ccp* mutant (left bar) or mixtures the WT and a complemented *ccp* mutant (right bar) and the competitive index determined at the indicated time point after infection. (B) A functional T3SS is required for the *ccp*-mediated growth advantage. Conventional mice (C57BL/6J) were infected intragastrically with a 1:1 mixture of the indicated *C. rodentium* strain mixtures and the competitive index determined at the indicated time point after infection. (A and B) Each symbol (circles or squares) represents data from one animal. **, $P < 0.01$.

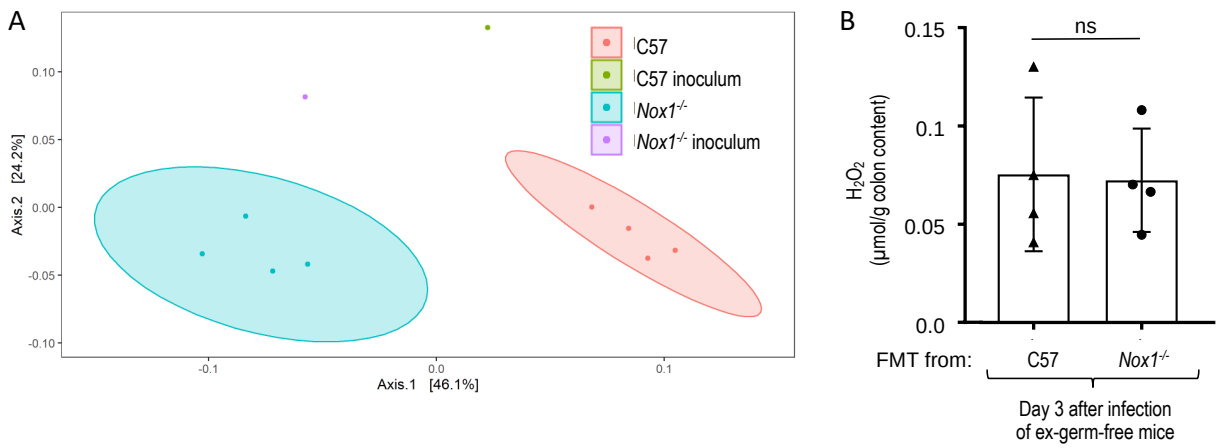

Fig. S3.3: Related to Figure 3.3. The microbiota composition does not govern H_2O_2 levels in the colon.

Germ-free mice (Swiss Webster, $N = 4$) received a fecal microbiota transplant (FMT) from conventional mice (C57) or congenic *Nox1*-deficient mice (*Nox1*$^{-/-}$) and seven days later mice were challenged with a 1:1 mixture of the *C. rodentium* wild type (WT) and a *ccp* mutant. (A) DNA was isolated from fecal contents and the microbiota composition analyzed by 16S rRNA gene amplicon sequencing. The graph shows a principal coordinates analysis of microbiota profiling data. (B) Hydrogen peroxide was measured in the supernatant of colon contents using Amplex Red and horseradish peroxidase on day 3 after infection. ns, $P > 0.05$.

Table S3.1: Related to Star Methods. Bacterial strains, plasmids and primers used in this study

Bacterial strains		
Species and strain	**Genotype**	**Reference**
C. rodentium DBS100	wild type; ATCC 51459	(Barthold et al., 1976)
C. rodentium CAL247	DBS100 Δ*cydAB*::Kan^R	(Lopez et al., 2016)
C. rodentium CAL286	DBS100 *escN*::pEP185.2	(Lopez et al., 2016)
C. rodentium CAL287	DBS100 *escN*::pEP185.2 Δ*cydAB*::Kan^R	(Lopez et al., 2016)
C. rodentium BMM39	DBS100 Δ*escN*::Kan^R	This study
C. rodentium BMM86	DBS100 Δ*cydAB*::Kan^R (pKD46)	This study
C. rodentium BMM87	DBS100 Δ*ccp*::Cm^R	This study
C. rodentium BMM88	DBS100 Δ*cydAB*::Kan^R Δ*ccp*::Cm^R	This study
C. rodentium BMM101	DBS100 Δ*cyxA*::Tet^R	This study
C. rodentium BMM104	DBS100 Δ*cydAB*::Kan^R Δ*ccp*::Cm^R Δ*cyxA*::Tet^R	This study
C. rodentium BMM109	DBS100 Δ*ccp*::Cm^R Δ*escN*::Kan^R	This study
E. coli DH5α *λpir*	F- *endA1 hsdR17* (r^-m^+) *supE44 thi-1 recA1 gyrA relA1 Δ(lacZYA-argF)$_{u189}$ Φ*80lacZΔM15	(Pal et al., 2005)
E. coli S17-1*λpir*	C600::RP4 2-(*tet::Mu*) (*kan::Tn7*) λ*pir recA1 thi pro hsdR* (r^-m^+)	(Simon et al., 1983)
S. Typhimurium AJB715	ATCC14028 nal^R *phoN::*KSAC	(Kingsley et al., 2003)
S. Typhimurium FF183	ATCC14028 nal^R Δ*invA* Δ*spiB phoN::*Tn10dCm	(Faber et al., 2016)
Plasmids		
Name	**Genotype**	**Reference**
pRDH10	*sacRB cat ori*R6K *mobRP4* Tet^R	(Kingsley et al., 1999)
pUC4 KSAC	ori(pMB1) bla Kan^R	(Lopez et al., 2016)
pSW172	ori(R101) *repA*101ts Carb^R	(Spees et al., 2013)

pEP185.2	oriR6K *mobRP4* Cm^R	(Kinder et al., 1993)
pBMM6	pRDH10 with regions upstream and downstream of *escN* flanking a KSAC cassette	This study
pKD46	Red recombinase system, arabinose inducible, 30°C permissive, $Spec^R$	(Datsenko and Wanner, 2000)
pSPN23	pBluescriptII KS+, $Carb^R$, Tet^R	(Raffatellu et al., 2009)
pWSK129	Cloning vector; Kan^R	(Wang and Kushner, 1991)
pBMM18	pWSK129::*ccp*	This study
Primers		
Gene	**Sequence**	**Organism**
escN	5'-TTCTGGCTGGCCTGAAAAGAGAGCACGGGT-3' 5'-GGCTTTCCCCAGCGAATCGTTTGAGGGAGT-3 5'-ACGATTCGCTGGGGAAAGCCACGTTGTGTC-3' 5'-TCTTTTCAGGCCAGCCAGAAAGTGAGGGAG-3'	*C. rodentium*
ccp	5'- TTGAAAATCATTACTCGTCTTACCGCGATCGCTATCGC AGGCATTGTTATTTGTTATTCAGGATTATCTGCGTGATC GGCACGTAAGAGG-3' 5'- GAGTGGCAGGGCGGGGCGTAAGATTGACGATATTGTC GCTTTTCTCGAAAGCCTGACCGGGGTGTATACGCCTTA TATGCAGGGCAAGTAA-3'	*C. rodentium*
cyxA	5'- ACGCTTCGCTTAACTTTTTCTGGATGTTGTTATTTCCAT GCGCAGGTATCGTCATATAAACGGGAGAAAATATACG ACCCGGGCCTGCAGG-3' 5'- CAGCAGGACGCTGGCGCACCAGATAGCAATCAGCCAC GCCACGCGATGCGACCATTTCCTGATTTTCGCCAATAC GACCCGGGCCTGCAGG-3'	*C. rodentium*
18s	5'-TGCATGGCCGTTCTTAGTTG-3' 5'-AGTTAGCATGCCAGAGTCTCGTT-3'	Mouse
Ifng	5'-CAACAGCAAGGCGAAAAAGGATGC-3' 5'-CCCCGAATCAGCAGCGACTCC-3'	Mouse
Nos2	5'-CCTCTTTCAGGTCACTTTGGTAGG-3' 5'-TTGGGTCTTGTTCAGCCACGG-3'	Mouse
Il6	5'-TCCAGAAACCGCTATGAAGTTCC-3' 5'-CACCAGCATCAGTCCCAAGAAG-3'	Mouse
Lcn2	5'-ACATTTGTTCCAAGCTCCAGGGC-3' 5'-CATGGCGAACTGGTTGTAGTCCG-3'	Mouse
Il22	5'-GGCCAGCCTTGCAGATAACA-3' 5'-GCTGATGTGACAGGAGCTGA-3'	Mouse

Table S3.2: Related to Star Methods. Criteria used for histopathological grading of colonic lesions

Histologic feature	Score	Criteria
Infiltration by polymorphonuclear cells	0	rare neutrophils within lamina propria
	1	occasional multifocal increased frequency of neutrophils within lamina propria
	2	diffuse infiltration of the lamina propria by low numbers of neutrophils
	3	diffuse infiltration of the submucosa and lamina propria by moderate numbers of neutrophils
	4	diffuse transmural infiltration of the submucosa, lamina propria, and muscle layers by high numbers of neutrophils
Infiltration by mononuclear cells	0	no detectable increase in mononuclear infiltration of the lamina propria
	1	mild multifocal expansion of the lamina propria by low numbers of infiltrating lymphocytes and plasma cells
	2	mild regional expansion of the lamina propria by moderate numbers of lymphocytes and plasma cells
	3	moderate regional to diffuse expansion of the lamina propria and epithelia by infiltrating lymphocytes and plasma cells
	4	severe diffuse expansion of the lamina propria and epithelia by infiltrating lymphocytes and plasma cells with distortion of the mucosal architecture
Edema	0	no observable edema
	1	mild multifocal perivascular expansion of the tunica adventitia
	2	moderate multifocal expansion of the submucosa with lymphatic dilation
	3	marked circumferential expansion of the submucosa with marked lymphatic dilation
	4	severe circumferential expansion of the submucosa with marked lymphatic dilation
Luminal suppurative exudate	0	no observable accumulation of suppurative exudate within the lumen
	1	mild accumulation of exudate
	2	moderate accumulation exudate
	3	marked accumulation of exudate
	4	severe accumulation of exudate

Crypt abscessation	0	no crypt abscessation observed
	1	rare small crypt abscess formation
	2	occasional small crypt abscess formation
	3	frequent small and medium crypt abscess
	4	abundant large crypt abscess formation
Brush border bacterial colonization	0	no bacterial colonization of brush border
	1	multifocal surface colonization
	2	regional surface colonization
	3	diffuse surface colonization
	4	diffuse surface colonization with extension into colonic crypt epithelium
Superficial epithelial injury	0	no observable disruption to the brush border or surface epithelium
	1	occasional multifocal brush border attenuation with increased apoptosis
	2	frequent to confluent brush border attenuation with abundant apoptosis
	3	marked brush border attenuation with loss of epithelial adhesion
	4	severe brush border attenuation with cell loss leading to erosive lesions of the superficial mucosa
Mucosal epithelial hyperplasia (number of cells per individual crypt height)	0	no observable hyperplasia (<20)
	1	mild crypt elongation (21-25)
	2	moderate crypt elongation (26-30)
	3	marked crypt elongation (31-35)
	4	severe crypt elongation (>35)
Goblet cell depletion	0	no observable depletion of goblet cells
	1	minimal depletion of goblet cells
	2	mild depletion of goblet cells
	3	moderate depletion of goblet cells
	4	marked depletion of goblet cells

Chapter 4

Salmonella Typhimurium modulates host IL-22 production to compete with the gut microbiota via the *gabTP*-dependent consumption of GABA

Brittany M. Miller[1], Lillian F. Zhang[1], Christopher A. Lopez[1,2], Eric M. Velazquez[1], Megan J. Liou[1], Henry Nguyen[1], Lauren C. Radlinski[1], Andreas J. Bäumler[1].

Affiliations:

[1] Department of Medical Microbiology and Immunology, School of Medicine, University of California, Davis, One Shields Avenue, Davis, CA, USA.

[2] Department of Biological Sciences, California State University, Sacramento, CA 95819, USA.

ABSTRACT

Salmonella *enterica* encodes an impressive array of metabolic pathways, however the significance of many of these pathways during infection remains to be determined. Interestingly, a recent *in silico* analysis revealed *Salmonella* serovars that cause intestinal disease, but not those that cause extra-intestinal disease, are able to uptake and catabolize gamma-aminobutyric acid (GABA). GABA is a major inhibitory neurotransmitter in the mammalian nervous system that may play a role in gastrointestinal function via involvement in the enteric nervous system. To explore the consequences of GABA utilization during infection, we first measured GABA concentration in the cecal contents of CBA/J mice infected with *S.* Typhimurium. Mice infected with a mutant in the GABA utilization operon (*gabTP*), had significantly more GABA compared to uninfected and wild-type infected mice, confirming that *S.* Typhimurium consumes GABA during infection. As GABA can be both host and microbiota derived, we next wanted to find the source of GABA. We conducted the same experiment in germ-free (GF) Swiss Webster mice, and intriguingly, we found no difference in GABA levels between the wild type and *gabTP*-infected GF mice. Additionally, cecal contents of GF mice contained approximately 100 times less GABA than those of conventional mice, indicating GABA in the cecal contents of conventional mice is primarily microbiota-derived. While GABA levels changed, the wild type had no growth advantage over the mutant in CBA/J mice in single or competitive infections. The significance of GABA to host gut physiology is still unclear, but could contribute to GI motor activity as well as modulation of immune cells. We therefore reasoned that *S.* Typhimurium GABA consumption could alter host physiology or immune responses during infection. To test this idea, we first measured whole gut transit time of infected mice using the Evans blue dye method. Gut transit time was decreased in mutant infected mice compared to wild-type and mock, suggesting that GABA concentrations alone could affect gut motility. We next used qPCR to determine differences in inflammatory status in the cecal tissue of infected mice. At ten- and fourteen-days post infection in CBA/J mice, we found a trend towards decreasing pro-inflammatory cytokines in the mutant infected mice compared to the wild-type, including Kc, a murine neutrophil chemoattractant. Interestingly,

gabTP infected mice did not upregulate IL-22 significantly, as expected from a wild-type infection. Because IL-22 has an effect on iron withholding and competition with *Enterobacteriaceae*, we next asked whether *gabTP* affects competition through modulating IL-22 levels. When *S.* Typhimurium was in competition with *Escherchia coli* JB2, it was able to outcompete JB2, however, the *gabTP* mutant was not able to outcompete, and both strains grew to similar numbers. Our results indicate that *gabTP*-dependent consumption of GABA boosts *S.* Typhimurium growth over related *Enterobactericeae* by modulating levels of IL-22. This work helps further illustrate the effect of the gut microbiota-derived metabolic profile on the host, and how *Salmonella* is able to engineer the host immune response to the benefit of the pathogen.

INTRODUCTION

Gamma-aminobutyric acid (GABA) has well defined roles in the human body as the main inhibitory neurotransmitter of the central nervous system (CNS) (Ognen, 2002). However, less is known of the role of GABA in the enteric nervous system (ENS). Because enteric GABA sources include both mucosal endocrine like-cells and neurons, GABA is thought to play both a neural and endocrine regulating role in the gut (Auteri et al., 2015). There are three types of GABA receptors, and all are found in the gut, including on neuronal and non-neuronal tissues, and interestingly, on certain immune cells, such as T cells (Mendu et al., 2012), dendritic cells (Jin et al., 2013), as well as on murine intestinal epithelial cells (Ma et al., 2018). In animals and plants, GABA is produced by the cytosolic enzyme glutamate decarboxylase (Buddhala et al., 2009). GABA seems to negatively regulate pro-inflammatory cytokine production, as well as immune cell proliferation (Auteri et al., 2015). Additionally, GABA can modulate gut GI motility, as well as peristalsis, and gastrointestinal secretion (Auteri et al., 2014).

Members of the gut microbiota of both mouse and humans have been shown to have the ability to produce and excrete GABA (Strandwitz et al., 2019). In particular, species of lactic acid bacteria and *Bacteroides* ssp. are known to be major GABA producers (Dhakal et al., 2012; Strandwitz et al., 2019). One common way GABA is produced is from the precursor glutamate, in a process that becomes a proton sink, aiding with acid tolerance for the bacterium (Foster, 2004). Glutamate decarboxylase (GAD) genes are widely spread throughout plants, animals, and bacteria, in fact, the first isolation of GABA from a microbe was from yeast (Reed, 1950). Microbes having GAD genes in the family *Enterobacteriaceae* include *Escherichia coli*, but interestingly, not *Salmonella enterica* (Smith et al., 1992). Another manner through which GABA is produced is from the breakdown of putrescine, which may be important during times of nitrogen starvation (Kurihara et al., 2010). The microbiota also has the potential to consume GABA. Some species of the order *Clostridiales* can ferment GABA to butyrate and acetate (Gerhardt et al., 2000). More recently, a previously unculturable gut microbiota bacterial isolate was found to require GABA for growth (Strandwitz et al., 2019). Besides acid tolerance, the metabolism of GABA is generally known

as the GABA shunt, by which GABA is converted to succinate, which then enters the TCA cycle (Feehily and Karatzas, 2013).

While the effects of GABA on host physiology are becoming increasingly appreciated, so too is the role of the microbiota in this gut-brain axis. *Lactobacillus rhamnosus* JB-1 given orally was shown to decrease anxiety in mice, via modulating GABA receptor RNA in the brain (Bravo et al., 2011). Another study found that by administering the same probiotic, GABA levels in the brain were affected 4 weeks after administration, indicating that a member of the gut microbiota producing GABA is capable of having long-lasting effects on the host nervous system (Janik et al., 2016). It is therefore of great importance to understand the connection between a microbiota metabolite, GABA, and the host.

In a large analysis of *Salmonella* genomes, it was found that *Salmonella* serovars associated with gastrointestinal disease have an operon (*gabDTP*) capable of importing and metabolizing GABA, a feature that is degraded in many serovars associated with extraintestinal disease (i.e. Typhi, Dublin, and Gallinarum), indicating that this operon may be important for the intestinal lifestyle of those *Salmonella* serovars (Nuccio and Bäumler, 2014). The *gabDTP* operon encodes a specific GABA permease (*gabP*), a GABA transaminase (*gabT*), as well as *gabD*, a succinic semialdehyde dehydrogenase, which converts succinate semialdehyde to succinate (Metzer et al., 1979). Interestingly, *gabD* is not degraded in many extraintestinal strains, however, another gene performing the same function, *sad*, is degraded (Nuccio and Bäumler, 2014). Here, we explore the role of the *gabDTP* operon during infection with *S.* Typhimurium. The physiological role of *gabDTP* remains unknown for the pathogen, as *S.* Typhimurium cannot use GABA as a sole carbon or nitrogen source *in vitro* (Gutnick et al., 1969). We uncovered a previously unknown mechanism by which *S.* Typhimurium can outcompete similar *Enterobacteriaceae* by modulating levels of GABA, leading to changes in IL-22 expression, favoring the pathogen growth over a commensal *E. coli*.

RESULTS

The *S.* Typhimurium *gabTP* operon changes GABA levels but does not enhance *S.* Typhimurium growth

The role of GABA uptake by *S.* Typhimurium during infection is not well understood. To investigate whether GABA promotes the growth of *Salmonella* in the mouse gut, we constructed an *S.* Typhimurium mutant strain lacking *gabT* and *gabP*, which encode proteins involved in GABA uptake and catabolism (Metzer et al., 1979). We then infected mice treated with a single dose of streptomycin one day prior to infection and saw no difference in recovery between the wild type (wt) and the mutant *S.* Typhimurium at day 4 post infection in cecal contents, colon contents, and in the spleen (**Fig. 4.1A**).

As GABA can be produced by the microbiota, we reasoned that the streptomycin mouse model may not be ideal to investigate whether *S.* Typhimurium can benefit from GABA, as streptomycin is known to change the gut microbiota composition and density (Stecher et al., 2007; Rivera-Chávez et al., 2016). We therefore decided to use the genetically resistant CBA mouse model, which does not require streptomycin pre-treatment for infection. When *S.* Typhimurium wt was competed against the mutant in this model, both were recovered in equal ratios in the cecal contents and the spleen at day 14 post infection (**Fig 4.1B**). Upon infection of CBA mice with either a single gavage of wt or *gabTP*, there was no significant difference between CFUs recovered from feces at any day tested (**Fig 4.1C**). CFUs for both strains tend to peak around day 10 but mice stay highly infected through day 14. CFUs from organs from the single infected mice were also plated to compare disseminated bacterial CFUs, however, in the spleen, liver, Peyer's patches, as well as the mesenteric lymph node, there was no significant difference in CFUs recovered (**Fig 4.1D**). The use of these models indicates that *gabTP* does not provide a fitness benefit to *S.* Typhimurium during infection.

We next wondered if *gabTP* played another function during infection of mice. As *gabP* encodes a specific GABA permease, we next looked at whether there was a difference in the amount of GABA in the cecal contents of mice infected with the wild type or the mutant, which is unable to take up GABA. Whereas infection of mice with *gabTP* mutant alone raised the fecal concentration of GABA, this was not observed during infection with the wild type, indicative of a *gabTP*-dependent GABA depletion during infection (**Fig**

4.1E). In summary, *S.* Typhimurium consumes GABA in the inflamed mouse gut, which does not provide a growth benefit to the pathogen but does change the levels of GABA in the gut lumen.

S. Typhimurium *gabTP* affects the host GI physiology

While the functions of GABA in the gut remain to be fully elucidated, it has been shown to play a role in peristalsis of the gut (Auteri et al., 2014)., To assess peristalsis rates, CBA mice were infected with either *S.* Typhimurium wtor *gabTP*, or LB as a mock control, and on day 10 post infection, the peak of infection in this model (**Fig 4.1C**), mice were gavaged with a mixture of Evans Blue dye and gum arabic, and the time until the first blue fecal pellet was passed was measured (Seerden et al., 2005). Mice infected with wild type *S.* Typhimurium had a significantly longer gut transit time than either mock or *gabTP* infected mice (**Fig. 4.2A**), despite both groups of infected mice having similar CFUs recovered from fecal pellets (**Fig. 4.2B**).

Next, we wanted to determine the source of the increase in GABA in mice infected with *gabTP*. Mice are capable of GABA production, via two isoforms of glutamate decarboxylase, GAD65 and GAD67 (Obata et al., 2008). Whether infected with the wt or *gabTP* strain, there was not an increased expression in host GAD isoforms in the cecal tissue compared to mock treated animals at day 10 post infection (**Fig 4.2C**), indicating that infection with *S.* Typhimurium does not increase host cecal production of GABA.

GABA is known to be produced by the microbiota, with *Bacteroides* species in particular producing large quantities of the neurotransmitter (Strandwitz et al., 2019). To determine whether GABA is produced by the microbiota in mice, we obtained cecal contents from germ-free mice, either mock infected, or infected with *S.* Typhimurium wt or *gabTP*, and measured levels of GABA via ELISA. We observed a 1-2 log fold decrease in GABA per gram of cecal content in germ-free mice compared to SPF mice (**Fig 4.2D**), indicating that while there is some GABA produced by the host, much of the neurotransmitter is indeed produced by the gut microbiota. Intriguingly, there was no significant difference between the GABA levels of germ-free mice infected with wild type or *gabTP*, indicating that the change in GABA seen in the SPF mice is likely due to the microbiota (**Fig 4.2D**). It is unclear, however, whether *S.* Typhimurium

inflammation-dependent microbiota reshaping is responsible for the change in GABA levels, or if another host cell type is involved.

GABA consumption by *S.* Typhimurium upregulates IL-22 expression

Another well described role of GABA in the gut is that of immunity, as GABA has been shown to negatively regulate pro-inflammatory cytokines as well as immune cell proliferation (Auteri et al., 2015). To test whether *S.* Typhimurium *gabTP*-dependent consumption of GABA leads to an increase in inflammatory cytokines, we used real-time PCR to measure various cytokines in cecal tissue at day 14 post infection. We found that mice infected with *gabTP* had significantly less upregulation of pro-inflammatory genes, such as *Il6*, *Ifng*, and *Kc* (*Cxcl1*) compared to wild type infected animals, however, these genes were still significantly upregulated compared to mock infected animals (**Fig 4.3A**). This change occurred not because of an increase in *S.* Typhimurium CFUs in the cecum, as there was no significant difference in CFUs recovered between wild type and *gabTP* infected animals (**Fig 4.3B**). This indicates that *Salmonella* infection leads to less GABA in the cecum, which leads to higher levels of inflammation. Interestingly, IL-22 expression was not significantly upregulated in *gabTP* mice compared to mock treated animals, but there was significant upregulation in mice infected with wild type *S.* Typhimurium (**Fig 4.3A**).

Consuming GABA helps *S.* Typhimurium compete against the microbiota

We next focused on IL-22, based on a recent report showing that dietary GABA inhibits IL-22 synthesis (Chen et al., 2019). Furthermore, during *S.* Typhimurium infection, IL-22 is highly upregulated in mice and rhesus macques (Godinez et al., 2009; Raffatellu et al., 2008). IL-22 has various functions during infection as a modulator of tissue repair and host defense (Valeri and Raffatellu, 2016). Expression of IL-22 has been shown to suppress the microbiota during infection via metal sequestration, which *S.* Typhimurium is able to overcome and thus bloom in the gut (Behnsen et al., 2014). Behnsen et al. showed that IL-22 enhances the ability of *S.* Typhimurium to compete with commensal *E. coli* strains that rely on enterobactin for iron acquisition, because IL-22 stimulates release of lipocalin-2 by epithelial cells to block

their growth. Production of salmochelin renders *S.* Typhimurium lipocalin-2 resistant, therefore providing the pathogen with a growth advantage over *E. coli*, but this growth advantage is no longer observed in IL-22-deficient mice. In essence, these observations supported a scenario in which *gabTP*-mediated GABA depletion increases IL-22 levels during colitis, thereby inducing epithelial lipocalin-2 release, which in turn provides a growth advantage for *S.* Typhimurium over commensal *E. coli* strains that rely on enterobactin for iron acquisition. This hypothesis suggested that our initial experiments did not detect a contribution of *gabTP* to fitness (**Fig. 4.1A,B**) because the experiment had been performed in the absence of an *E. coli* competitor. To test this idea, we first infected CBA mice with *S.* Typhimurium wild type or *gabTP*, then gave mice *E. coli* JB2, a murine commensal isolate that produces enterobactin but not salmochelin via oral gavage one day post infection with *Salmonella* (Behnsen et al., 2014). By day 6 post infection, wild type *Salmonella* grew to significantly higher CFU than *E. coli* JB2 in fecal pellets, however, *gabTP* did not outcompete *E. coli* significantly (**Fig 4.3C**). By day 10 post infection, wild type *S.* Typhimurium grew to higher CFUs than *E. coli* and had significantly higher colonization than the *gabTP* strain (**Fig 4.3C**). Consistent with our hypothesis, the *gabTP* genes enhanced *S.* Typhimurium recovery from the feces in the presence of commensal *E.* coli JB2, showing that GABA depletion provides a benefit to *S.* Typhimurium during its competition with endogenous *E. coli.*

DISCUSSION

The function of GABA in the gut is still not fully elucidated. Here, we found that an enteric pathogen, *S.* Typhimurium, could modulate GABA levels for the benefit of the pathogen to outcompete the gut microbiota. Studies on *S.* Typhimurium have shown that the pathogen is able to induce inflammation in the gut, and paradoxically benefit from this immune response meant to fend off the pathogenic invader (Barman et al., 2008; Stecher et al., 2007). It is therefore no surprise that *S.* Typhimurium can modulate many host processes, including the innate inflammatory response, or by modulating levels of a host neurotransmitter as shown here. The discovery that *S.* Typhimurium is able to induce IL-22 expression, in part by the consumption of GABA, an anti-inflammatory compound, melds nicely with what is known

about *S.* Typhimurium promoting inflammation during infection. This IL-22 expression leads to the pathogen being able to outcompete a closely related *Enterobacteriaceae*, *E. coli* JB2. We additionally saw that GABA levels during infection were able to change not only inflammation status, but gut transit time as well. This agrees with the body of literature of GABA playing a role in gut peristalsis (Auteri et al., 2014).

This study, however, has left much to be explored. The source of the increase in GABA seen in mice infected with *gabTP* remains to be found. Because *S.* Typhimurium is able to change both the composition and density of the gut microbiota during infection, an attractive possibility would be that this inflammation is reducing a gut member that consumes GABA, or perhaps the inflammation is benefitting a GABA producer as well (Stecher et al., 2007). Although we saw slight differences in cytokines, overall, there was still heavy inflammation, with *gabTP* affecting IL-22 most significantly. Perhaps a reduction in a immune cell population related to the action of IL-22 during inflammation is the answer. Another possibility is that the host is upregulating GABA production. As mentioned before, while we did not see changes in glutamate decarboxylase expression in whole cecal tissue (**Fig 4.2C**), a certain cell type could be overlooked that is producing GABA in the gut during infection. This is a less likely scenario, due to not finding a difference in GABA levels between wild type and *gabTP* infected germ-free mice (**Fig 4.2D**). The source of IL-22 following infection is as well still being studied. Knowing the source of IL-22 is important, as it could then be tested whether this cell type is directly influenced by GABA levels, or if there is another indirect way of modulation. The link between GABA and IL-22 therefore is a key question left unanswered by this work. A recent study showed that oral supplementation of GABA to weaning piglets decreased IL-22 expression, but the mechanism there as well as in this study is unclear (Chen et al., 2019).

Overall, we show that *Salmonella* infection leads to less GABA being available, which leads to higher levels of inflammation, as well as normal upregulation of IL-22, which helps dampen growth of *E. coli* JB2 while boosting growth of *S.* Typhimurium. This study adds to the body of literature explaining how *S.* Typhimurium is able to finely modulate the host to carve out a niche for pathogen expansion, and outcompete the gut microbiota.

Figures

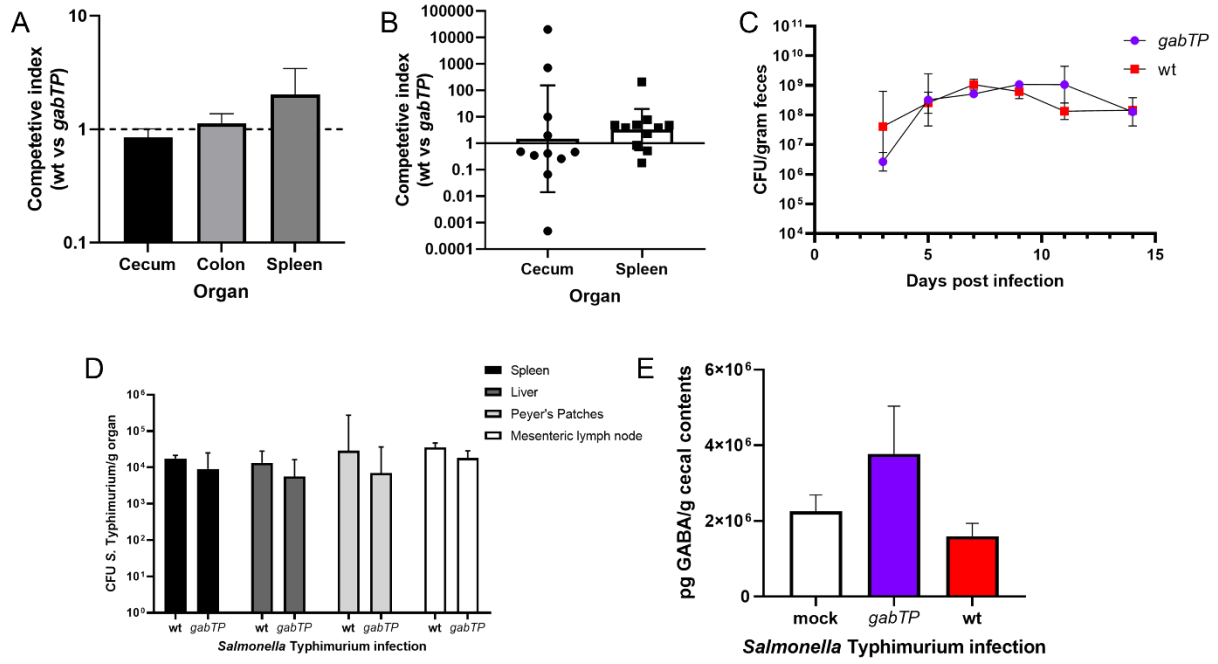

Figure 4.1: (A) Mice (C57BL/6J, N=6) were treated with streptomycin and infected intragastrically with a 1:1 mixture of both *S.* Typhimurium wild type (wt) and *gabTP* mutant one day later. The graph shows the competitive index calculated from the cecal contents, colon contents, and spleen 4 days after infection. (B) Mice (CBA/J, N=11) were infected intragastrically with a 1:1 mixture of *S.* Typhimurium wt and *gabTP*. The graph shows the competitive index determined from the cecal contents and spleen 14 days after infection. (C-D) Mice (CBA/J, N=6) were infected intragastrically with *S.* Typhimurium wt or *gabTP*. (C) Graph shows recovery from fecal contents on indicated days. (D) Graph shows recovery from indicated organs on day 14 post infection. (E) Mice (CBA/J, N=6) were infected intragastrically with *S.* Typhimurium wild type (wt), or *gabTP*, or with LB as mock control. 14 days post infection, cecal contents were obtained, and GABA was quantified via ELISA.

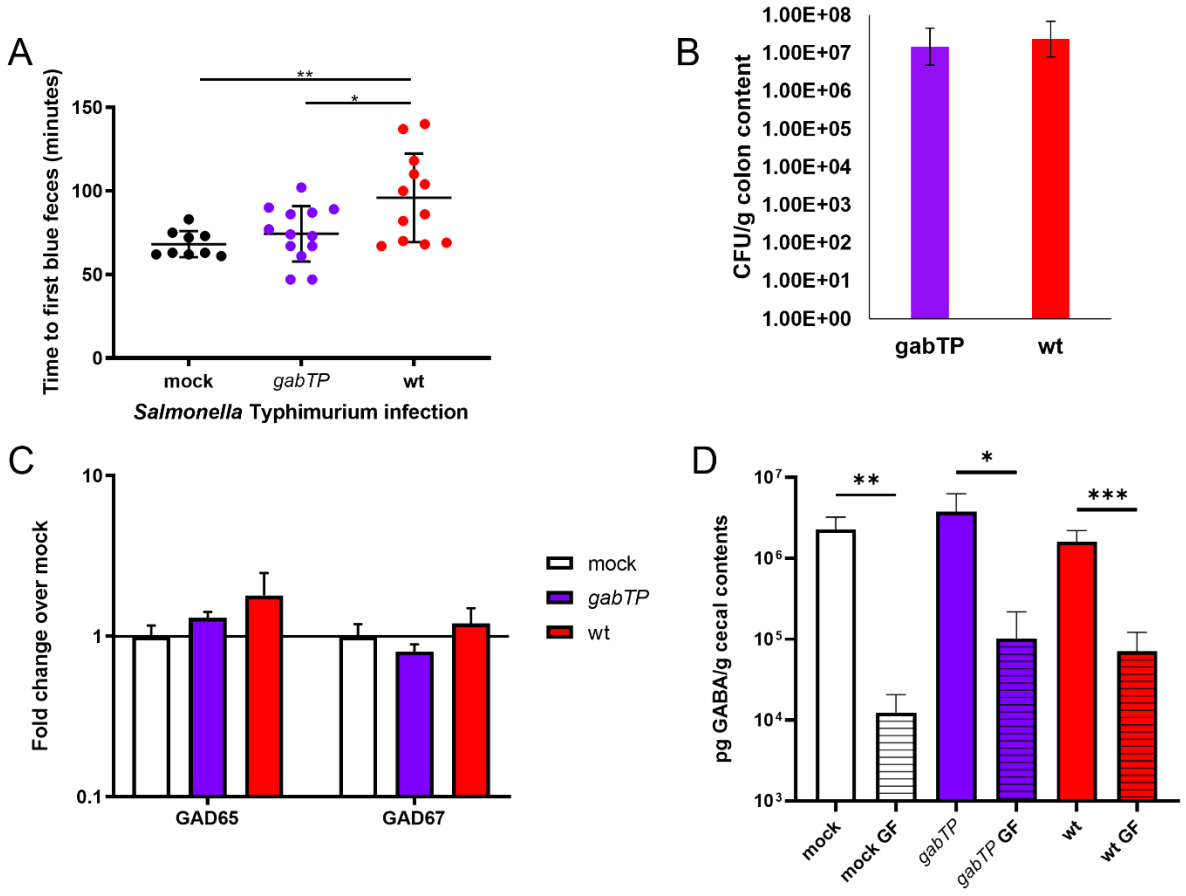

Figure 4.2: (A-C) Mice (CBA/J, N =11-13) were infected intragastrically with LB as mock control, *S.* Typhimurium wild type (wt), or *gabTP*. (A) Gut transit time was measured and (B) CFUs were determined at day 10 post infection. (C) Glutamate decarboxylase expression was quantified by real-time PCR from cecal tissue at day 10 post infection. (D) Mice (germ-free Swiss Webster [GF] N=4 or CBA/J N=6) were infected intragastrically with LB as mock control, *S.* Typhimurium wt, or *gabTP*. GABA was measured via ELISA from the cecal contents at day 3 (for germ-free mice) or day 14 (for CBA/J mice) post infection. $^{*}p < 0.05$; $^{**}p < 0.01$; $^{***}p < 0.005$.

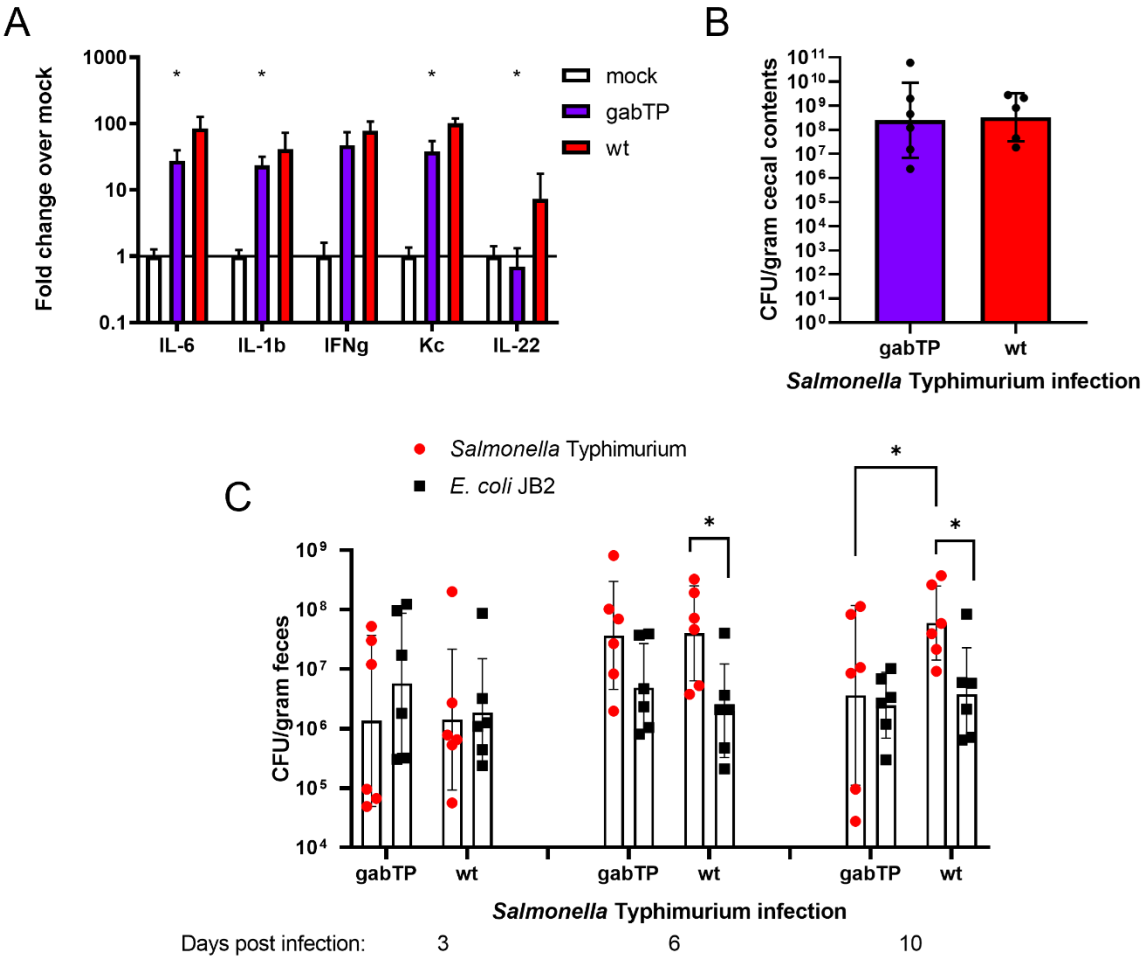

Figure 4.3: (A-B) Mice (CBA/J, N=5-6) were infected with LB as mock control, or *S.* Typhimurium wild type (wt), or *gabTP*. (A) Real-time PCR was used to measure the indicated gene expression levels at 14 days post infection. Statistical analysis indicated whether expression was significantly different between the wt and *gabTP* infected samples. (B) CFUs recovered were determined at day 14 post infection. (C) Mice (CBA/J, N=6) were intragastrically infected with *S.* Typhimurium wt or *gabTP*. One day post infection, mice were infected intragastrically with *E. coli* JB2. CFUs of *S.* Typhimurium and *E. coli* were determined in fecal contents at the indicated days post infection. $^{*}p < 0.05$.

Materials and Methods

Bacterial strains and culture conditions

For the *Salmonella enterica* Typhimurium and *Escherichia coli* strains used in this study, see Table S4.1. Strains were grown routinely in Luria-Burtani broth (BD Biosciences #244620) or on LB plates unless otherwise indicated, at 37°C. Antibiotics were used, when necessary, at the following concentrations: carbenicillin (carb), 0.1 mg/ml; chloramphenicol (Cm), 0.03 mg/ml; kanamycin (Kan), 0.1 mg/ml.

Mutant construction

To construct a *gabTP* mutant, regions of approximately 800 bp in length flanking the *gabTP* genes were amplified via PCR using Q5 High Fidelity 2X Master Mix (NEB) using the primers listed in Table S4.2. Products were run on an agarose gel and purified using the Zymoclean Gel DNA Recovery Kit (Zymo Research). The fragments were ligated into pRDH10 using Gibson Assembly Master Mix (NEB). The plasmid, pBMM2, was propagated in *E. coli* DH5*α λpir,* and transformed into chemically competent *E. coli* S17-1 *λpir*, which was then conjugated with AJB715 or IR715. Double crossover events were selected via sucrose selection, and mutants were screened for loss of Cm resistance, and PCR was used to confirm the deletion. The strain was then named BMM19 (containing *phoN::KSAC*) and BMM16.

For construction of an *iroN* mutant, regions of approximately 600 bp in length flanking the *iroN* gene were amplified via PCR using Q5 High Fidelity 2X Master Mix (NEB) using the primers listed in Table S4.2. Products were run on an agarose gel and purified using the Zymoclean Gel DNA Recovery Kit (Zymo Research). The carbenicillin cassette was obtained in a similar manner via PCR using pRE107 as template, followed by gel purification. The three fragments were ligated into pRE118 using Gibson Assembly Master Mix (NEB). The plasmid, pBMM25, was propagated in *E. coli* DH5*α λpir,* and transformed into chemically competent E. coli S17-1 *λpir*, which was then conjugated with BMM16 and FF176. Double crossover events were selected for via sucrose selection, and mutants were screened for resistance to carb, loss of Cm

resistance, and PCR was used to confirm the deletions. The strains were then named BMM148 and BMM147. To create a Kan resistant BMM148, phage P22 HT *int-105* was used for generalized transduction. A P22 lysate of the strain FF176 was generated, and used to transduce the *phoN::KSAC* into BMM148 to generate BMM149. Transductants were cleaned from phage contamination on Evans blue-Uranine (EBU) plates, and transductants were tested for phage sensitivity by cross-streaking against P22 H5.

To create a carb resistant *E. coli* JB2, pCAL62 was electroporated into JB2. The resultant colonies were selected via plating on LB plates containing carb.

Mouse experiments

The Institutional Animal Care and Use Committee at the University of California, Davis, approved all animal experiments. For experiments involving specific pathogen free mice, C57BL6/J or CBA/J mouse strains (Jackson Laboratories) aged 5-8 weeks were inoculated with $1x10^9$ colony forming units (CFU) per mouse of a single *S.* Typhimurium strain in LB broth intragastrically, or 0.1 ml sterile LB broth as mock infection. For some experiments, mice were given an equal ratio of $5x10^8$ CFU wild type and $5x10^8$ CFU mutant strain. For experiments involving C57BL/6J mice, mice were given a single dose of 20 mg streptomycin per mouse one day prior to infection unless otherwise indicated. Fecal pellets were collected on days 0 through 14 post infection, and mice were sacrificed between days 3 and 14 post infection. Cecal contents were collected in sterile phosphate-buffered saline (PBS) on ice. Cecal tissue collected for histopathology was stored in 10% phosphate buffered formalin overnight, followed by storage in 70% ethanol. Cecal tissue collected for murine RNA analysis were flash frozen and stored at -80°C. *S.* Typhimurium from feces and cecal contents were enumerated by plating serial ten-fold dilutions of samples on LB agar (BD Biosciences) containing the appropriate antibiotics. Plates were incubated overnight at 37°C under atmospheric oxygen conditions.

Germ-free Swiss Webster mice were bred and housed at the Teaching and Research Animal Care Services facilities at UC Davis. Male and female mice aged 5-10 weeks were used and were infected and euthanized as described above. Mice were kept in sterile cages in a biosafety cabinet for the duration of the experiments.

To measure whole gut transit time of mice, mice were individually housed in a cage containing no bedding but with shredding enrichment paper an hour prior to the experiment. At 6 p.m. (to account the nocturnal nature of mice), mice were gavaged with 100 µl of a mixture of 5% Evans blue and 5% gum arabic in sterile water. The time was noted for the gavage of each individual mouse, and gut transit time was calculated as the minutes until the first blue fecal pellet was passed.

Isolation of RNA from mouse tissue and quantitative real-time PCR

Murine cecal tissue samples were homogenized in TRI Reagent (Molecular Research Center, Inc.) using a Mini-Beadbeater (BioSpec Products) and RNA was isolated following the manufacturer's protocol. RNA was eluted in DNase buffer and contaminating DNA was removed using the DNA-free kit (Applied Biosystems), and RNA was stored at -80°C.

RNA concentration and quality were measured spectrophotometrically using a Nanodrop (ND-1000, Nanodrop Technologies). Isolated RNA from murine samples was reverse transcribed using random hexamers and MuLV reverse transcriptase (Applied Biosystems). Quantitative real-time PCR (qPCR) was performed using SYBR green PCR mix (Applied Biosystems) and the primer sets listed in Table S4.2 to a concentration of 0.25 mM. Delta delta Ct was used to calculate fold change between groups.

ELISA

To measure GABA in cecal contents of mice, cecal contents were collected on ice in sterile PBS, homogenized, centrifuged, and the supernatant was used in the Mouse GABA ELISA kit (Neogen, discontinued) or QuickDetect GABA (Mouse) ELISA Kit (Biovision, #E4456). The assay was performed

according to kit instructions, and the optical density of standards and supernatants was determined using a microplate reader (BioRad).

Statistical analysis

Geometric means were determined throughout the study. For most experiments, data points were converted logarithmically to obtain a normal distribution prior to analysis. Student's *t* tests or ANOVA followed by Fisher's LSD post hoc test (for comparison of more than two groups) were used to assess significance, and a *P* value of 0.05 or less was considered significant. If appropriate, outliers were removed using Grubb's test.

Table S4.1: *S.* Typhimurium and *E. coli* strains used in this study

Bacterial strains		
Species and strain	**Genotype**	**Reference**
***S.* Typhimurium strains**		
AJB715	IR715 Δ*phoN::*KSAC	(Kingsley et al., 2003)
ATCC 14028	Nalidixic acid-resistant derivative of ATCC14028	(Stojiljkovic et al., 1995)
FF176	IR715 *phoN::*Tn*10d-Cm*	(Faber et al., 2016)
BMM16	IR715 Δ*gabTP*	This study
BMM19	IR715 Δ*phoN::*KSAC Δ*gabTP*	This study
BMM147	IR715 Δ*phoN::*Tn*10d-Cm* Δ*iroN::*Carb^R	This study
BMM148	Δ*gabTP* Δ*iroN::*Carb^R	This study
BMM149	IR715 Δ*phoN::*KSAC Δ*gabTP* Δ*iroN::*Carb^R	This study
***E. coli* strains**		
E. coli DH5α *λpir*	F- *endA1 hsdR17* (r$^-$m$^+$) *supE44 thi-1 recA1 gyrA relA1 Δ(lacZYA-argF)$_{u189}$ Φ*80lacZΔM15	Lab stock
E. coli S17-1*λpir*	C600::RP4 2-(*tet::Mu*) (*kan::Tn7*) *λpir recA1 thi pro hsdR* (r$^-$ m$^+$)	Lab stock
E. coli JB2	Wild type (commensal isolated from mouse gut)	(Behnsen et al., 2014)
E. coli JB2 pCAL62	pCAL 62 (carb^R strep^R)	This study
Plasmids		
Name	**Genotype**	**Reference**
pRDH10	*sacRB cat ori*R6K *mobRP4* Tet^R	(Kingsley et al., 1999)
pCAL62	*ori*(R101) *Carb^R Strep^R*	(Spees et al., 2013)
pRE107	*sacRB carb^R ori*R6K	(Edwards et al., 1998)
pRE118	*sacRB KSAC ori*R6K	(Edwards et al., 1998)
pBMM2	pRDH10 with regions upstream and downstream of *gabTP*	This study
pBMM25	pRE118 with regions upstream and downstream of *iroN* flanking carbenicillin resistance cassette	This study

Table S4.2: Primers used in this study

Primers		
Gene	**Sequence**	**Organism**
gabTP	5'-CACACCCGTCCTGTGCCGAAGAGGGGAAGCGTATC-3' 5'-CTACGGTTAGGCGAAAATCGGGTGAATCTG-3 5'-TTTTCGCCTAACCGTAGCAAAACGCCCT-3' 5'-GCGTCCGGCGTAGAGGACAATGGCGGAATGGAACG-3'	*S.* Typhimurium
iroN	5'-TTCATGGCCATATCAATGGGCCGAATATCGCTGATAAAGG-3' 5'-ATTGGTAATGGATTATGCCCGCCGCT-3' 5'-GGGCATAATCCATTACCAATGCTTAATCAGTGAGG-3' 5'-TTTAGGGACGCGGAACCCCTATTTGTTTATTTTTC-3' 5'-GTTCCGCGTCCCTAAATAATGTCTAAAGTAG-3' 5'-AATTCATGCAGTTCACTTATATTCGTCCACCTAAAGAG-3'	*S.* Typhimurium
18s	5'-TGCATGGCCGTTCTTAGTTG-3' 5'-AGTTAGCATGCCAGAGTCTCGTT-3'	Mouse
Il1b	5'-CCTGAACTCAACTGTGAAATGCC-3' 5'-TCTTTTGGGGTCCGTCAACTTC-3	Mouse
Ifng	5'-CAACAGCAAGGCGAAAAAGGATGC-3' 5'-CCCCGAATCAGCAGCGACTCC-3'	Mouse
Nos2	5'-CCTCTTTCAGGTCACTTTGGTAGG-3' 5'-TTGGGTCTTGTTCAGCCACGG-3'	Mouse
Il6	5'-TCCAGAAACCGCTATGAAGTTCC-3' 5'-CACCAGCATCAGTCCCAAGAAG-3'	Mouse
Lcn2	5'-ACATTTGTTCCAAGCTCCAGGGC-3' 5'-CATGGCGAACTGGTTGTAGTCCG-3'	Mouse
Il22	5'-GGCCAGCCTTGCAGATAACA-3' 5'-GCTGATGTGACAGGAGCTGA-3'	Mouse
Kc	5'-TGCACCCAAACCGAAGTCAT-3' 5'-TTGTCAGAAGCCAGCGTTCAC-3'	Mouse
RegIIIg	5'-GCTCCTATTGCTATGCCTTGTTTAG-3' 5'-CATGGAGGACAGGAAGGAAGC-3'	Mouse
Gad65	5'-GCTGGAACCACCGTGTATGG-3' 5'-TCCACGTGCATCCAGATCTTAT-3'	Mouse
Gad67	5'-TCCACCATCAACGGCATTAT-3' 5'-AGCGGCAGGTGTTGGATAAC-3'	Mouse

References

Auteri, M., Zizzo, M.G., Mastropaolo, M., and Serio, R. (2014). Opposite role played by GABAA and GABAB receptors in the modulation of peristaltic activity in mouse distal colon. Eur. J. Pharmacol. *731*, 93–99.

Auteri, M., Zizzo, M.G., and Serio, R. (2015). GABA and GABA receptors in the gastrointestinal tract: from motility to inflammation. Pharmacol. Res. *93*, 11–21.

Aviello, G., Singh, A.K., O'Neill, S., Conroy, E., Gallagher, W., D'Agostino, G., Walker, A.W., Bourke, B., Scholz, D., and Knaus, U.G. (2019). Colitis susceptibility in mice with reactive oxygen species deficiency is mediated by mucus barrier and immune defense defects. Mucosal Immunol. *12*, 1316–1326.

Barman, M., Unold, D., Shifley, K., Amir, E., Hung, K., Bos, N., and Salzman, N. (2008). Enteric salmonellosis disrupts the microbial ecology of the murine gastrointestinal tract. Infect. Immun. *76*, 907–915.

Behnsen, J., Jellbauer, S., Wong, C.P., Edwards, R.A., George, M.D., Ouyang, W., and Raffatellu, M. (2014). The cytokine IL-22 promotes pathogen colonization by suppressing related commensal bacteria. Immunity *40*, 262–273.

Berger, C.N., Crepin, V.F., Roumeliotis, T.I., Wright, J.C., Serafini, N., Pevsner-Fischer, M., Yu, L., Elinav, E., Di Santo, J.P., Choudhary, J.S., et al. (2018). The Citrobacter rodentium type III secretion system effector EspO affects mucosal damage repair and antimicrobial responses. PLoS Pathog. *14*, e1007406.

Borisov, V.B., and Verkhovsky, M.I. (2015). Oxygen as Acceptor. EcoSal Plus *6*.

Bravo, J.A., Forsythe, P., Chew, M.V., Escaravage, E., Savignac, H.M., Dinan, T.G., Bienenstock, J., and Cryan, J.F. (2011). Ingestion of Lactobacillus strain regulates emotional behavior and central GABA receptor expression in a mouse via the vagus nerve. Proc. Natl. Acad. Sci. U. S. A. *108*, 16050–16055.

Buddhala, C., Hsu, C.-C., and Wu, J.-Y. (2009). A novel mechanism for GABA synthesis and packaging into synaptic vesicles. Neurochem. Int. *55*, 9–12.

Carson, D., Barry, R., Hopkins, E.G.D., Roumeliotis, T.I., García-Weber, D., Mullineaux-Sanders, C., Elinav, E., Arrieumerlou, C., Choudhary, J.S., and Frankel, G. (2020). Citrobacter rodentium induces rapid and unique metabolic and inflammatory responses in mice suffering from severe disease. Cell. Microbiol. *22*, e13126.

Chatterjee, S., Lekmeechai, S., Constantinou, N., Grzybowska, E.A., Kozik, Z., Choudhary, J.S., Berger, C.N., Frankel, G., and Clements, A. The type III secretion system effector EspO of enterohaemorrhagic Escherichia coli inhibits apoptosis through an interaction with HAX-1. Cell. Microbiol. *n/a*, e13366.

Chen, S., Tan, B., Xia, Y., Liao, S., Wang, M., Yin, J., Wang, J., Xiao, H., Qi, M., Bin, P., et al. (2019). Effects of dietary gamma-aminobutyric acid supplementation on the intestinal functions in weaning piglets. Food Funct. *10*, 366–378.

Dhakal, R., Bajpai, V.K., and Baek, K.-H. (2012). Production of gaba (γ – Aminobutyric acid) by microorganisms: a review. Braz. J. Microbiol. *43*, 1230–1241.

Edwards, R.A., Keller, L.H., and Schifferli, D.M. (1998). Improved allelic exchange vectors and their use to analyze 987P fimbria gene expression. Gene *207*, 149–157.

Faber, F., Tran, L., Byndloss, M.X., Lopez, C.A., Velazquez, E.M., Kerrinnes, T., Nuccio, S.-P., Wangdi, T., Fiehn, O., Tsolis, R.M., et al. (2016). Host-mediated sugar oxidation promotes post-antibiotic pathogen expansion. Nature *534*, 697–699.

Feehily, C., and Karatzas, K. a. G. (2013). Role of glutamate metabolism in bacterial responses towards acid and other stresses. J. Appl. Microbiol. *114*, 11–24.

Foster, J.W. (2004). Escherichia coli acid resistance: tales of an amateur acidophile. Nat. Rev. Microbiol. *2*, 898–907.

Gerhardt, A., Cinkaya, I., Linder, D., Huisman, G., and Buckel, W. (2000). Fermentation of 4-aminobutyrate by Clostridium aminobutyricum: cloning of two genes involved in the formation and dehydration of 4-hydroxybutyryl-CoA. Arch. Microbiol. *174*, 189–199.

Godinez, I., Raffatellu, M., Chu, H., Paixão, T.A., Haneda, T., Santos, R.L., Bevins, C.L., Tsolis, R.M., and Bäumler, A.J. (2009). Interleukin-23 orchestrates mucosal responses to Salmonella enterica serotype Typhimurium in the intestine. Infect. Immun. *77*, 387–398.

Gutnick, D., Calvo, J.M., Klopotowski, T., and Ames, B.N. (1969). Compounds which serve as the sole source of carbon or nitrogen for Salmonella typhimurium LT-2. J. Bacteriol. *100*, 215–219.

Hughes, E.R., Winter, M.G., Duerkop, B.A., Spiga, L., Furtado de Carvalho, T., Zhu, W., Gillis, C.C., Büttner, L., Smoot, M.P., Behrendt, C.L., et al. (2017). Microbial Respiration and Formate Oxidation as Metabolic Signatures of Inflammation-Associated Dysbiosis. Cell Host Microbe *21*, 208–219.

Janik, R., Thomason, L.A.M., Stanisz, A.M., Forsythe, P., Bienenstock, J., and Stanisz, G.J. (2016). Magnetic resonance spectroscopy reveals oral Lactobacillus promotion of increases in brain GABA, N-acetyl aspartate and glutamate. NeuroImage *125*, 988–995.

Jin, Z., Mendu, S.K., and Birnir, B. (2013). GABA is an effective immunomodulatory molecule. Amino Acids *45*, 87–94.

Jones, R.M., Luo, L., Ardita, C.S., Richardson, A.N., Kwon, Y.M., Mercante, J.W., Alam, A., Gates, C.L., Wu, H., Swanson, P.A., et al. (2013). Symbiotic lactobacilli stimulate gut epithelial proliferation via Nox-mediated generation of reactive oxygen species. EMBO J. *32*, 3017–3028.

Kingsley, R.A., Reissbrodt, R., Rabsch, W., Ketley, J.M., Tsolis, R.M., Everest, P., Dougan, G., Bäumler, A.J., Roberts, M., and Williams, P.H. (1999). Ferrioxamine-Mediated Iron(III) Utilization by Salmonella enterica. Appl. Environ. Microbiol. *65*, 1610–1618.

Kingsley, R.A., Humphries, A.D., Weening, E.H., de Zoete, M.R., Winter, S., Papaconstantinopoulou, A., Dougan, G., and Bäumler, A.J. (2003). Molecular and Phenotypic Analysis of the CS54 Island of Salmonella enterica Serotype Typhimurium: Identification of Intestinal Colonization and Persistence Determinants. Infect. Immun. *71*, 629–640.

Kruis, W., Fric, P., Pokrotnieks, J., Lukás, M., Fixa, B., Kascák, M., Kamm, M.A., Weismueller, J., Beglinger, C., Stolte, M., et al. (2004). Maintaining remission of ulcerative colitis with the probiotic Escherichia coli Nissle 1917 is as effective as with standard mesalazine. Gut *53*, 1617–1623.

Kurihara, S., Kato, K., Asada, K., Kumagai, H., and Suzuki, H. (2010). A putrescine-inducible pathway comprising PuuE-YneI in which gamma-aminobutyrate is degraded into succinate in Escherichia coli K-12. J. Bacteriol. *192*, 4582–4591.

Larsson, E., Tremaroli, V., Lee, Y.S., Koren, O., Nookaew, I., Fricker, A., Nielsen, J., Ley, R.E., and Bäckhed, F. (2012). Analysis of gut microbial regulation of host gene expression along the length of the gut and regulation of gut microbial ecology through MyD88. Gut *61*, 1124–1131.

Ma, X., Sun, Q., Sun, X., Chen, D., Wei, C., Yu, X., Liu, C., Li, Y., and Li, J. (2018). Activation of GABAA Receptors in Colon Epithelium Exacerbates Acute Colitis. Front. Immunol. *0*.

Mendu, S.K., Bhandage, A., Jin, Z., and Birnir, B. (2012). Different subtypes of GABA-A receptors are expressed in human, mouse and rat T lymphocytes. PloS One *7*, e42959.

Metzer, E., Levitz, R., and Halpern, Y.S. (1979). Isolation and properties of Escherichia coli K-12 mutants impaired in the utilization of gamma-aminobutyrate. J. Bacteriol. *137*, 1111–1118.

Nuccio, S.-P., and Bäumler, A.J. (2014). Comparative analysis of Salmonella genomes identifies a metabolic network for escalating growth in the inflamed gut. MBio *5*, e00929-00914.

Obata, K., Hirono, M., Kume, N., Kawaguchi, Y., Itohara, S., and Yanagawa, Y. (2008). GABA and synaptic inhibition of mouse cerebellum lacking glutamate decarboxylase 67. Biochem. Biophys. Res. Commun. *370*, 429–433.

Ognen, P.A.C. (2002). GABA and Glutamate in the Human Brain. Neuroscientist *8*, 562–573.

Patterson, E., Ryan, P.M., Wiley, N., Carafa, I., Sherwin, E., Moloney, G., Franciosi, E., Mandal, R., Wishart, D.S., Tuohy, K., et al. (2019). Gamma-aminobutyric acid-producing lactobacilli positively affect metabolism and depressive-like behaviour in a mouse model of metabolic syndrome. Sci. Rep. *9*, 16323.

Raffatellu, M., Santos, R.L., Verhoeven, D.E., George, M.D., Wilson, R.P., Winter, S.E., Godinez, I., Sankaran, S., Paixao, T.A., Gordon, M.A., et al. (2008). Simian immunodeficiency virus-induced mucosal interleukin-17 deficiency promotes Salmonella dissemination from the gut. Nat. Med. *14*, 421–428.

Reed, L.J. (1950). THE OCCURRENCE OF γ-AMINOBUTYRIC ACID IN YEAST EXTRACT; ITS ISOLATION AND IDENTIFICATION. J. Biol. Chem. *183*, 451–458.

Rivera-Chávez, F., and Bäumler, A.J. (2015). The Pyromaniac Inside You: Salmonella Metabolism in the Host Gut. Annu. Rev. Microbiol. *69*, 31–48.

Rivera-Chávez, F., Zhang, L.F., Faber, F., Lopez, C.A., Byndloss, M.X., Olsan, E.E., Xu, G., Velazquez, E.M., Lebrilla, C.B., Winter, S.E., et al. (2016). Depletion of Butyrate-Producing Clostridia from the Gut Microbiota Drives an Aerobic Luminal Expansion of Salmonella. Cell Host Microbe *19*, 443–454.

Rogers, A.W.L., Tsolis, R.M., and Bäumler, A.J. (2021). Salmonella versus the Microbiome. Microbiol. Mol. Biol. Rev. MMBR *85*, e00027-19.

Seerden, T.C., De Winter, B.Y., Van Den Bossche, R.M., Herman, A.G., Pelckmans, P.A., and De Man, J.G. (2005). Regional differences in gastrointestinal motility disturbances during acute necrotising pancreatitis. Neurogastroenterol. Motil. Off. J. Eur. Gastrointest. Motil. Soc. *17*, 671–679.

Smith, D.K., Kassam, T., Singh, B., and Elliott, J.F. (1992). Escherichia coli has two homologous glutamate decarboxylase genes that map to distinct loci. J. Bacteriol. *174*, 5820–5826.

Spees, A.M., Wangdi, T., Lopez, C.A., Kingsbury, D.D., Xavier, M.N., Winter, S.E., Tsolis, R.M., and Bäumler, A.J. (2013). Streptomycin-Induced Inflammation Enhances Escherichia coli Gut Colonization Through Nitrate Respiration. MBio *4*, e00430-13.

Stecher, B., Robbiani, R., Walker, A.W., Westendorf, A.M., Barthel, M., Kremer, M., Chaffron, S., Macpherson, A.J., Buer, J., Parkhill, J., et al. (2007). Salmonella enterica Serovar Typhimurium Exploits Inflammation to Compete with the Intestinal Microbiota. PLOS Biol. *5*, e244.

Stojiljkovic, I., Bäumler, A.J., and Heffron, F. (1995). Ethanolamine utilization in Salmonella typhimurium: nucleotide sequence, protein expression, and mutational analysis of the cchA cchB eutE eutJ eutG eutH gene cluster. J. Bacteriol. *177*, 1357–1366.

Strandwitz, P., Kim, K.H., Terekhova, D., Liu, J.K., Sharma, A., Levering, J., McDonald, D., Dietrich, D., Ramadhar, T.R., Lekbua, A., et al. (2019). GABA-modulating bacteria of the human gut microbiota. Nat. Microbiol. *4*, 396–403.

Suay-García, B., and Pérez-Gracia, M.T. (2019). Present and Future of Carbapenem-resistant Enterobacteriaceae (CRE) Infections. Antibiotics *8*, 122.

Valeri, M., and Raffatellu, M. (2016). Cytokines IL-17 and IL-22 in the host response to infection. Pathog. Dis. *74*, ftw111.

Concluding Remarks

Brittany M. Miller

The family *Enterobacteriaceae* spans many different bacterial lifestyles, from pathogen to harmless commensal, yet all sharing the core characteristic of thriving in a mammalian gut environment. Mechanisms of gut colonization by pathogens and commensals alike are still being elucidated, as well as the host barriers that prevent unwanted colonization. The differences in colonization strategy between an attaching and effacing pathogen, *Citrobacter rodentium*, and the invasive *Salmonella enterica* serovar Typhimurium vary wildly as illustrated in part through this thesis. In a nutshell, enteric pathogens have a slew of methods of colonizing their hosts, via bacterial factors like toxins, adhesins, and virulence factors, or some via host susceptibilities, such as antibiotic administration, or immune system status of the host. As pathogens, *Enterobacteriaceae* are responsible for a large burden of illnesses and deaths. In the United States, pathogenic *Enterobacteriaceae* such as *Salmonella* spp. and *Shigella* spp. represent a large proportion of hospitalizations and deaths from food-borne illnesses (Scallan et al.). In 2017, the WHO estimated that diarrheal disease is the second leading cause worldwide of death in children under five years old, with enteropathogenic *E. coli* representing one of the top causes (Lanata et al., 2013). Alarmingly, carbapenem-resistant *Enterobacteriaceae* (CRE) infections are on the rise in the United States and worldwide, which represent a huge public health threat, as these bacteria are resistant to a last line of defense antibiotic (Suay-García and Pérez-Gracia, 2019). CREs are not just limited to pathogens, but include many otherwise harmless bacteria that have been associated more with nosocomial infections. Therefore, much more work is needed to understand strategies *Enterobacteriaceae* employ, to help prevent and treat infections.

There are many host factors that shape the gut microbiota, acting as habitat filters, in addition to the innate and responsive responses of the host to a pathogen (see Chapter 1). Host control mechanisms guide the formation of the microbiota, which in turn helps further in conferring colonization resistance to pathogens. Pathogenesis research has for many years focused on elucidating molecular mechanisms of how bacterial virulence factors and toxins can cause disease in hosts. There is still much unknown about certain virulence strategies, yet, for many pathogens such as *Salmonella* spp. and enterohemorrhagic *E. coli*, elegant studies have described in detail how virulence factors mechanistically act on host cells, down to the

protein interaction level. Research coming out from the past few years in host-pathogen interactions has begun to focus on bacterial metabolism in the context of host-pathogen interactions. If a bacterium cannot overcome the hurdles in the form of habitat filters that the host provides, the bacterium will not be able to obtain nutrients, grow, and successfully colonize the host. Therefore, it is vitally important to learn more about the lifestyle of enteric bacteria as they infect the host GI tract. The respiratory mechanisms described for *C. rodentium* in the previous chapters 2 and 3, as well as *Salmonella* Typhimurium's engineering of a host neurotransmitter in chapter 4, add to the body of scientific literature that elucidate how enteric pathogens are able to grow in the gut. This is partially shown here via respiration, as well as through competition with other similar *Enterobacteriaceae* who would otherwise fill a desirable nutritional niche in the gut, which allows for the pathogen to spread to another host, thus propagating the pathogen species. In addition to filling gaps in knowledge, these strategies may be able to inform treatment and prevention methods. The linking of bacterial metabolism and virulence in future studies beyond the scope of this thesis will provide a more complete knowledge of host-pathogen interactions.

In chapter 2, we discovered that *C. rodentium*, via action of its type 3 secretion system (T3SS), causes colonic crypt hyperplasia, which leads to the availability of oxygen, a valuable new electron acceptor, for the pathogen. This was a significant discovery, as it was unknown why the pathogen would cause hyperplasia – could it benefit from this immune reaction? We found indeed that hyperplasia led to a change in colonocyte metabolism, shifting away from beta-oxidation of fatty acids, which is an oxygen intense process, towards a more fermentative metabolism, leaving host oxygen available for the pathogen (Fan et al., 2015). This could be a key to answering "why" attaching and effacing pathogens infect the host in this manner – it provides them access to oxygen, the electron acceptor with the highest reduction potential, thus providing the most ATP, and the most benefit to the cell (Borisov and Verkhovsky, 2015). Many questions remain to be answered. It is unclear how exactly the host senses bacterial infection and respond in a manner such as hyperplasia. Atarashi et al. found that epithelial cells respond in a similar way to segmented filamentous bacteria (SFB) attachment as with *C. rodentium* attachment (Atarashi et al.,

2015). Both bacteria triggered a Th17 response, and mutants that could not attach did not trigger the same response (6). The induction of hyperplasia, however, must therefore be downstream of colonocyte sensing of adhesion. Adhesion alone is also not the signal for hyperplasia, as SFB colonization does not lead to hyperplasia. It is still not clear what the signals are that eventually culminate in hyperplasia. We know from previous studies that hyperplasia is worse in susceptible mice, which have the *Cri1* locus, coding for *R-spondin2* (*Rspo2*) gene (Papapietro et al., 2013). *Rspo2* expression induces proliferation of intestinal precursor cells and inhibited the differentiation of mature enterocytes and goblet cells, a hallmark of colonic crypt hyperplasia. The authors note that the regulation of *Rspo2* is unclear, and because resistant mice such as C57BL/6J mice lack this locus, it is unclear what contributes to hyperplasia in these models. An elegant study showed that IL-22 production as a result of infection increases epithelial cell proliferation, which contributed in part to hyperplasia (Zheng et al., 2008). A recent study also showed that a *C. rodentium* effector protein, EspO, was responsible for causing hyperplasia in their mouse model, and translocation of this effector during infection affected secretion of IL-22 (Berger et al., 2018). Another group recently added to the knowledge of EspO function, showing it could inhibit apoptosis (Chatterjee et al.). This is an interesting concept, that preventing cell apoptosis could contribute to colonic crypt hyperplasia, although the authors did all their work *in vitro*, so whether apoptosis is an important process in the development of colonic crypt hyperplasia remains to be seen. It is also not clear what other cellular metabolic changes are happening during hyperplasia, and of special interest would be elucidating the metabolic status of the transient amplifying (TA) cells, the undifferentiated cells which accumulate during hyperplasia (Carson et al., 2020; Lopez et al., 2016). A picture of colonocyte metabolism is emerging, where under homeostatic conditions the colon maintains physiological hypoxia by high mitochondrial oxygen consumption (Chapter 1, 13). However, under conditions of hyperplasia, these TA cells obtain energy by converting glucose into lactate, which shifts the mitochondrial oxidative phosphorylation to aerobic glycolysis, leading to hypoxia being lost (Chapter 1). Other factors of TA cell metabolism might help us learn which carbon sources *C. rodentium* is obtaining during this stage of infection. In addition, colonocyte metabolism affects the

composition of the microbiota, which is important for understanding conditions outside of pathogen infection, such as dysbiosis during Inflammatory Bowel Disease (IBD) (Litvak et al., 2018).

In chapter 3, we found that *C. rodentium* is able to respire hydrogen peroxide before hyperplasia occurs, and the source of the hydrogen peroxide is host NOX1. This was an important discovery, as it showed that a host factor that presumably exists as an antibacterial defense mechanism was able to not only be survived by the pathogen, but able to be harnessed for energy and thus pathogen growth. On the bacterial side, anaerobic respiration is much more beneficial in terms of energy gain than fermentation (Borisov and Verkhovsky, 2015), and this is the first study to show that a pathogen can respire hydrogen peroxide in the gut. Like the major benefit from respiring oxygen, respiring hydrogen peroxide is also another reason attaching and effacing pathogens like *C. rodentium* make their niche attaching near the epithelial surface. Although hydrogen peroxide does not have as high a reduction potential as an electron acceptor as oxygen, anaerobic respiration is still much more beneficial in terms of energy production over fermentation (Borisov and Verkhovsky, 2015). In other words, the ability to respire hydrogen peroxide poises the pathogen to be able to rapidly outcompete the gut microbiota.

Much is still unknown about the function of NOX1 in the gut, and the conclusions of this study suggest that NOX1 could be a factor that shapes the gut biogeography, that is, which microbes are where in the gut environment. The colon is largely made up of strict anaerobes, which lack the ability to defend against reactive oxygen species (ROS), as they lack catalase and other peroxidases that would otherwise shield the cell from ROS damage (Albenberg et al., 2014). As we saw that NOX1 was constitutively expressed, as seen by the level of hydrogen peroxide, it seems that a gradient of hydrogen peroxide would be a good defense against obligate anaerobes getting too close to the epithelial barrier. The dogma in the field for a long time has been that oxygen radiating from the epithelial barrier in the colon is why only oxygen-tolerant organisms are found in this niche (Albenberg et al., 2014), however, these organisms would also be hydrogen peroxide-tolerant. Consistent with this hypothesis, Aviello et al. found that upon the breakdown of this habitat filter, mice faced mucus layer disruption and bacteria penetration into the crypts

(Aviello et al., 2019). Further work is needed to confirm the hypothesis that NOX1 specifically aids in keeping the gut microbiota away from the epithelial surface. Another interesting avenue of research would be understanding the regulation of NOX1, as it has been previously reported that germ-free mice express much less NOX1 in their colonic epithelium than SPF mice, as well as less ROS (Jones et al., 2013; Larsson et al., 2012). This is consistent with the hypothesis that NOX1 is a habitat filter that protects the colonic epithelium from the gut microbiota via a hydrogen peroxide gradient, in that its regulation is dependent on microbes. NOX1 expression seems to be induced by the gut microbiota, but whether it is induced by certain gut microbiota members, or just signals of bacteria, like TLR ligands, remains to be discovered.

In contrast to the strategies of *C. rodentium,* Chapter 4 showed another mechanism by which a related enteric pathogen, *Salmonella enterica* serovar Typhimurium, can modulate the gut environment for its own benefit. Years of research in *S.* Typhimurium pathogenic strategy has shown that the pathogen causes inflammation, and is able to benefit heavily from it, at the cost of the gut microbiota and the host (Rivera-Chávez and Bäumler, 2015; Rogers et al., 2021). In Chapter 4, we show *S.* Typhimurium can consume GABA in the mouse gut, which led to a change in IL-22 levels. This upregulation of IL-22 leads to the production of lipocalin-2, which sequesters iron from the gut lumen. *S.* Typhimurium produces salmochelin, which renders it lipocalin-2 resistant, allowing the pathogen to bloom when other bacteria are unable to grow due to lack of iron (Behnsen et al., 2014). Therefore, the *gabTP*-dependent consumption of GABA allows *S.* Typhimurium to compete with other *Enterobacteriaceae* that lack salmochelin. This was an important discovery, as it showed a pathogen could modulate levels of a neurotransmitter to benefit its own growth.

Much about the function of GABA in the gut is still unknown, and there are many unanswered questions left by this study. One large question remaining is how *S.* Typhimurium modulates GABA levels. We found that although host expression of glutamate decarboxylase does not change in whole cecal tissue during infection, this could be an artifact of essentially averaging all the cell types that are present in the gut during infection. That is to say, a small cell population could be producing the GABA, while other cell

types are not, and the signal is therefore diluted out. Another interesting mechanism would be whether *S.* Typhimurium-induced inflammation, which is known to alter the composition of the microbiota is responsible for the change in GABA levels in the lumen (Rivera-Chávez et al., 2016). The mechanism of how GABA levels influence IL-22 is also currently unknown, although a recent study showed that by supplementing weaning piglets with GABA, IL-22 levels decreased (Chen et al., 2019). Finding the cell type in the gut that is affected by GABA would help elucidate the link between GABA and IL-22. *S.* Typhimurium causes inflammation in the gut, that is characterized by an influx of neutrophils, and infection is later resolved by adaptive immunology (Rivera-Chávez and Bäumler, 2015). Many immune cells have been found to express GABA receptors on their surface (Auteri et al., 2015), including gut epithelial cells themselves (Ma et al., 2018). Interestingly, because GABA levels also affected whole gut transit time as shown in Chapter 4, the effect of GABA levels changing in the lumen must extend past the gut lumen as well, to be able to transduce the signal to the enteric plexi, affecting peristalsis. Outside of the *gabTP*-dependent changes in gut transit time, it is unknown what other effects are exerted on the host in this model. The gut-brain axis is a hot field of study, and *S.* Typhimurium may serve as a good tool to study how GABA levels in the gut are affecting the brain. It has been shown previously that *Lactobacillus* production of GABA was able to affect anxiety behaviors in mice, and even affected mRNA levels of GABAB receptor mRNA in the brain (Bravo et al., 2011). More recently, Patterson et al. saw GABA-producing *Lactobacillus brevis* was able to attenuate metabolic dysfunction and despair-like behavior in diet-induced obese mice (Patterson et al., 2019). The implication of gut microbes being able to "communicate" in this manner with the brain may serve as a useful tool in understanding numerous behavioral conditions that are thought to have a gut component, such as anxiety and depression.

While determining how enteric pathogens cause disease is of general scientific interest, the ultimate goal of pathogen research is to treat and prevent infection in humans. Learning more about strategies that bacterial pathogens use, especially in regards to their metabolism, is an open avenue through which to design treatments or preventions to disease. A recent study found that tungstate was able to specifically

block the molybdenum cofactor-dependent respiratory pathways that are important for *Enterobacteriaceae* anaerobic expansion under inflammatory conditions (Hughes et al., 2017; Zhu et al., 2018). The authors were furthermore able to show that under non-inflammatory conditions in mice, there were no overt changes to the microbiota, yet during inflammation, tungstate was able to exquisitely block the *Proteobacteria* expansion normally seen, without affecting the host immune response. Another treatment option for infections and IBD has been the oral administration of probiotics, where it was found that *E. coli* Nissle 1917 was able to suppress the growth of pathogens in patients with IBD, presumably through Nissle filling the ecological niche that a related *Enterobacteriaceae* pathogen would (Kruis et al., 2004). Probiotics that would be used in this manner clinically depend on their administration prior to infection, and *Salmonella* spp. have methods of outcompeting other *Enterobacteriaceae*, as shown in Chapter 4 that may render such treatments not useful. Chapter 4 also brings up the interesting possibility of treating humans with GABA for the treatment of *S.* Typhimurium infection. GABA is found in some foods, and as a dietary supplement widely available for individual purchase. Indeed, many individuals have gut microbes already capable of producing and using GABA (Strandwitz et al., 2019). While it is still contested whether GABA can penetrate the blood-brain barrier, GABA could potentially be used as a treatment to modulate levels of IL-22, in the gut during conditions such as infection, but much work is needed before that is realized. A large hurdle is that GABA is most likely absorbed by the body upstream of the colon, and levels of GABA are not affected in the colon by oral supplementation (unpublished data). Ultimately, research about pathogenic strategies for infection such as this thesis will lead to better treatments for affected humans, and a better understanding of host-microbe interactions as a whole.

References

Albenberg, L., Esipova, T.V., Judge, C.P., Bittinger, K., Chen, J., Laughlin, A., Grunberg, S., Baldassano, R.N., Lewis, J.D., Li, H., et al. (2014). Correlation between intraluminal oxygen gradient and radial partitioning of intestinal microbiota. Gastroenterology *147*, 1055-1063.e8.

Atarashi, K., Tanoue, T., Ando, M., Kamada, N., Nagano, Y., Narushima, S., Suda, W., Imaoka, A., Setoyama, H., Nagamori, T., et al. (2015). Th17 Cell Induction by Adhesion of Microbes to Intestinal Epithelial Cells. Cell *163*, 367–380.

Auteri, M., Zizzo, M.G., Mastropaolo, M., and Serio, R. (2014). Opposite role played by GABAA and GABAB receptors in the modulation of peristaltic activity in mouse distal colon. Eur. J. Pharmacol. *731*, 93–99.

Auteri, M., Zizzo, M.G., and Serio, R. (2015). GABA and GABA receptors in the gastrointestinal tract: from motility to inflammation. Pharmacol. Res. *93*, 11–21.

Aviello, G., Singh, A.K., O'Neill, S., Conroy, E., Gallagher, W., D'Agostino, G., Walker, A.W., Bourke, B., Scholz, D., and Knaus, U.G. (2019). Colitis susceptibility in mice with reactive oxygen species deficiency is mediated by mucus barrier and immune defense defects. Mucosal Immunol. *12*, 1316–1326.

Barman, M., Unold, D., Shifley, K., Amir, E., Hung, K., Bos, N., and Salzman, N. (2008). Enteric salmonellosis disrupts the microbial ecology of the murine gastrointestinal tract. Infect. Immun. *76*, 907–915.

Behnsen, J., Jellbauer, S., Wong, C.P., Edwards, R.A., George, M.D., Ouyang, W., and Raffatellu, M. (2014). The cytokine IL-22 promotes pathogen colonization by suppressing related commensal bacteria. Immunity *40*, 262–273.

Berger, C.N., Crepin, V.F., Roumeliotis, T.I., Wright, J.C., Serafini, N., Pevsner-Fischer, M., Yu, L., Elinav, E., Di Santo, J.P., Choudhary, J.S., et al. (2018). The Citrobacter rodentium type III secretion system effector EspO affects mucosal damage repair and antimicrobial responses. PLoS Pathog. *14*, e1007406.

Borisov, V.B., and Verkhovsky, M.I. (2015). Oxygen as Acceptor. EcoSal Plus *6*.

Bravo, J.A., Forsythe, P., Chew, M.V., Escaravage, E., Savignac, H.M., Dinan, T.G., Bienenstock, J., and Cryan, J.F. (2011). Ingestion of Lactobacillus strain regulates emotional behavior and central GABA receptor expression in a mouse via the vagus nerve. Proc. Natl. Acad. Sci. U. S. A. *108*, 16050–16055.

Buddhala, C., Hsu, C.-C., and Wu, J.-Y. (2009). A novel mechanism for GABA synthesis and packaging into synaptic vesicles. Neurochem. Int. *55*, 9–12.

Carson, D., Barry, R., Hopkins, E.G.D., Roumeliotis, T.I., García-Weber, D., Mullineaux-Sanders, C., Elinav, E., Arrieumerlou, C., Choudhary, J.S., and Frankel, G. (2020). Citrobacter rodentium induces rapid and unique metabolic and inflammatory responses in mice suffering from severe disease. Cell. Microbiol. *22*, e13126.

Chatterjee, S., Lekmeechai, S., Constantinou, N., Grzybowska, E.A., Kozik, Z., Choudhary, J.S., Berger, C.N., Frankel, G., and Clements, A. The type III secretion system effector EspO of enterohaemorrhagic Escherichia coli inhibits apoptosis through an interaction with HAX-1. Cell. Microbiol. *n/a*, e13366.

Chen, S., Tan, B., Xia, Y., Liao, S., Wang, M., Yin, J., Wang, J., Xiao, H., Qi, M., Bin, P., et al. (2019). Effects of dietary gamma-aminobutyric acid supplementation on the intestinal functions in weaning piglets. Food Funct. *10*, 366–378.

Dhakal, R., Bajpai, V.K., and Baek, K.-H. (2012). Production of gaba (γ – Aminobutyric acid) by microorganisms: a review. Braz. J. Microbiol. *43*, 1230–1241.

Edwards, R.A., Keller, L.H., and Schifferli, D.M. (1998). Improved allelic exchange vectors and their use to analyze 987P fimbria gene expression. Gene *207*, 149–157.

Faber, F., Tran, L., Byndloss, M.X., Lopez, C.A., Velazquez, E.M., Kerrinnes, T., Nuccio, S.-P., Wangdi, T., Fiehn, O., Tsolis, R.M., et al. (2016). Host-mediated sugar oxidation promotes post-antibiotic pathogen expansion. Nature *534*, 697–699.

Fan, Y.-Y., Davidson, L.A., Callaway, E.S., Wright, G.A., Safe, S., and Chapkin, R.S. (2015). A bioassay to measure energy metabolism in mouse colonic crypts, organoids, and sorted stem cells. Am. J. Physiol. Gastrointest. Liver Physiol. *309*, G1-9.

Feehily, C., and Karatzas, K. a. G. (2013). Role of glutamate metabolism in bacterial responses towards acid and other stresses. J. Appl. Microbiol. *114*, 11–24.

Foster, J.W. (2004). Escherichia coli acid resistance: tales of an amateur acidophile. Nat. Rev. Microbiol. *2*, 898–907.

Gerhardt, A., Cinkaya, I., Linder, D., Huisman, G., and Buckel, W. (2000). Fermentation of 4-aminobutyrate by Clostridium aminobutyricum: cloning of two genes involved in the formation and dehydration of 4-hydroxybutyryl-CoA. Arch. Microbiol. *174*, 189–199.

Godinez, I., Raffatellu, M., Chu, H., Paixão, T.A., Haneda, T., Santos, R.L., Bevins, C.L., Tsolis, R.M., and Bäumler, A.J. (2009). Interleukin-23 orchestrates mucosal responses to Salmonella enterica serotype Typhimurium in the intestine. Infect. Immun. *77*, 387–398.

Gutnick, D., Calvo, J.M., Klopotowski, T., and Ames, B.N. (1969). Compounds which serve as the sole source of carbon or nitrogen for Salmonella typhimurium LT-2. J. Bacteriol. *100*, 215–219.

Hughes, E.R., Winter, M.G., Duerkop, B.A., Spiga, L., Furtado de Carvalho, T., Zhu, W., Gillis, C.C., Büttner, L., Smoot, M.P., Behrendt, C.L., et al. (2017). Microbial Respiration and Formate Oxidation as Metabolic Signatures of Inflammation-Associated Dysbiosis. Cell Host Microbe *21*, 208–219.

Janik, R., Thomason, L.A.M., Stanisz, A.M., Forsythe, P., Bienenstock, J., and Stanisz, G.J. (2016). Magnetic resonance spectroscopy reveals oral Lactobacillus promotion of increases in brain GABA, N-acetyl aspartate and glutamate. NeuroImage *125*, 988–995.

Jin, Z., Mendu, S.K., and Birnir, B. (2013). GABA is an effective immunomodulatory molecule. Amino Acids *45*, 87–94.

Jones, R.M., Luo, L., Ardita, C.S., Richardson, A.N., Kwon, Y.M., Mercante, J.W., Alam, A., Gates, C.L., Wu, H., Swanson, P.A., et al. (2013). Symbiotic lactobacilli stimulate gut epithelial proliferation via Nox-mediated generation of reactive oxygen species. EMBO J. *32*, 3017–3028.

Kingsley, R.A., Reissbrodt, R., Rabsch, W., Ketley, J.M., Tsolis, R.M., Everest, P., Dougan, G., Bäumler, A.J., Roberts, M., and Williams, P.H. (1999). Ferrioxamine-Mediated Iron(III) Utilization by Salmonella enterica. Appl. Environ. Microbiol. *65*, 1610–1618.

Kingsley, R.A., Humphries, A.D., Weening, E.H., de Zoete, M.R., Winter, S., Papaconstantinopoulou, A., Dougan, G., and Bäumler, A.J. (2003). Molecular and Phenotypic Analysis of the CS54 Island of Salmonella enterica Serotype Typhimurium: Identification of Intestinal Colonization and Persistence Determinants. Infect. Immun. *71*, 629–640.

Kruis, W., Fric, P., Pokrotnieks, J., Lukás, M., Fixa, B., Kascák, M., Kamm, M.A., Weismueller, J., Beglinger, C., Stolte, M., et al. (2004). Maintaining remission of ulcerative colitis with the probiotic Escherichia coli Nissle 1917 is as effective as with standard mesalazine. Gut *53*, 1617–1623.

Kurihara, S., Kato, K., Asada, K., Kumagai, H., and Suzuki, H. (2010). A putrescine-inducible pathway comprising PuuE-YneI in which gamma-aminobutyrate is degraded into succinate in Escherichia coli K-12. J. Bacteriol. *192*, 4582–4591.

Lanata, C.F., Fischer-Walker, C.L., Olascoaga, A.C., Torres, C.X., Aryee, M.J., Black, R.E., and Unicef, for the C.H.E.R.G. of the W.H.O. and (2013). Global Causes of Diarrheal Disease Mortality in Children <5 Years of Age: A Systematic Review. PLOS ONE *8*, e72788.

Larsson, E., Tremaroli, V., Lee, Y.S., Koren, O., Nookaew, I., Fricker, A., Nielsen, J., Ley, R.E., and Bäckhed, F. (2012). Analysis of gut microbial regulation of host gene expression along the length of the gut and regulation of gut microbial ecology through MyD88. Gut *61*, 1124–1131.

Litvak, Y., Byndloss, M.X., and Bäumler, A.J. (2018). Colonocyte metabolism shapes the gut microbiota. Science *362*.

Lopez, C.A., Miller, B.M., Rivera-Chávez, F., Velazquez, E., Byndloss, M.X., Chávez-Arroyo, A., Lokken, K.L., Tsolis, R.M., Winter, S.E., and Bäumler, A.J. (2016). Virulence factors enhance Citrobacter rodentium expansion through aerobic respiration. Science *353*, 1249–1253.

Ma, X., Sun, Q., Sun, X., Chen, D., Wei, C., Yu, X., Liu, C., Li, Y., and Li, J. (2018). Activation of GABAA Receptors in Colon Epithelium Exacerbates Acute Colitis. Front. Immunol. *0*.

Mendu, S.K., Bhandage, A., Jin, Z., and Birnir, B. (2012). Different subtypes of GABA-A receptors are expressed in human, mouse and rat T lymphocytes. PloS One *7*, e42959.

Metzer, E., Levitz, R., and Halpern, Y.S. (1979). Isolation and properties of Escherichia coli K-12 mutants impaired in the utilization of gamma-aminobutyrate. J. Bacteriol. *137*, 1111–1118.

Nuccio, S.-P., and Bäumler, A.J. (2014). Comparative analysis of Salmonella genomes identifies a metabolic network for escalating growth in the inflamed gut. MBio *5*, e00929-00914.

Obata, K., Hirono, M., Kume, N., Kawaguchi, Y., Itohara, S., and Yanagawa, Y. (2008). GABA and synaptic inhibition of mouse cerebellum lacking glutamate decarboxylase 67. Biochem. Biophys. Res. Commun. *370*, 429–433.

Ognen, P.A.C. (2002). GABA and Glutamate in the Human Brain. Neuroscientist *8*, 562–573.

Papapietro, O., Teatero, S., Thanabalasuriar, A., Yuki, K.E., Diez, E., Zhu, L., Kang, E., Dhillon, S., Muise, A.M., Durocher, Y., et al. (2013). R-Spondin 2 signalling mediates susceptibility to fatal infectious diarrhoea. Nat. Commun. *4*, 1898.

Patterson, E., Ryan, P.M., Wiley, N., Carafa, I., Sherwin, E., Moloney, G., Franciosi, E., Mandal, R., Wishart, D.S., Tuohy, K., et al. (2019). Gamma-aminobutyric acid-producing lactobacilli positively affect metabolism and depressive-like behaviour in a mouse model of metabolic syndrome. Sci. Rep. *9*, 16323.

Raffatellu, M., Santos, R.L., Verhoeven, D.E., George, M.D., Wilson, R.P., Winter, S.E., Godinez, I., Sankaran, S., Paixao, T.A., Gordon, M.A., et al. (2008). Simian immunodeficiency virus-induced mucosal interleukin-17 deficiency promotes Salmonella dissemination from the gut. Nat. Med. *14*, 421–428.

Reed, L.J. (1950). THE OCCURRENCE OF γ-AMINOBUTYRIC ACID IN YEAST EXTRACT; ITS ISOLATION AND IDENTIFICATION. J. Biol. Chem. *183*, 451–458.

Rivera-Chávez, F., and Bäumler, A.J. (2015). The Pyromaniac Inside You: Salmonella Metabolism in the Host Gut. Annu. Rev. Microbiol. *69*, 31–48.

Rivera-Chávez, F., Zhang, L.F., Faber, F., Lopez, C.A., Byndloss, M.X., Olsan, E.E., Xu, G., Velazquez, E.M., Lebrilla, C.B., Winter, S.E., et al. (2016). Depletion of Butyrate-Producing Clostridia from the Gut Microbiota Drives an Aerobic Luminal Expansion of Salmonella. Cell Host Microbe *19*, 443–454.

Rogers, A.W.L., Tsolis, R.M., and Bäumler, A.J. (2021). Salmonella versus the Microbiome. Microbiol. Mol. Biol. Rev. MMBR *85*, e00027-19.

Scallan, E., Hoekstra, R.M., Angulo, F.J., Tauxe, R.V., Widdowson, M.-A., Roy, S.L., Jones, J.L., and Griffin, P.M. Foodborne Illness Acquired in the United States—Major Pathogens - Volume 17, Number 1—January 2011 - Emerging Infectious Diseases journal - CDC.

Smith, D.K., Kassam, T., Singh, B., and Elliott, J.F. (1992). Escherichia coli has two homologous glutamate decarboxylase genes that map to distinct loci. J. Bacteriol. *174*, 5820–5826.

Spees, A.M., Wangdi, T., Lopez, C.A., Kingsbury, D.D., Xavier, M.N., Winter, S.E., Tsolis, R.M., and Bäumler, A.J. (2013). Streptomycin-Induced Inflammation Enhances Escherichia coli Gut Colonization Through Nitrate Respiration. MBio *4*, e00430-13.

Stecher, B., Robbiani, R., Walker, A.W., Westendorf, A.M., Barthel, M., Kremer, M., Chaffron, S., Macpherson, A.J., Buer, J., Parkhill, J., et al. (2007). Salmonella enterica Serovar Typhimurium Exploits Inflammation to Compete with the Intestinal Microbiota. PLOS Biol. *5*, e244.

Stojiljkovic, I., Bäumler, A.J., and Heffron, F. (1995). Ethanolamine utilization in Salmonella typhimurium: nucleotide sequence, protein expression, and mutational analysis of the cchA cchB eutE eutJ eutG eutH gene cluster. J. Bacteriol. *177*, 1357–1366.

Strandwitz, P., Kim, K.H., Terekhova, D., Liu, J.K., Sharma, A., Levering, J., McDonald, D., Dietrich, D., Ramadhar, T.R., Lekbua, A., et al. (2019). GABA-modulating bacteria of the human gut microbiota. Nat. Microbiol. *4*, 396–403.

Suay-García, B., and Pérez-Gracia, M.T. (2019). Present and Future of Carbapenem-resistant Enterobacteriaceae (CRE) Infections. Antibiotics *8*, 122.

Valeri, M., and Raffatellu, M. (2016). Cytokines IL-17 and IL-22 in the host response to infection. Pathog. Dis. *74*, ftw111.

Zheng, Y., Valdez, P.A., Danilenko, D.M., Hu, Y., Sa, S.M., Gong, Q., Abbas, A.R., Modrusan, Z., Ghilardi, N., de Sauvage, F.J., et al. (2008). Interleukin-22 mediates early host defense against attaching and effacing bacterial pathogens. Nat. Med. *14*, 282–289.

Zhu, W., Winter, M.G., Byndloss, M.X., Spiga, L., Duerkop, B.A., Hughes, E.R., Büttner, L., de Lima Romão, E., Behrendt, C.L., Lopez, C.A., et al. (2018). Precision editing of the gut microbiota ameliorates colitis. Nature *553*, 208–211.